

Time-Dependent Self Consistent Harmonic Approximation: Anharmonic nuclear quantum dynamics and time correlation functions

Lorenzo Monacelli and Francesco Mauri
Physics Department, University of Rome "Sapienza"
 (Dated: May 26, 2022)

Most material properties of great physical interest are directly related to nuclear dynamics, e.g. the ionic thermal conductivity, Raman/IR vibrational spectra, inelastic X-ray, and Neutron scattering. A theory able to compute from first principles these properties, fully accounting for the quantum nature of the nuclei and the anharmonicity in the nuclear energy landscape that can be implemented in systems with hundreds of atoms is missing. Here, we derive an approximated theory for the quantum time evolution of lattice vibrations at finite temperature. This theory introduces the time dynamics in the Self-Consistent Harmonic Approximation (SCHA) and shares with the static case the same computational cost. It is nonempirical, as pure states evolve according to the Dirac least action principle and the dynamics of the thermal ensemble conserves both energy and entropy. The static SCHA is recovered as a stationary solution of the dynamical equations. We apply perturbation theory around the static SCHA solution and derive an algorithm to compute efficiently quantum dynamical correlation functions. Thanks to this new algorithm, we have access to the response function of any general external time-dependent perturbation, enabling the simulation of phonon spectra without following any perturbative expansion of the nuclear potential or empirical methods. We benchmark the method on the IR and Raman spectroscopy of high-pressure hydrogen phase III, with a simulation cell of 96 atoms. Our work also explores the nonlinear regime of the dynamical nuclear motion, providing a paradigm to simulate the interaction with intense or multiple probes, as in pump-probe spectroscopy, or chemical reactions involving light atoms, as the proton transfer in biomolecules.

I. INTRODUCTION

The computational power available for research dramatically increased in the last decades paving the way to the birth of a new field of science: material design. We can predict the physical properties of a material *in silico*, anticipating the experimental data and enabling for an automatic search of target compounds before their synthesis. An example of an impressive result is the prediction of record-breaking high-temperature superconductivity in hydrates, like hydrogen sulfide[1] and LaH_{10} [2] that came together with experimental result[3–5], thanks to the success of *ab initio* crystal structure prediction[6–8].

Material science can also assist in interpreting experimental data, as it is possible, in principle, to anticipate the outcome of almost any experimental technique by calculating dynamical correlation functions. For example, IR and optical spectroscopy are obtained by simulating the dipole-dipole time correlation functions, Raman signal with the polarizability-polarizability dynamical correlation function, while Neutron and X-Ray scattering can be simulated calculating the dynamical structure factor.

However, still, first-principle calculations are far from being perfect, and they often miss the required precision. One of the most difficult aspect to describe are ionic vibrations. Even if the energy of ionic vibration is orders of magnitude smaller than the typical energy involved in chemical bonds, the nuclear excited states are in the same range of energy as thermal excitation available at room temperature. Therefore, ionic motion is responsible for almost all properties of materials that depend on

temperature as thermal expansion and thermal conductivity.

While the development of time-dependent Hartree-Fock (TD-HF) and time-dependent density functional theory[9, 10] (TD-DFT) paved the way to the simulation of these quantum correlation functions fully *ab initio* for electrons, still a full quantum theory of nuclear motion that can be routinely applied in realistic systems (with hundreds of atoms in the simulation cell) is missing.

The usual approach to lattice dynamics is through perturbation theory, where the ionic motion is expanded as a small perturbation around the static position (minimum of the total electronic energy of the system with frozen ions). Needless to say, this approach fails in many cases, as when ions are located in a saddle point of the energy landscape and their position is stabilized by entropy, or if a very strong anharmonicity is present.

Ionic time correlation functions can be computed also in the presence of strong anharmonicity with *ab initio* molecular dynamics (AIMD)[11, 12], but it neglects nuclear quantum dispersion. This is critical for molecular crystals or systems with light atoms, where the Debye temperature comparable or above room temperature. In these cases, AIMD provides untrustable results.

The quantum equivalent of AIMD is path-integral molecular dynamics (PIMD), but this is a static theory, in which time is replaced by an imaginary variable. Thus, PIMD describes only equilibrium quantities. It is possible to obtain dynamical correlation function by performing an analytical continuation to real time[13], but this is computationally heavy and achievable only in prototypical cases where the correlation function has few poles and if a force-field is available to clean stochastic

noise[14]. Empirical methods have been developed[15–18], but, still, their application is computationally expensive as it requires a PIMD calculation.

Relevant cases where all these techniques fail are materials with light atoms or close to structural instability, where ionic fluctuations are sizable. For example, the simulation of high-pressure hydrates requires a full quantum and anharmonic treatment of the nuclear motion. These materials are attracting a lot of attention due to the discovery of room-temperature superconductivity[19]. On the other side, systems close to a structural instability play a fundamental role in technological and industrial applications; among them, we have multiferroics, charge density waves in 2D layers, and ferroelectrics, where the huge anharmonic phonon scattering is exploited also to increase their thermoelectric efficiency. Moreover, quantum nuclear dynamics beyond the linear regime is fundamental for studying chemical reactions involving light atoms. A significant example is the proton transfer in biomolecules.

In this work, we formulate a new dynamical theory of quantum nuclear motion at finite temperature and derive an algorithm to calculate time-dependent correlation functions fully *ab initio*. This method has a computational cost of the same order of standard AIMD but fully accounts for the effect of quantum fluctuations non empirically. Our theory is a time-dependent (TD) extension of the Stochastic Self-Consistent Harmonic Approximation (SCHA), that already proved to be very efficient in describing equilibrium properties of many materials, as high-pressure hydrates[20–23], hydrogen[24–26], charge density waves[27–29] and thermoelectric materials[30–32].

In Sec. II we introduce the theoretical framework of this paper. We revise the general dynamical response to an external time-dependent perturbation and the relationship between the nuclear time-correlation functions to some common experimental techniques. In Sec. III we revise the static SCHA, redefining it in a context in which it is easier to link with the full time-dependent theory. The Time-Dependent SCHA (TD-SCHA) is introduced in Sec. IV, where we derive the master equation for the density matrix by imposing that a Gaussian wave-packet must minimize the Dirac action. We also discuss generic features of the time-evolution as energy and entropy conservation. We also discuss steady-state solutions and the thermodynamic equilibrium (where the SCHA solution is recovered). In Sec. V, we linearize the TD-SCHA equations of motion around the equilibrium solution. We derive the explicit formula to compute the quantum time-correlation functions and derive a new Lanczos based algorithm to compute them. We show in Sec. VD that we recover the dynamical *ansatz* formulated by Bianco et al[33] for one-phonon Green functions. In Sec. VII B, we benchmark the method in the complex case of high-pressure hydrogen phase III, where quantum dispersion and anharmonicity strongly affect the vibrational spectra. We prove, comparing the simulation of IR

and Raman spectra to experiments, how the TD-SCHA can easily handle such a complex system with 96 atoms in the simulation cell computing forces between ions fully *ab initio* within Density Functional Theory (DFT).

A. Notation

First of all, let us introduce the notation used in the paper.

We use bold fonts to indicate vectors or matrices; products between them are the standard rows-by-columns product. Each index indicates both atomic and Cartesian components, so, if not differently specified, it ranges from 1 to $3N$ (N is the number of atoms). Therefore, vectors and matrices have dimension $3N$ and $3N \times 3N$, respectively. For quantum operators and wave-functions, we use the Dirac notation: we distinguish quantum operators with a hat $\hat{\cdot}$ from real numbers. So, for example, R_i is the position of the i -th atom/Cartesian component, \hat{R}_i is quantum position operator and $|R_i\rangle$ is the eigenvector of the position operator with R_i as eigenvalue:

$$\hat{R}_i |R_i\rangle = R_i |R_i\rangle \quad (1)$$

The bracket $\langle \cdot \rangle_\rho$ indicates an average on the distribution specified in the lower index. The average is a standard average on the nuclear probability distribution $\rho(\mathbf{R})$ if we do not indicate the operator, otherwise it is a quantum average computed on the density matrix:

$$\langle O \rangle_\rho = \int d\mathbf{R} O(\mathbf{R}) \rho(\mathbf{R}) \quad (2)$$

$$\langle \hat{O} \rangle_{\hat{\rho}} = \text{Tr} [\hat{\rho} \hat{O}] \quad (3)$$

Moreover, if the density matrix, the wave-function and any parameter that represent the status of the system does not have an explicit time dependency, it represents the equilibrium solution, unless differently stated.

II. THE QUANTUM NUCLEAR EVOLUTION

Almost all experimental techniques used to characterize materials involve an exchange in energy between the probe and the sample below hundreds of eV. At this energy scale, the only components of the material that interact with the probe are valence electrons and ions, which include the atomic nucleus plus the core electrons. These are the degrees of freedom we are interested in studying. In the Born-Oppenheimer (BO) approximation, electrons are fast moving with respect to ions. For this reason, the electrons feel the ionic lattice frozen, and relax to their ground state for each ionic configuration. Thus, the full electron-ion wave-function $|\Psi\rangle$ can be factorized in a ionic and electronic part:

$$\langle \mathbf{R}, \mathbf{r} | \Psi \rangle = \langle \mathbf{R} | \psi_{\text{ion}} \rangle \langle \mathbf{r} | \psi_{\text{el}} | \mathbf{R} \rangle \quad (4)$$

where \mathbf{r} are the electron positions, $|\psi_{\text{ion}}\rangle$ is the wave-function of ions and $|\psi_{\text{el}}[\mathbf{R}]\rangle$ is the electronic ground state with the ions fixed in the \mathbf{R} position.

In this work, we focus in physical properties that depends only on ions. For this reason, we will drop the ion index from the wave-function, and $|\psi\rangle$ always refers to the nuclear wave-function $|\psi_{\text{ion}}\rangle$. Within BO approximation, the ionic wave-function obeys to the Schroedinger equation with a BO Hamiltonian \hat{H} :

$$\hat{H} = \sum_{i=1}^{3N} \frac{\hat{p}_i^2}{2m_i} + V(\hat{\mathbf{R}}) \quad (5)$$

where \hat{p}_i is the momentum operator of nucleus i , m_i the mass of the i -th atom. The BO potential $V(\mathbf{R})$ is the ionic energy landscape, obtained as the ground state energy of the electronic problem with ions fixed in positions \mathbf{R} . The BO energy landscape $V(\mathbf{R})$ is usually obtained *ab initio* by solving the electronic problem with fixed nuclei within DFT or HF approximations.

This work aims to describe how (nuclear) physical properties change in time when the system in equilibrium is perturbed by an external probe. This is the typical setup for any experiment: when $t < t_0$, the system is in equilibrium. At $t = t_0$, it starts interacting with an external time-dependent perturbation $V^{(1)}(\mathbf{R}, t)$. We are interested in the expectation value of a generic nuclear observable $\hat{\mathcal{A}}$ at time $t > t_0$.

At $T = 0\text{ K}$, the nuclear wave-function in equilibrium satisfies the static Schroedinger equation:

$$\hat{H} |\psi\rangle = E_{\text{GS}} |\psi\rangle \quad (6)$$

The presence of a time-dependent perturbation for $t \geq t_0$ introduces a time dependency in the nuclear wave-function $|\psi(t)\rangle$. The time-dependent external perturbation is:

$$V^{(1)}(\hat{\mathbf{R}}, t) = \mathcal{B}(\hat{\mathbf{R}}) \mathcal{V}(t) \quad (7)$$

$$\mathcal{V}(t) = 0 \quad \text{for} \quad t < t_0 \quad (8)$$

where $\hat{\mathcal{B}} = \mathcal{B}(\hat{\mathbf{R}})$ is the observable that couples the external perturbation (the probe) with the ionic positions and $\mathcal{V}(t)$ is the time envelope of our perturbation. Thus, the quantum expectation value of the $\hat{\mathcal{A}}$ observable at time t is:

$$\mathcal{A}(t) = \langle \psi(t) | \hat{\mathcal{A}} | \psi(t) \rangle \quad (9)$$

The Schroedinger equation governs the time-evolution of $|\psi(t)\rangle$:

$$i\hbar \frac{d}{dt} |\psi(t)\rangle = \hat{H}_{\text{td}}(t) |\psi(t)\rangle. \quad (10)$$

where the $\hat{H}_{\text{td}}(t)$ time-dependent Hamiltonian is:

$$\hat{H}_{\text{td}}(t) = \hat{H} + V^{(1)}(\hat{\mathbf{R}}, t), \quad (11)$$

and Eq. (10) is solved with the initial condition that the wave-function at $t = t_0$ is in the ground state:

$$|\psi(t_0)\rangle = |\psi\rangle. \quad (12)$$

At finite temperature ($T > 0\text{ K}$), we just need to replace the wave-function with a density matrix $\hat{\rho}$ that can describe also mixture of states. At equilibrium (when $t \leq t_0$), the density matrix is $\hat{\rho}$:

$$\hat{\rho} = \sum_i p_i |\psi_i\rangle \langle \psi_i|. \quad (13)$$

where the $|\psi_i\rangle$ are the eigenstates of the \hat{H} Hamiltonian with E_i energy, and p_i are the Boltzmann occupations (k_b is the Boltzmann constant and T the temperature):

$$\hat{H} |\psi_i\rangle = E_i |\psi_i\rangle \quad (14)$$

$$p_i = \frac{e^{-\beta E_i}}{Z} \quad Z = \sum_i e^{-\beta E_i} \quad \beta = \frac{1}{k_b T} \quad (15)$$

After t_0 , the system interacts with the external perturbation, and the density matrix depends on time $\hat{\rho}(t)$. This time evolution is simply given by the evolution of each state in the mixture according to the Schroedinger equation:

$$\hat{\rho}(t) = \sum_i p_i |\psi_i(t)\rangle \langle \psi_i(t)|. \quad (16)$$

Where $|\psi_i(t)\rangle$ are the same eigenstates of the BO Hamiltonian \hat{H} (Eq. 14) at $t = t_0$ evolving with the time dependent Hamiltonian $\hat{H}_{\text{td}}(t)$. In this work, we focus on isolated systems, therefore p_i does not depend on time, and the density matrix satisfy the Liouville-Von Neumann equation:

$$i\hbar \frac{d}{dt} \hat{\rho}(t) = \hat{H}_{\text{td}}(t) \hat{\rho}(t) - \hat{\rho}(t) \hat{H}_{\text{td}}(t) \quad (17)$$

In this case, the average of the observable is:

$$\mathcal{A}(t) = \langle \hat{\mathcal{A}} \rangle_{\hat{\rho}(t)} = \text{Tr} [\hat{\rho}(t) \hat{\mathcal{A}}] \quad (18)$$

A case of particular interest is the linear regime (when the interaction between the probe and the system is small compared to the typical interaction between the ions). In this case, the time-dependence of an observable is given by the response function:

$$\mathcal{A}(t) = \mathcal{A}(t_0) + \int_{-\infty}^{\infty} \chi_{\mathcal{AB}}(t-t') \mathcal{V}(t') dt' \quad (19)$$

The response function $\chi_{\mathcal{AB}}(t)$ is directly related to time-correlation function through the Kubo equation:

$$\chi_{\mathcal{AB}}(t) = -\frac{i}{\hbar} \left\langle [e^{\frac{i}{\hbar} \hat{H} t} \hat{\mathcal{A}} e^{-\frac{i}{\hbar} \hat{H} t}, \hat{\mathcal{B}}] \right\rangle_{\hat{\rho}(t_0)} \vartheta(t) \quad (20)$$

Here, $e^{-\frac{i}{\hbar}\hat{H}t}$ is the time evolution operator in absence of the external perturbation and $\vartheta(t)$ is the Heaviside function. In particular, the convolution of Eq. (19) between χ_{AB} and \mathcal{V} becomes a simple product in the frequency domain:

$$\mathcal{A}(\omega) - \mathcal{A}(t_0) = \chi_{AB}(\omega)\mathcal{V}(\omega). \quad (21)$$

The $\hat{\mathcal{A}}$ and $\hat{\mathcal{B}}$ operators depend on the particular experiment we want to simulate. For example, IR spectroscopy studies the absorption of IR light across the sample. Absorbed light is related to the imaginary part of the refractive index $n(\omega)$, that is obtained from the dielectric tensor $\epsilon(\omega)$:

$$n(\omega) = \sqrt{\epsilon(\omega)} \quad (22)$$

The dielectric tensor of a material is directly related to the polarization-polarization susceptibility $\chi_{MM}(\omega)$, for which we have an electronic and ionic contribution. The electronic contribution is almost always constant in the IR light for an insulator, and the features of IR spectroscopies (peaks) are given by the ionic contribution to the dipole-dipole response function:

$$n(\omega) = \sqrt{1 + 4\pi\chi_{MM}^{(el)}(\omega) + 4\pi\chi_{MM}^{(ion)}(\omega)}. \quad (23)$$

Therefore, to simulate IR spectra, we need to compute the dynamical nuclear correlation function $\chi_{MM}^{(ion)}(\omega)$, where $\hat{\mathcal{A}} = \hat{\mathcal{B}} = M(\hat{\mathbf{R}})$, and $M(\hat{\mathbf{R}})$ is the dipole moment along the probe polarization of the system when nuclei are located in \mathbf{R} . Analogously, the Raman signal is obtained measuring the energy exchanged between the incoming and outgoing radiation. This energy exchange occurs thanks to the polarizability tensor $\alpha(\mathbf{R})$ of the system caused by the displacements in the ionic position \mathbf{R} , induced by the probe. In this case, $\hat{\mathcal{A}} = \hat{\mathcal{B}} = \alpha_{xy}(\hat{\mathbf{R}})$, where the xy directions are the incoming and outgoing polarization of light[34]. In the same way, the dynamical structure factor and the thermal conductivity are dynamical nuclear correlation functions[35].

Indeed, we can also simulate experiments beyond linear regime, in which the system interacts with multiple probes, as in impulsive vibrational spectroscopy[36]. Here, the system is perturbed with two pulses: a first optical pulse at $t = t_0$ brings the system out-of-equilibrium, then, the probe pulse interacts with the sample at time $t_1 > t_0$ measuring its polarizability.

The numerical simulation of such an experiment requires the solution of Eq. (17) and Eq. (18). This is computationally unfeasible for a system with more than few atoms, as the memory required to store the density matrix goes as $M^{(3N)^2}$, where M is the dimension of the basis of the wave-function and N the number of atoms in the simulation cell. Also, the easier linear regime requires the calculation of the time-correlation function in Eq. (20), that involves the full diagonalization of the static interacting Hamiltonian \hat{H} to calculate the free time-evolution $e^{-\frac{i}{\hbar}\hat{H}t}$.

In this work, we derive an approximated theory for the time evolution of the nuclear density matrix. Our theory allows simulating the time evolution of systems with hundreds of atoms with the BO energy landscape $V(\hat{\mathbf{R}})$ calculated *ab initio* from the solution of the electronic problem. For the case of linear perturbations, we also derive a new algorithm to calculate the nuclear time-correlation functions $\chi_{AB}(t)$. We present an *ab initio* application of a system with 96 atoms in the unit cell.

In the next section, we revise the static SCHA theory, a theory for the equilibrium density matrix that is the starting point of our derivation.

III. STATIC SELF-CONSISTENT HARMONIC APPROXIMATION

The SCHA is a mean-field theory developed to deal with interacting phonons and to compute thermodynamic properties of solids.

Here, the interacting many-body ionic density matrix is replaced with a non-interacting one. Starting from now through the rest of the paper, $\hat{\rho}$ is the SCHA equilibrium density matrix. As done in Hartree-Fock for electrons, in the SCHA, the $\hat{\rho}$ density matrix minimizes the free energy functional of a trial density matrix $\hat{\rho}$:

$$F[\hat{\rho}] = \min_{\hat{\rho}} F[\hat{\rho}]. \quad (24)$$

$$F[\hat{\rho}] = \langle \hat{H} \rangle_{\hat{\rho}} - TS[\hat{\rho}], \quad (25)$$

where $S[\hat{\rho}]$ is the entropy functional:

$$S[\hat{\rho}] = -k_b \text{Tr} [\hat{\rho} \ln \hat{\rho}]. \quad (26)$$

The $\hat{\rho}$ is restricted only among Gaussian matrices:

$$\begin{aligned} \langle \mathbf{R} | \hat{\rho} | \mathbf{R}' \rangle = \mathcal{N} \exp \Bigg[& - \sum_{ab} \frac{\Theta_{ab}}{4} (R_a - \mathcal{R}_a)(R_b - \mathcal{R}_b) + \\ & - \sum_{ab} \frac{\Theta'_{ab}}{4} (R'_a - \mathcal{R}_a)(R'_b - \mathcal{R}_b) + \\ & + \sum_{ab} A_{ab} (R_a - \mathcal{R}_a)(R'_b - \mathcal{R}'_b) \Bigg] \end{aligned} \quad (27)$$

The parameters that uniquely determines $\hat{\rho}$ are the vector \mathcal{R} , that represent the average ionic positions, and the real Hermitian matrices Θ and \mathbf{A} , that represent the quantum and thermal fluctuations around the average positions, respectively. The \mathcal{N} factor is the normalization of the density matrix. The Θ and \mathbf{A} matrices are not independent: they commute and are constrained so that $\hat{\rho}$ must be normalized. This condition is obtained if the real symmetric matrix Υ has only positive eigenvalues:

$$\Upsilon = \Theta - 2\mathbf{A} \quad (28)$$

Eq. (27) is a bit more general than the one introduced in ref.[20]: it is the density matrix of a quantum harmonic oscillator, where each normal mode is thermally populated by a different temperature. However, as we prove later in Sec. IVE and Appendix D, in the minimum of the free energy, all the modes are always populated by the same temperature, and the result coincides with ref.[20].

The SCHA is solved by substituting the expression of the trial density matrix $\hat{\rho}$ (Eq. 27) into the free energy functional (Eq. 25), and minimizing with respect to \mathbf{R} , Θ and \mathbf{A} .

Interestingly, the SCHA equilibrium density matrix $\hat{\rho}$ satisfies the self-consistent equation:

$$\hat{\rho} = \frac{\exp\left(-\beta\hat{\mathcal{H}}[\rho]\right)}{Z[\rho]}, \quad (29)$$

where $\hat{\mathcal{H}}[\rho]$ is a harmonic Hamiltonian that depends self-consistently on the nuclear equilibrium density $\rho(\mathbf{R})$:

$$\rho(\mathbf{R}) = \langle \mathbf{R} | \hat{\rho} | \mathbf{R} \rangle \quad (30)$$

$$\hat{\mathcal{H}}[\rho] = \sum_{i=1}^{3N} \frac{\hat{p}_i^2}{2m_i} + \sum_{ij} \left\langle \frac{\partial^2 V}{\partial R_i \partial R_j} \right\rangle_{\rho} (\hat{R}_i - \mathcal{R}_i[\rho])(\hat{R}_j - \mathcal{R}_j[\rho]). \quad (31)$$

The functional $\mathcal{R}_i[\rho]$ is the average position of the i -th atom, and coincides with the \mathcal{R}_i solution of the SCHA:

$$\mathcal{R}[\rho] = \int d\mathbf{R} \rho(\mathbf{R}) \mathbf{R}, \quad (32)$$

and the averages are computed with the $\rho(\mathbf{R})$ probability density

$$\left\langle \frac{\partial^2 V}{\partial R_a \partial R_b} \right\rangle_{\rho} = \int d\mathbf{R} \rho(\mathbf{R}) \frac{\partial^2 V(\mathbf{R})}{\partial R_a \partial R_b}. \quad (33)$$

When $\hat{\rho}$ is the equilibrium solution $\hat{\rho}$, we have:

$$A_{ab} = \sqrt{m_a m_b} \sum_{\mu} \frac{2\omega_{\mu} n_{\mu} (n_{\mu} + 1)}{\hbar(2n_{\mu} + 1)} e_{\mu}^a e_{\mu}^b \quad (34)$$

$$\Upsilon_{ab} = \sqrt{m_a m_b} \sum_{\mu} \frac{2\omega_{\mu}}{\hbar(2n_{\mu} + 1)} e_{\mu}^a e_{\mu}^b \quad (35)$$

Where e_{μ} and ω_{μ} are the normal modes and frequencies of the self-consistent harmonic Hamiltonian $\hat{\mathcal{H}}[\rho]$, and n_{μ} is the Bose-Einstein occupation number:

$$n_{\mu} = \frac{1}{e^{\beta\hbar\omega_{\mu}} - 1} \quad (36)$$

The SCHA in its stochastic implementation[20, 33, 37] proved to be a practical tool for many equilibrium calculations thanks to its cheap numerical cost. Both the

kinetic energy and the entropy of Eq. (25) are analytical when a Gaussian density matrix is employed. The only remaining term is the average of the potential energy on ionic configurations. This can be efficiently calculated with a Monte Carlo integral, sampling stochastically the ionic configurations, distributed according to $\rho(\mathbf{R})$.

A particular case is the $T = 0$ K limit, when the equilibrium SCHA density matrix is a pure state. Here, the SCHA equilibrium pure state $|\psi\rangle$ is the ground state of the self-consistent Hamiltonian $\hat{\mathcal{H}}[\rho]$:

$$\hat{\mathcal{H}}[\rho] |\psi\rangle = E_{GS} |\psi\rangle \quad (37)$$

and the density $\rho(\mathbf{R})$ is:

$$\rho(\mathbf{R}) = \langle \mathbf{R} | \psi \rangle \langle \psi | \mathbf{R} \rangle = |\langle \mathbf{R} | \psi \rangle|^2 \quad (38)$$

The pure state is a Gaussian wave-packet:

$$\langle \mathbf{R} | \psi \rangle = \mathcal{N}^{\frac{1}{2}} \exp \left[-\frac{1}{4} \sum_{ab} \Upsilon_{ab} (R_a - \mathcal{R}_a)(R_b - \mathcal{R}_b) \right] \quad (39)$$

IV. TIME-DEPENDENT SELF-CONSISTENT HARMONIC APPROXIMATION

The SCHA introduced in Sec. III is a static theory: it cannot describe dynamical properties, like phonons observed experimentally.

In this section, we derive a new theory, the Time-Dependent Self-Consistent Harmonic Approximation (TD-SCHA), to describe correctly, without any empirical approximation, the response of the system to any (small or not) external time-dependent probe that interacts with ions.

We start from a pure state, i.e. the equilibrium solution at $T = 0$ K. At time $t = t_0$, we switch on a perturbation $V^{(1)}(\mathbf{R}, t)$ and the overall Hamiltonian becomes $\hat{H}_{td}(t)$ defined in Eq. (11).

We constrain the wave-packet to the most general time-dependent Gaussian:

$$\begin{aligned} \langle \mathbf{R} | \psi(t) \rangle = & \mathcal{N}^{\frac{1}{2}}(t) \exp \left(i \sum_a Q_a(t) [R_a - \mathcal{R}_a(t)] + \right. \\ & \left. - \sum_{ab} \left[\frac{\Theta_{ab}(t)}{4} - iC_{ab}(t) \right] [R_a - \mathcal{R}_a(t)] [R_b - \mathcal{R}_b(t)] \right). \end{aligned} \quad (40)$$

In Eq. (40) we have two new parameters with respect to the static solution of Eq. (38): \mathbf{Q} and \mathbf{C} . They add a complex phase to our wave-packet, and represent the momentum of the \mathbf{R} and Θ variables. The time-dependency of the \mathbf{Q} , \mathbf{R} , Θ , and \mathbf{C} parameters is found by minimizing the Dirac action along the time-evolution path:

$$A = \frac{1}{t - t_0} \int_{t_0}^t \langle \psi(t') | \hat{H}_{td}(t') - i\hbar \frac{d}{dt'} |\psi(t')\rangle dt' \quad (41)$$

The full equations of motion are derived in Appendix C.

It can be proved (as we show in Sec. IV A) that the same equations of motion are obtained if Eq. (40) is evolved by a self-consistent Schroedinger equation:

$$i\hbar \frac{d}{dt} |\psi(t)\rangle = \hat{\mathcal{H}}[\rho(t)] |\psi(t)\rangle \quad (42)$$

The self-consistent Hamiltonian that defines the time-evolution in the TD-SCHA is:

$$\begin{aligned} \hat{\mathcal{H}}[\rho(t)] = & \sum_{i=1}^N \frac{\hat{p}_i^2}{2m_i} + \sum_i \left\langle \frac{\partial V^{(\text{tot})}}{\partial R_i} \right\rangle_{\rho(t)} (\hat{R}_i - \mathcal{R}_i[\rho(t)]) + \\ & + \sum_{ij} \left\langle \frac{\partial^2 V^{(\text{tot})}}{\partial R_i \partial R_j} \right\rangle_{\rho(t)} (\hat{R}_i - \mathcal{R}_i[\rho(t)])(\hat{R}_j - \mathcal{R}_j[\rho(t)]), \end{aligned} \quad (43)$$

where

$$V^{(\text{tot})}(\mathbf{R}, t) = V(\mathbf{R}) + V^{(1)}(\mathbf{R}, t) \quad (44)$$

The $\hat{\mathcal{H}}[\rho(t)]$ Hamiltonian depends on the $\rho(\mathbf{R}, t)$ probability distribution of finding the ions in the \mathbf{R} configurations at time t :

$$\rho(\mathbf{R}, t) = |\langle \mathbf{R} | \psi(t) \rangle|^2 \quad (45)$$

The time-dependent self-consistent Hamiltonian (Eq. 43) has one extra linear term in $\hat{\mathbf{R}}$ compared to the static one (Eq. 31). This extra linear term is zero when the self-consistency of the equilibrium SCHA is achieved, as the average of the derivative of the BO potential (forces) on the equilibrium SCHA distribution is a necessary condition for the SCHA self-consistency[20].

The nuclear self-consistent Schroedinger equation (Eq. 42) has the same shape of other mean-field theories for electrons, as TD-HF or TD-DFT. It is worth to notice that Eq. (42) minimizes the action only if the wave-function is a Gaussian wave-packet. Notably, as we show in the next section, if $|\psi\rangle$ is Gaussian, Eq. (42) is a closed equation: a Gaussian wave-packet evolving in a general self-consistent harmonic Hamiltonian keeps its Gaussian form.

A. Dynamics of a mixture of states

Eq. (42) describes the dynamics just of pure states. The equilibrium solution of the SCHA is a pure state only if $T = 0$ K.

We can extend the nuclear time-dependent evolution of a mixture of states by replacing the time-dependent Schroedinger equation (Eq. 42) with the Liouville-von Neumann equation (Eq. 17), as usually done in TD-DFT[38] and TD-HF:

$$i\hbar \frac{d}{dt} \hat{\rho}(t) = \hat{\mathcal{H}}[\rho(t)] \hat{\rho}(t) - \hat{\rho}(t) \hat{\mathcal{H}}[\rho(t)] \quad (46)$$

$$\rho(\mathbf{R}, t) = \langle \mathbf{R} | \hat{\rho}(t) | \mathbf{R} \rangle \quad (47)$$

Thanks to Eq. (46), we can describe the dynamics also of mixtures of states, starting from the equilibrium SCHA solution at any temperature. Moreover, as Eq. (42), this is a closed equation for a Gaussian wave-packet (as we show in this section). We also prove in Sec. IV B and IV C that Eq. (46) correctly conserves both the energy and the entropy, as expected from the correct evolution of an isolated quantum system.

As we did for the pure state, we can get the explicit equation of motion for the Gaussian mixed states wave-packet.

$$\begin{aligned} \langle \mathbf{R}' | \hat{\rho}(t) | \mathbf{R} \rangle = & \mathcal{N}(t) \exp \left(i \sum_a Q_a(t) (R'_a - R_a) + \right. \\ & - \sum_{ab} \left[\frac{\Theta_{ab}(t)}{4} - iC_{ab}(t) \right] [R_a - \mathcal{R}_a(t)][R_b - \mathcal{R}_b(t)] + \\ & - \sum_{ab} \left[\frac{\Theta_{ab}(t)}{4} + iC_{ab}(t) \right] [R'_a - \mathcal{R}_a(t)][R'_b - \mathcal{R}_b(t)] \\ & \left. + \sum_{ab} A_{ab}(t) [R_a - \mathcal{R}_a(t)][R'_b - \mathcal{R}_b(t)] \right). \end{aligned} \quad (48)$$

With respect to the pure state introduced in Eq. (40), the time-dependent density matrix (Eq. 48) has one more parameter: the $\mathbf{A}(t)$ complex Hermitian matrix. \mathcal{R}_i is the average position of the i -th atom and coincides with the definition of Eq. (32). The variable Q_i is a linear phase modulation; multiplied by \hbar , it represents the momentum of the i -th atom. In a flat potential (where $\hat{\mathcal{H}}$ only contains the kinetic operator) the i -th atom average position drifts with constant velocity $v_i = \frac{\hbar Q_i(t)}{m_i}$. The \mathbf{Q} and \mathbf{R} variables are similar to those of a classical molecular dynamics. The $\mathbf{\Theta}$, \mathbf{A} matrices describe the quantum and thermal fluctuations. In particular, by looking at the diagonal elements of the density operator (the density distribution, Eq. 45), we get the covariance matrix of quantum-thermal fluctuations:

$$\frac{\rho(\mathbf{R}, t)}{\mathcal{N}(t)} = \exp \left\{ - \sum_{ab} \frac{1}{2} \Upsilon_{ab}(t) [R_a - \mathcal{R}_a(t)][R_b - \mathcal{R}_b(t)] \right\} \quad (49)$$

$$\Upsilon_{ab}(t) = \Theta_{ab}(t) - 2\text{Re}A_{ab}(t), \quad (50)$$

where Re and Im identify the real and imaginary part. $\mathbf{\Upsilon}$ is the inverse the covariance matrix of the Gaussian distribution:

$$(\mathbf{\Upsilon}^{-1})_{ab}(t) = \langle [R_a - \mathcal{R}_a(t)][R_b - \mathcal{R}_b(t)] \rangle_{\rho(t)}. \quad (51)$$

We give intuitive picture on the physical meaning of the parameters. The $\mathbf{\Theta}$ matrix encodes pure quantum fluctuations and $\text{Re}\mathbf{A}$ the thermal ones: if $\mathbf{A} = 0$, Eq. (48) is a pure state and we recover Eq. (40). \mathbf{C} is a quadratic phase and represents the *chirp* along the quantum fluctuations. Its role is very similar to the chirp in signal

propagation, and represent a gradient in the speed of particles in different positions in the wave-packet, as discussed in ref.[36]. On the other side, the $\text{Im}\mathbf{A}$ plays the role of the momentum for the thermal fluctuations. It is nonzero only when there are more than 1 degree of freedom ($\text{Im}\mathbf{A}$ is anti symmetric) and if the system is not in a pure quantum state.

The $\mathcal{N}(t)$ is the density matrix normalization:

$$\mathcal{N}(t) = \sqrt{\frac{\det \mathbf{\Upsilon}(t)}{(2\pi)^{3N}}} \quad (52)$$

Eq. (48) can be substituted in Eq. (46) to get the dynamical equations for the parameters. For a convenient choice of the notation, it is better to express the parameters rescaled by the masses. We indicate with a $\tilde{\cdot}$ the rescaled matrices and vectors as:

$$\tilde{C}_{ab}(t) = \frac{C_{ab}(t)}{\sqrt{m_a m_b}}, \quad \tilde{A}(t) = \frac{A_{ab}(t)}{\sqrt{m_a m_b}}, \quad (53a)$$

$$\tilde{\Upsilon}_{ab}(t) = \frac{\Upsilon_{ab}(t)}{\sqrt{m_a m_b}}, \quad \tilde{\Theta}(t) = \frac{\Theta_{ab}(t)}{\sqrt{m_a m_b}}, \quad (53b)$$

$$\tilde{\mathcal{R}}_a(t) = \sqrt{m_a} \mathcal{R}_a(t) \quad \tilde{Q}_a(t) = \frac{Q_a(t)}{\sqrt{m_a}} \quad (53c)$$

The final equation of motion are:

$$\frac{d\tilde{\mathcal{R}}}{dt} = \hbar \tilde{\mathcal{Q}} \quad \frac{dQ_a}{dt} = \frac{\left\langle f_a^{(\text{tot})} \right\rangle_{\rho(t)}}{\hbar} \quad (54a)$$

$$\frac{d\tilde{\Upsilon}}{dt} = \hbar \left[\tilde{\Upsilon}(2\tilde{\mathcal{C}} + \text{Im}\tilde{\mathbf{A}}) + (2\tilde{\mathcal{C}} - \text{Im}\tilde{\mathbf{A}})\tilde{\Upsilon} \right] \quad (54b)$$

$$\frac{d\text{Re}\tilde{\mathbf{A}}}{dt} = \frac{\hbar}{2} \left(4\tilde{\mathcal{C}}\text{Re}\tilde{\mathbf{A}} + 4\text{Re}\tilde{\mathbf{A}}\tilde{\mathcal{C}} - \tilde{\Theta}\text{Im}\tilde{\mathbf{A}} + \text{Im}\tilde{\mathbf{A}}\tilde{\Theta} \right) \quad (54c)$$

$$\frac{d\text{Im}\tilde{\mathbf{A}}}{dt} = \frac{\hbar}{2} \left(4\tilde{\mathcal{C}}\text{Im}\tilde{\mathbf{A}} + 4\text{Im}\tilde{\mathbf{A}}\tilde{\mathcal{C}} + \tilde{\Theta}\text{Re}\tilde{\mathbf{A}} - \text{Re}\tilde{\mathbf{A}}\tilde{\Theta} \right) \quad (54d)$$

$$\frac{d\tilde{\mathcal{C}}}{dt} = \frac{1}{2\hbar} \left\langle \frac{\partial^2 V^{(\text{tot})}}{\partial \tilde{\mathcal{R}} \partial \tilde{\mathcal{R}}} \right\rangle_{\rho(t)} + \frac{\hbar}{2} \left[4\tilde{\mathcal{C}}^2 - \frac{1}{4}\tilde{\Theta}^2 + \text{Re}(\tilde{\mathbf{A}}\tilde{\mathbf{A}}^\dagger) \right]. \quad (54e)$$

Here, we dropped the explicit time-dependency of these variables for brevity: they represent the $\hat{\rho}(t)$ density matrix and not the equilibrium one.

The products of matrices is the standard rows-by-columns. The symbol \cdot^\dagger after a matrix indicates the Hermitian conjugate, and $\left\langle f_a^{(\text{tot})} \right\rangle_{\rho(t)}$ is the average of BO forces on the a -th atom:

$$f_a^{(\text{tot})}(\mathbf{R}, t) = -\frac{\partial V^{(\text{tot})}(\mathbf{R}, t)}{\partial R_a}, \quad (55)$$

while the derivative with respect the $\tilde{\mathbf{R}}$ variable indicates the mass rescale:

$$\frac{\partial^2 V^{(\text{tot})}}{\partial \tilde{R}_a \partial \tilde{R}_b} = \frac{1}{\sqrt{m_a m_b}} \frac{\partial^2 V^{(\text{tot})}}{\partial R_a \partial R_b} \quad (56)$$

Eq. (54a) are the semi-classical equation of motion: they resemble the Newton dynamics, but the force is averaged on the ionic probability distribution. The dynamics preserves $\mathbf{\Upsilon}$, $\text{Re}\mathbf{A}$ and \mathbf{C} symmetric and $\text{Im}\mathbf{A}$ antisymmetric. The details of the derivation of Eq. (54) is reported in appendix A. These equations reduce to the evolution of the pure state that minimizes the Dirac action, if we set $\mathbf{A} = 0$ (see Appendix C).

Notably, substituting the Gaussian wave-packet Eq. (48) into TD-SCHA equation of motion Eq. (46), we get an extra condition on the time-dependency of the $\mathcal{N}(t)$ parameter.

$$\frac{d\mathcal{N}(t)}{dt} = 2\hbar \mathcal{N}(t) \text{Tr} \left[\tilde{\mathcal{C}}(t) \right] \quad (57)$$

This condition is automatically satisfied by Eq. (54) if we substitute Eq. (52) into Eq. (57). Since Eq. (57) does not depend explicitly on $\tilde{\mathbf{R}}$ operators and it is automatically satisfied by the equation of motions, the Gaussian wave-packet evolution is closed with the TD-SCHA equation (Eq. 46). In fact, the application of the Liouville operator on a Gaussian density matrix:

$$\hat{\mathcal{H}}[\rho(t)]\hat{\rho}(t) - \hat{\rho}(t)\hat{\mathcal{H}}[\rho(t)] \quad (58)$$

with $\hat{\mathcal{H}}[\rho(t)]$ Harmonic, generates a polynomial of the same order than the time derivative for the density matrix $i\hbar \frac{d}{dt}\hat{\rho}(t)$. This means that, if the density matrix is Gaussian at $t = t_0$ (equilibrium), it remains Gaussian for the whole time-evolution, as Eq. (58) does not provide any term shifting $i\hbar \frac{d}{dt}\hat{\rho}(t)$ from a Gaussian.

Very interestingly, the full dynamics is just obtained by standard rows-by-columns product of small matrices (they are $3N \times 3N$, with N the number of atoms in the simulation cell). The only two quantities depending from the physical system (the real BO Hamiltonian \hat{H}) are

$$\left\langle \mathbf{f}^{(\text{tot})} \right\rangle_{\rho(t)} \quad \left\langle \frac{\partial^2 V^{(\text{tot})}}{\partial \tilde{\mathcal{R}} \partial \tilde{\mathcal{R}}} \right\rangle_{\rho(t)}. \quad (59)$$

The calculation of these averages is also needed for a static SCHA calculation and can be computed stochastically as described in [20, 33].

In particular, an efficient method to compute the average of the second derivatives of the BO potential is obtained exploiting the methodology introduced in ref.[33], that takes advantage of integration by parts:

$$\left\langle \frac{\partial^2 V^{(\text{tot})}}{\partial R_a \partial R_b} \right\rangle_{\rho(t)} = \sum_p \Upsilon_{ap} \langle (R_p - \mathcal{R}_p) f_a \rangle_{\rho(t)} \quad (60)$$

In this way, only *ab initio* forces are required. Therefore, the implementation of the TD-SCHA equations has the same overall computational cost as a static calculation.

Derivation of Gaussian wave-packet dynamics is discussed in literature following different approaches[39–44]. For example, refs.[42–44] project the real dynamics into the manifold of Gaussian states, while refs.[39–41] exploit the Wentzel-Kramers-Brillouin (WKB) method to derive semiclassical equations expanding the Schroedinger equation linearly around $\hbar = 0$.

B. Energy conservation

Here we show that the TD-SCHA equation of motion (Eq. 46) satisfies energy conservation when we switch off the time-dependent perturbation, as we expect from a closed system. This is not trivial, as, for example, does not happen in other methods for finite temperature dynamics of ions, as the finite temperature multi-configurational time-dependent Hartree method[45].

The total energy is computed as the average of the BO Hamiltonian on the time-dependent density matrix:

$$E(t) = \langle \hat{H} \rangle_{\hat{\rho}(t)} = \text{Tr} [\hat{\rho}(t) \hat{H}]. \quad (61)$$

By dividing into kinetic and potential contribution, the total energy is:

$$E(t) = \langle \hat{K} \rangle_{\hat{\rho}(t)} + \langle \hat{V} \rangle_{\hat{\rho}(t)} \quad (62)$$

The kinetic energy can be evaluated analytically directly from the density matrix of Eq. (48):

$$\begin{aligned} \langle \hat{K} \rangle_{\hat{\rho}(t)} &= \frac{\hbar^2}{2} \left[\text{Tr} \left(4\tilde{C}(\tilde{\mathbf{Y}})^{-1}\tilde{C} - \text{Im}\tilde{\mathbf{A}}(\tilde{\mathbf{Y}})^{-1}\text{Im}\tilde{\mathbf{A}} \right) + \right. \\ &\quad \left. - 2 \text{Tr} \left(\tilde{C}(\tilde{\mathbf{Y}})^{-1}\text{Im}\tilde{\mathbf{A}} \right) + \right. \\ &\quad \left. + \frac{1}{4} \text{Tr} \tilde{\mathbf{Y}} + \text{Tr} \tilde{\mathbf{A}} \right] + \sum_{i=1}^n \frac{\hbar^2 Q_i^2}{2m_i} \end{aligned} \quad (63)$$

Also here, we dropped the exploit time dependency of the parameters that represent $\hat{\rho}(t)$.

The last term is the kinetic energy of classical particles, the rest is the contribution of the quantum and thermal fluctuations to the kinetic energy.

To prove that $\frac{d}{dt} E(t) = 0$, we compute the derivative

of the average kinetic energy:

$$\begin{aligned} \frac{d \langle \hat{K} \rangle_{\hat{\rho}(t)}}{dt} &= \frac{\hbar^2}{2} \left[\frac{1}{4} \text{Tr} \frac{d\tilde{\mathbf{Y}}}{dt} + \sum_{i=1}^{3n} \frac{Q_i}{m_i} \frac{dQ_i}{dt} + \right. \\ &\quad \left. + 2 \text{Tr} \left(4\tilde{C}(\tilde{\mathbf{Y}})^{-1} \frac{d\tilde{C}}{dt} - \tilde{C}(\tilde{\mathbf{Y}})^{-1} \frac{d\text{Im}\tilde{\mathbf{A}}}{dt} \right) + \right. \\ &\quad \left. + \text{Tr} \frac{d\text{Re}\tilde{\mathbf{A}}}{dt} - 2 \text{Tr} \left(\frac{d\tilde{C}}{dt} (\tilde{\mathbf{Y}})^{-1} \text{Im}\tilde{\mathbf{A}} \right) + \right. \\ &\quad \left. - 2 \text{Tr} \left(\text{Im}\tilde{\mathbf{A}}(\tilde{\mathbf{Y}})^{-1} \text{Im}\tilde{\mathbf{A}} + \tilde{C} \frac{d(\tilde{\mathbf{Y}})^{-1}}{dt} \text{Im}\tilde{\mathbf{A}} \right) + \right. \\ &\quad \left. + \text{Tr} \left(4\tilde{C} \frac{d(\tilde{\mathbf{Y}})^{-1}}{dt} \tilde{C} - \text{Im}\tilde{\mathbf{A}} \frac{d(\tilde{\mathbf{Y}})^{-1}}{dt} \text{Im}\tilde{\mathbf{A}} \right) \right]. \end{aligned} \quad (64)$$

By substituting the equation of motion (Eq. 54) we get the final derivative of the kinetic energy:

$$\begin{aligned} \frac{d \langle \hat{K} \rangle_{\hat{\rho}(t)}}{dt} &= \sum_i \frac{\hbar Q_i \langle f_i \rangle_{\rho}}{m_i} + \\ &\quad + 2\hbar \text{Tr} \left[\left\langle \frac{\partial^2 V}{\partial \tilde{\mathbf{R}} \partial \tilde{\mathbf{R}}} \right\rangle_{\rho(t)} (\tilde{\mathbf{Y}})^{-1} \tilde{C} \right] + \\ &\quad - \hbar \text{Tr} \left[\left\langle \frac{\partial^2 V}{\partial \tilde{\mathbf{R}} \partial \tilde{\mathbf{R}}} \right\rangle_{\rho(t)} (\tilde{\mathbf{Y}})^{-1} \text{Im}\tilde{\mathbf{A}} \right] \end{aligned} \quad (65)$$

In the same way, we can compute the derivative of the average potential:

$$\begin{aligned} \frac{d \langle \hat{V} \rangle_{\hat{\rho}(t)}}{dt} &= - \sum_{ab} \langle (R_a - \mathcal{R}_a)(R_b - \mathcal{R}_b)V \rangle_{\rho(t)} \frac{1}{2} \frac{d\Upsilon_{ab}}{dt} + \\ &\quad + \sum_{ab} \langle (R_a - \mathcal{R}_a)V \rangle_{\rho(t)} \Upsilon_{ab} \frac{d\mathcal{R}_b}{dt} + \langle V \rangle_{\rho(t)} \frac{1}{\mathcal{N}} \frac{d\mathcal{N}}{dt} \end{aligned} \quad (66)$$

By substituting the equation of motion and integrating by parts the averages, it is possible to show that (see appendix B):

$$\frac{d}{dt} \langle V \rangle_{\hat{\rho}(t)} = - \frac{d}{dt} \langle K \rangle_{\hat{\rho}(t)} \quad (67)$$

C. Entropy conservation

The equations of motion (54) conserve also the entropy. This is a general feature of any Hamiltonian dynamics, and the TD-SCHA makes no exception, even if the Hamiltonian depends self-consistently from the density matrix. The entropy defined on the many-body density matrix is:

$$S[\hat{\rho}(t)] = -k_b \text{Tr} [\hat{\rho}(t) \log \hat{\rho}(t)] \quad (68)$$

for simplicity, we drop the explicit t dependence of $\hat{\rho}(t)$.

$$B(\hat{\rho}) = \hat{\rho} \log \hat{\rho} \quad (69)$$

$$\frac{dS}{dt} = -k_b \text{Tr} \left[\frac{d\hat{\rho}}{dt} \frac{dB(\hat{\rho})}{d\hat{\rho}} \right] \quad (70)$$

$$\frac{dS}{dt} = \frac{ik_b}{\hbar} \left[\text{Tr} \left(\hat{\mathcal{H}}[\rho] \hat{\rho} \frac{dB(\hat{\rho})}{d\hat{\rho}} \right) - \text{Tr} \left(\hat{\rho} \hat{\mathcal{H}}[\rho] \frac{dB(\hat{\rho})}{d\hat{\rho}} \right) \right] \quad (71)$$

By exploiting the cyclic permutation of the trace and the commutation between $dB(\hat{\rho})/d\hat{\rho}$ and $\hat{\rho}$, Eq. (71) is zero.

The entropy conservation derives from the unitary time evolution: we are evolving a closed quantum system and there is no de-coherence in the dynamics. In other words, the dynamics is reversible, as if we change the initial sign of $\text{Im}\mathbf{A}$, \mathbf{C} , and \mathbf{Q} , the evolution proceeds backward in time.

D. Steady-state solutions

Thanks to Eq. (46), the steady state solution of the dynamical equations occurs when the density matrix $\hat{\rho}$ commutes with the self-consistent Hamiltonian $\hat{\mathcal{H}}[\rho]$. This means that there is a basis that simultaneously diagonalizes both the Hamiltonian $\hat{\mathcal{H}}[\rho]$ and the density matrix. This condition can also be inferred from the equation of motions Eq. (54), imposing that the time-derivatives are zero. In this case we have:

$$C_{ab} = 0 \quad \text{Im}A_{ab} = 0 \quad Q_a = 0 \quad (72)$$

This is quite intuitive, as discussed in Sec. IV A, these variables are related to the instantaneous average momentum and chirp.

Substituting Eq. (72) inside Eq. (54) we get the following conditions:

$$\langle f_a \rangle_\rho = 0 \quad (73a)$$

$$\frac{1}{2\hbar} \left\langle \frac{\partial^2 V}{\partial \tilde{R}_a \partial \tilde{R}_b} \right\rangle_\rho = \frac{\hbar}{2} \left(\frac{1}{4} \tilde{\Theta}_{ab}^2 - \text{Re} \tilde{A}_{ab}^2 \right) \quad (73b)$$

Eq. (73a) is a necessary condition for the equilibrium SCHA: the average of the BO forces is the gradient of the SCHA free energy versus the centroids positions \mathcal{R} [20]. Moreover, from Eq. (54d) we have that $\tilde{\Theta}$ and $\text{Re}\tilde{\mathbf{A}}$ commute in the static solution, from which also $\tilde{\mathbf{Y}}$ and $\text{Re}\tilde{\mathbf{A}}$ commute (that is a direct consequence of the commutation between $\hat{\rho}$ and $\hat{\mathcal{H}}[\rho]$). Since it is better to express our quantity as a function of the total dispersion $\tilde{\mathbf{Y}}$ (Eq. 50) we have:

$$\frac{\tilde{\mathbf{Y}}^2}{4} + \tilde{\mathbf{Y}} \text{Re}\tilde{\mathbf{A}} = \frac{1}{\hbar^2} \left\langle \frac{\partial^2 V}{\partial \tilde{\mathbf{R}} \partial \tilde{\mathbf{R}}} \right\rangle_\rho. \quad (74)$$

If we express Eq. (74) in the basis that diagonalizes both $\tilde{\mathbf{Y}}$ and $\text{Re}\tilde{\mathbf{A}}$, the same basis must diagonalize also $\left\langle \frac{\partial^2 V}{\partial \tilde{\mathbf{R}} \partial \tilde{\mathbf{R}}} \right\rangle$. Let us define \mathbf{e}_μ the eigenvector of $\left\langle \frac{\partial^2 V}{\partial \tilde{\mathbf{R}} \partial \tilde{\mathbf{R}}} \right\rangle$, $\tilde{\mathbf{Y}}$ and $\text{Re}\tilde{\mathbf{A}}$ and ω_μ^2 , $\tilde{\mathbf{Y}}_\mu$ and $\text{Re}\tilde{A}_\mu$ the corresponding eigenvalues:

$$\sum_b \left\langle \frac{\partial^2 V}{\partial \tilde{R}_a \partial \tilde{R}_b} \right\rangle_\rho e_\mu^b = \omega_\mu^2 e_\mu^a, \quad (75)$$

Eq. (74) becomes:

$$\frac{\tilde{\mathbf{Y}}_\mu^2}{4} + \tilde{\mathbf{Y}}_\mu \text{Re}\tilde{A}_\mu = \frac{\omega_\mu^2}{\hbar^2}. \quad (76)$$

Without loss of generality, if we change variable introducing a new parameter n_μ and define:

$$\tilde{\mathbf{Y}}_\mu = \frac{2\omega_\mu}{\hbar(2n_\mu + 1)}, \quad (77a)$$

from Eq. (76), we get:

$$\text{Re}\tilde{A}_\mu = \frac{2\omega_\mu n_\mu (n_\mu + 1)}{\hbar(2n_\mu + 1)}. \quad (77b)$$

In these equations, n_μ is a free parameter for each frequency: the TD-SCHA equations are stationary for any choice of n_μ . In particular, we can write n_μ as the Bose-Einstein occupation number with a temperature that depends on μ :

$$n_\mu = \frac{1}{e^{\beta_\mu \hbar \omega_\mu} - 1} \quad (78)$$

The stationary density matrix identified by Eq. (77) and (72) is the product of equilibrium densities matrices of harmonic oscillators of frequencies ω_μ and temperatures β_μ .

If we fix all $\beta_\mu = \beta$, we recover the standard finite temperature SCHA solution (Eq. 34, 35, and 36), with β the Boltzman factor[20].

$$\beta = \frac{1}{k_b T} \quad (79)$$

However, in principle, also solutions with different temperatures in different modes are a stationary point of the TD-SCHA equations. This is true also for the real dynamics: a perfectly harmonic oscillator is stationary even if each normal mode is populated with a different temperature (since there is no coupling and heat transfer between modes). In general, any mixture of eigenstates of the time-independent Hamiltonian is a stationary density matrix, even if the population is not the equilibrium one.

E. Equilibrium and thermodynamics

In the previous section, we showed that infinite steady states exist. The steady-state solutions are equal to

the product of equilibrium noninteracting quantum Harmonic oscillators, where each normal mode has a thermal occupation number n_μ with a temperature that depends on the mode. This is not, indeed, the equilibrium solution of the SCHA, which requires all normal modes populated by the same temperature. However, not all steady-states are equilibrium solutions: if we prepare the system in a mixture of state with eigenstates of the Hamiltonian, the exact time-dependent density matrix is stationary even if the occupation probabilities are not the Boltzmann factors.

The system reaches equilibrium if we introduce an interaction with an external bath (or a dephasing mechanism). In an isolated system, the equilibrium solution is the one that maximizes the entropy among all possible steady states at fixed energy. Maximizing the entropy fixing the energy is equivalent in minimizing the Helmholtz free energy. This is the starting point for the static SCHA. In Appendix D we prove that this condition correspond imposing an uniform β on each mode.

Therefore, we recover the SCHA as the static solution of the TD-SCHA that maximizes the entropy. It is worth noting that the TD-SCHA will not spontaneously evolve into the SCHA solution, unless the equations are modified to account for the coupling with a reservoir that provides a mechanism for quantum decoherence[46], allowing the entropy of the subsystem to increase. The extension of TD-SCHA to describe the dynamics of an open quantum system is beyond the scope of the current work.

V. LINEAR RESPONSE THEORY

Almost all experimental data are collected by probing the response of the system to a time-dependent external perturbation. This perturbation could be either electromagnetic radiation (static electric fields, IR, optical light, X-ray) or particles like electrons and neutrons. If the perturbation does not provide enough energy to heat the system, we are in the linear regime[47, 48]. Typical experiments that involve interactions with ionic degrees of freedom are Raman and IR spectroscopy, neutron, and X-Ray scattering. In this section, we present the dynamical linear response of the TD-SCHA equations on top of the static SCHA solution. This enables the computation of the response function for any experiment probing the nuclear motion fully *ab initio* and considering both quantum/thermal fluctuations and anharmonicity beyond perturbation theory.

Since the probe heating of the sample (Joule effect) enter at higher orders in the perturbation, the linear response does not depend on the coupling with the thermal bath[47, 48]. Therefore, even if the TD-SCHA introduced in this work describes closed quantum systems, the results we derive in this section are general, and apply also to systems coupled with a bath.

We start from the thermodynamic equilibrium (the

SCHA solution) and then we add “small” time-dependent external potential $V^{(1)}(\mathbf{R}, t)$ that acts on the nuclei for $t \geq t_0$. We study how the parameters of our density matrix changes under the effect of the external perturbation:

$$\mathcal{R}_i(t) = \mathcal{R}_i + \mathcal{R}_i^{(1)}(t) \quad Q_i(t) = Q_i^{(1)}(t) \quad (80a)$$

$$\Upsilon_{ab}(t) = \Upsilon_{ab} + \Upsilon_{ab}^{(1)}(t) \quad C_{ab}(t) = C_{ab}^{(1)}(t) \quad (80b)$$

$$A_{ab}(t) = A_{ab} + A_{ab}^{(1)}(t) \quad (80c)$$

$$V^{(\text{tot})}(\mathbf{R}, t) = V(\mathbf{R}) + V^{(1)}(\mathbf{R}, t) \quad (80d)$$

where the $^{(1)}$ indicates the small perturbation around the equilibrium SCHA solution. We restrict to cases in which \hat{A} and \hat{B} depend only on nuclear positions. For this reason, the only dynamics we are interested on is the diagonal elements of the density matrix, i.e the ionic probability distribution $\rho(\mathbf{R}, t)$. This depends only on $\Upsilon(t)$ and $\mathcal{R}(t)$. Substituting Eq. (80) into the equations of motion (Eq. 54) and keeping only linear terms in the perturbation, we get a system of linear differential equations. Since we are interested in $\Upsilon(t)$ and $\mathcal{R}(t)$, the minimal linear system that describe their dynamics is the following:

$$\frac{d^2 \tilde{\Upsilon}^{(1)}}{dt^2} = \bar{\mathbf{X}} \tilde{\Upsilon}^{(1)} + \bar{\mathbf{Y}} \text{Re} \tilde{\mathbf{A}}^{(1)} + \bar{\mathbf{Z}} \tilde{\mathcal{R}}^{(1)} + \mathbf{f}_{\Upsilon}^{(1)}, \quad (81a)$$

$$\frac{d^2 \text{Re} \tilde{\mathbf{A}}^{(1)}}{dt^2} = \bar{\mathbf{X}}' \tilde{\Upsilon}^{(1)} + \bar{\mathbf{Y}}' \text{Re} \tilde{\mathbf{A}}^{(1)} + \bar{\mathbf{Z}}' \tilde{\mathcal{R}}^{(1)} + \mathbf{f}_{\text{ReA}}^{(1)}, \quad (81b)$$

$$\frac{d^2 \tilde{\mathcal{R}}^{(1)}}{dt^2} = \bar{\mathbf{X}}'' \tilde{\Upsilon}^{(1)} + \bar{\mathbf{Z}}'' \tilde{\mathcal{R}}^{(1)} + \mathbf{f}_{\mathcal{R}}^{(1)}. \quad (81c)$$

Even if $\text{Re} \tilde{\mathbf{A}}(t)$ does not affect the average of the observable directly, we need to keep it, as $\Upsilon(t)$ depends explicitly on its dynamics. In Eq. (81), the bar $\bar{\cdot}$ over a symbol indicates a tensor. $\bar{\mathbf{X}}$, $\bar{\mathbf{Y}}$, $\bar{\mathbf{X}}'$, and $\bar{\mathbf{Y}}'$ are 4-rank tensors, $\bar{\mathbf{Z}}$, $\bar{\mathbf{Z}}'$, and $\bar{\mathbf{X}}''$ are 3-rank tensors, while $\bar{\mathbf{Z}}''$ is a 2-rank tensor. We recall that $\tilde{\Upsilon}^{(1)}$ and $\text{Re} \tilde{\mathbf{A}}^{(1)}$ are 2-rank tensor, as well as $\mathbf{f}_{\Upsilon}^{(1)}$ and $\mathbf{f}_{\text{ReA}}^{(1)}$, while $\tilde{\mathcal{R}}^{(1)}$ and $\mathbf{f}_{\mathcal{R}}^{(1)}$ are vectors (1-rank).

The product between tensors is the defined by the operator on the left. 4-rank tensors $\bar{\mathbf{X}}$, $\bar{\mathbf{Y}}$, $\bar{\mathbf{X}}'$, and $\bar{\mathbf{Y}}'$ are contracted on the last two indices:

$$\left(\bar{\mathbf{X}} \tilde{\Upsilon}^{(1)} \right)_{ab} = \sum_{cd} \bar{X}_{abcd} \tilde{\Upsilon}_{cd}^{(1)}, \quad (82a)$$

also 3-rank tensors $\bar{\mathbf{Z}}$, $\bar{\mathbf{Z}}'$ are contracted on the last two indices:

$$\left(\bar{\mathbf{Z}} \tilde{\Upsilon}^{(1)} \right)_a = \sum_{bc} \bar{Z}_{abc} \tilde{\Upsilon}_{bc}^{(1)}. \quad (82b)$$

The 3-rank tensor $\bar{\mathbf{X}}''$ is contracted only on the last index:

$$\left(\bar{\mathbf{X}}''\tilde{\mathbf{R}}^{(1)}\right)_{ab} = \sum_{bc} \bar{X}''_{abc} \tilde{\mathcal{R}}_c^{(1)}. \quad (82c)$$

The 2-rank tensor $\bar{\mathbf{Z}}''$ is contracted on the last index, as the standard matrix rows-by-columns product.

The details on the derivation of Eq. (81) are reported in Appendix E, and the explicit expression of the tensors in Appendix F.

It is convenient to express Eq. (81) in matricial form, as:

$$\frac{d^2}{dt^2} \begin{pmatrix} \tilde{\mathbf{Y}}^{(1)} \\ \text{Re}\tilde{\mathbf{A}}^{(1)} \\ \tilde{\mathbf{R}}^{(1)} \end{pmatrix} = \begin{pmatrix} \bar{\mathbf{X}} & \bar{\mathbf{Y}} & \bar{\mathbf{Z}} \\ \bar{\mathbf{X}}' & \bar{\mathbf{Y}}' & \bar{\mathbf{Z}}' \\ \bar{\mathbf{X}}'' & 0 & \bar{\mathbf{Z}}'' \end{pmatrix} \begin{pmatrix} \tilde{\mathbf{Y}}^{(1)} \\ \text{Re}\tilde{\mathbf{A}}^{(1)} \\ \tilde{\mathbf{R}}^{(1)} \end{pmatrix} + \begin{pmatrix} \mathbf{f}_{\tilde{\mathbf{Y}}}^{(1)} \\ \mathbf{f}_{\text{Re}\tilde{\mathbf{A}}}^{(1)} \\ \mathbf{f}_{\tilde{\mathbf{R}}}^{(1)} \end{pmatrix} \quad (83)$$

The tensors introduced in Eq. (81) account for the free time-evolution of the system with the full anharmonic interaction: they are defined by the static unperturbed Hamiltonian $\hat{\mathcal{H}}[\rho]$. In particular, they depend on phonon scattering vertexes: the 4-phonon scattering tensor $\bar{\mathbf{D}}^{(4)}$ and 3-phonon scattering tensor $\bar{\mathbf{D}}^{(3)}$, and the free evolution $\bar{\mathbf{D}}^{(2)}$

$$\bar{D}_{abcd}^{(4)} = \left\langle \frac{\partial^4 V}{\partial \tilde{R}_a \partial \tilde{R}_b \partial \tilde{R}_c \partial \tilde{R}_d} \right\rangle_{\rho}, \quad (84)$$

$$\bar{D}_{abc}^{(3)} = \left\langle \frac{\partial^3 V}{\partial \tilde{R}_a \partial \tilde{R}_b \partial \tilde{R}_c} \right\rangle_{\rho}, \quad (85)$$

$$\bar{D}_{ab}^{(2)} = \left\langle \frac{\partial^2 V}{\partial \tilde{R}_a \partial \tilde{R}_b} \right\rangle_{\rho} \quad (86)$$

where the averages are computed over the unperturbed ionic probability distribution $\rho(\mathbf{R})$. Due to the Gaussian constrain on the density matrix, the TD-SCHA does not account directly for higher-order phonon scattering processes. However, $\bar{\mathbf{D}}^{(3)}$, $\bar{\mathbf{D}}^{(4)}$, and $\bar{\mathbf{D}}^{(2)}$ depend “self-consistently” on higher-order anharmonicities, as they are averaged on the equilibrium distribution. In fact, they are temperature dependent.

In particular, $\bar{\mathbf{X}}$ and $\bar{\mathbf{X}}'$ depend on $\bar{\mathbf{D}}^{(4)}$, while $\bar{\mathbf{Z}}$, $\bar{\mathbf{Z}}'$ and $\bar{\mathbf{X}}''$ depend on $\bar{\mathbf{D}}^{(3)}$. The $\bar{\mathbf{X}}$, $\bar{\mathbf{X}}'$, $\bar{\mathbf{Y}}$, $\bar{\mathbf{Y}}'$ and $\bar{\mathbf{Z}}''$ contain terms of the free evolution, that are non zero even if the system is a perfect harmonic crystal. TABLE I summarizes these dependencies.

The $\mathbf{f}_{\tilde{\mathbf{Y}}}^{(1)}$, $\mathbf{f}_{\text{Re}\tilde{\mathbf{A}}}^{(1)}$, and $\mathbf{f}_{\tilde{\mathbf{R}}}^{(1)}$ represent how the bare perturbation $V^{(1)}(\mathbf{R}, t)$ enters in the equation of the motion. In the polarization basis (i.e. the basis that diagonalizes $\tilde{\mathbf{Y}}^{(0)}$ and $\text{Re}\tilde{\mathbf{A}}^{(0)}$ introduced in Sec. IV D), they are:

$$f_{\tilde{\mathbf{Y}}}^{(1)}{}_{\mu\nu} = \frac{1}{\hbar} \left(\frac{2\omega_{\mu}}{2n_{\mu}+1} + \frac{2\omega_{\nu}}{2n_{\nu}+1} \right) \left\langle \frac{\partial^2 V^{(1)}}{\partial \tilde{R}_{\mu} \partial \tilde{R}_{\nu}} \right\rangle_{\rho}, \quad (87a)$$

	$\bar{\mathbf{D}}^{(2)}$	$\bar{\mathbf{D}}^{(3)}$	$\bar{\mathbf{D}}^{(4)}$
$\bar{\mathbf{X}}$	o		o
$\bar{\mathbf{Y}}$	o		
$\bar{\mathbf{Z}}$		o	
$\bar{\mathbf{X}}'$	o		o
$\bar{\mathbf{Y}}'$	o		
$\bar{\mathbf{Z}}'$		o	
$\bar{\mathbf{X}}''$		o	
$\bar{\mathbf{Z}}''$	o		

TABLE I. Dependency of the coefficients of the linear response system (Eq. 81) on the free evolution $\bar{\mathbf{D}}^{(2)}$, on anharmonic coupling $\bar{\mathbf{D}}^{(3)}$ (Eq. 85) and $\bar{\mathbf{D}}^{(4)}$ (Eq. 84). A o in the grid indicates that the tensor on the first column depends on the corresponding term in the first row. This table helps to see which terms can be set to zero if we neglect $\bar{\mathbf{D}}^{(3)}$ or $\bar{\mathbf{D}}^{(4)}$, and to visualize how anharmonicity couples different degrees of freedom

$$f_{\text{Re}\tilde{\mathbf{A}}}^{(1)}{}_{\mu\nu} = \frac{1}{\hbar} \left(\frac{2(n_{\mu}+1)n_{\mu}\omega_{\mu}}{2n_{\mu}+1} + \frac{2(n_{\nu}+1)n_{\nu}\omega_{\nu}}{2n_{\nu}+1} \right) \left\langle \frac{\partial^2 V^{(1)}}{\partial \tilde{R}_{\mu} \partial \tilde{R}_{\nu}} \right\rangle_{\rho} \quad (87b)$$

$$f_{\tilde{\mathbf{R}}}^{(1)}{}_{\mu} = - \left\langle \frac{\partial V^{(1)}}{\partial \tilde{R}_{\mu}} \right\rangle_{\rho} \quad (87c)$$

If we rewrite the perturbation in frequency domain, we can define the Green function:

$$\mathbf{G}(\omega) = - \begin{pmatrix} \bar{\mathbf{X}} + \omega^2 & \bar{\mathbf{Y}} & \bar{\mathbf{Z}} \\ \bar{\mathbf{X}}' & \bar{\mathbf{Y}}' + \omega^2 & \bar{\mathbf{Z}}' \\ \bar{\mathbf{X}}'' & 0 & \bar{\mathbf{Z}}'' + \omega^2 \end{pmatrix}^{-1} \quad (88)$$

Given any possible time-dependent perturbation one nuclei $V^{(1)}(\mathbf{R}, \omega)$ we can compute the perturbation vector $\mathbf{f}_{\tilde{\mathbf{Y}}|\text{Re}\tilde{\mathbf{A}}|\tilde{\mathbf{R}}}^{(1)}$ and obtain the response as:

$$\begin{pmatrix} \tilde{\mathbf{Y}}^{(1)}(\omega) \\ \text{Re}\tilde{\mathbf{A}}^{(1)}(\omega) \\ \tilde{\mathbf{R}}^{(1)}(\omega) \end{pmatrix} = \mathbf{G}(\omega) \begin{pmatrix} \mathbf{f}_{\tilde{\mathbf{Y}}}^{(1)}(\omega) \\ \mathbf{f}_{\text{Re}\tilde{\mathbf{A}}}^{(1)}(\omega) \\ \mathbf{f}_{\tilde{\mathbf{R}}}^{(1)}(\omega) \end{pmatrix}. \quad (89)$$

A. The general response function

In this section, we derive the general expression of the response function $\chi_{AB}(\omega)$ within the TD-SCHA theory for any couple of ionic time-independent observables $\hat{\mathbf{A}}$ and $\hat{\mathbf{B}}$.

The $\chi_{AB}(\omega)$ describes how an external perturbation, interacting with the ions through $\hat{\mathbf{B}}$, affects the average

of $\hat{\mathcal{A}}$, as described in Sec. II.

$$V^{(1)}(\hat{\mathbf{R}}, t) = \mathcal{B}(\hat{\mathbf{R}})\mathcal{V}(t) \quad (90)$$

$$\langle \mathcal{A}(\mathbf{R}) \rangle_{\rho^{(1)}(\omega)} = \chi_{\mathcal{AB}}(\omega)\mathcal{V}(\omega) \quad (91)$$

Since we are in linear regime, we expand the average of $\hat{\mathcal{A}}$ at first order around the equilibrium solution:

$$\begin{aligned} \langle \mathcal{A}(\mathbf{R}) \rangle_{\rho^{(1)}(\omega)} &= \sum_{\mu\nu} \frac{\partial \langle \mathcal{A}(\mathbf{R}) \rangle_{\rho(\omega)}}{\partial \tilde{\Upsilon}_{\mu\nu}} \tilde{\Upsilon}_{\mu\nu}^{(1)} + \\ &+ \sum_{\mu\nu} \frac{\partial \langle \mathcal{A}(\mathbf{R}) \rangle_{\rho(\omega)}}{\partial \text{Re} \tilde{A}_{\mu\nu}} \text{Re} \tilde{A}_{\mu\nu}^{(1)} + \\ &+ \sum_{\mu} \frac{\partial \langle \mathcal{A}(\mathbf{R}) \rangle_{\rho(\omega)}}{\partial \tilde{\mathcal{R}}_{\mu}} \tilde{\mathcal{R}}_{\mu}^{(1)} \end{aligned} \quad (92)$$

where the derivatives in Eq. (92) are evaluated with the equilibrium SCHA density matrix. In particular, since the $\hat{\mathcal{A}}$ observable depends only on the ionic positions $\hat{\mathbf{R}}$, only the $\tilde{\Upsilon}^{(1)}$ and $\tilde{\mathcal{R}}^{(1)}$ affects its average.

By exploiting the integration by parts as illustrated in ref.[33], we get (in the polarization basis of Eq. (76)):

$$\frac{\partial \langle \mathcal{A}(\mathbf{R}) \rangle_{\rho(\omega)}}{\partial \tilde{\Upsilon}_{\mu\nu}} = -\hbar^2 \frac{(2n_{\mu} + 1)(2n_{\nu} + 1)}{8\omega_{\mu}\omega_{\nu}} \left\langle \frac{\partial^2 \mathcal{A}}{\partial \tilde{R}_{\mu} \partial \tilde{R}_{\nu}} \right\rangle_{\rho} \quad (93a)$$

$$\frac{\partial \langle \mathcal{A}(\mathbf{R}) \rangle_{\rho(\omega)}}{\partial \text{Re} \tilde{A}_{\mu\nu}} = 0 \quad (93b)$$

$$\frac{\partial \langle \mathcal{A}(\mathbf{R}) \rangle_{\rho(\omega)}}{\partial \tilde{\mathcal{R}}_{\mu}} = \left\langle \frac{\partial \mathcal{A}}{\partial \tilde{R}_{\mu}} \right\rangle_{\rho} \quad (93c)$$

In the same way, we employ Eq. (87) to express how the perturbation $\hat{\mathcal{B}}$ affects the density matrix dynamics:

$$f_{\tilde{\Upsilon} \mu\nu}^{(1)}(\omega) = \frac{1}{\hbar} \left(\frac{2\omega_{\mu}}{2n_{\mu} + 1} + \frac{2\omega_{\nu}}{2n_{\nu} + 1} \right) \left\langle \frac{\partial^2 \mathcal{B}}{\partial \tilde{R}_{\mu} \partial \tilde{R}_{\nu}} \right\rangle_{\rho} \mathcal{V}(\omega), \quad (94a)$$

$$\begin{aligned} f_{\text{Re} A \mu\nu}^{(1)}(\omega) &= \frac{1}{\hbar} \left(\frac{2(n_{\mu} + 1)n_{\mu}\omega_{\mu}}{2n_{\mu} + 1} + \right. \\ &\quad \left. + \frac{2(n_{\nu} + 1)n_{\nu}\omega_{\nu}}{2n_{\nu} + 1} \right) \left\langle \frac{\partial^2 \mathcal{B}}{\partial \tilde{R}_{\mu} \partial \tilde{R}_{\nu}} \right\rangle_{\rho} \mathcal{V}(\omega) \end{aligned} \quad (94b)$$

$$f_{\tilde{\mathcal{R}} \mu}^{(1)}(\omega) = - \left\langle \frac{\partial \mathcal{B}}{\partial \tilde{R}_{\mu}} \right\rangle_{\rho} \mathcal{V}(\omega) \quad (94c)$$

Since $\mathbf{f}^{(1)}$ is proportional to \mathcal{V} , it is convenient to define $\mathbf{f}^{(1)}$ as:

$$\mathbf{f}_x^{(1)}(\omega) = \mathbf{f}_x^{(1)}\mathcal{V}(\omega) \quad x = \tilde{\Upsilon}, \text{Re} \tilde{A}, \tilde{\mathcal{R}} \quad (95)$$

We can express the response function with a standard linear-algebra matrix-vector multiplications. We introduce the response vector \mathbf{p} and the perturbation vector \mathbf{q} as:

$$\mathbf{p} = \left(\frac{\partial \langle \hat{\mathcal{A}} \rangle_{\hat{\rho}(\omega)}}{\partial \tilde{\Upsilon}} \quad \frac{\partial \langle \hat{\mathcal{A}} \rangle_{\hat{\rho}(\omega)}}{\partial \text{Re} \tilde{A}} \quad \frac{\partial \langle \hat{\mathcal{A}} \rangle_{\hat{\rho}(\omega)}}{\partial \tilde{\mathcal{R}}} \right), \quad (96)$$

$$\mathbf{q} = \begin{pmatrix} \mathbf{f}_{\tilde{\Upsilon}}^{(1)} \\ \mathbf{f}_{\text{Re} A}^{(1)} \\ \mathbf{f}_{\tilde{\mathcal{R}}}^{(1)} \end{pmatrix}. \quad (97)$$

In this way, the average of $\hat{\mathcal{A}}$ (Eq. 92) is a simple scalar product:

$$\langle \hat{\mathcal{A}} \rangle_{\rho^{(1)}(\omega)} = \mathbf{p} \cdot \begin{pmatrix} \tilde{\Upsilon}^{(1)}(\omega) \\ \text{Re} \tilde{A}^{(1)}(\omega) \\ \tilde{\mathcal{R}}^{(1)}(\omega) \end{pmatrix} \quad (98)$$

The last vector in Eq. (98) is the result of the linear response system (Eq. 89), and it is the product between the Green function $\mathbf{G}(\omega)$ to the \mathbf{q} vector:

$$\begin{pmatrix} \tilde{\Upsilon}^{(1)}(\omega) \\ \text{Re} \tilde{A}^{(1)}(\omega) \\ \tilde{\mathcal{R}}^{(1)}(\omega) \end{pmatrix} = \mathbf{G}(\omega) \mathbf{q} \mathcal{V}(\omega). \quad (99)$$

Combining Eq. (98) with Eq. (99), we get the expression of the response function in the TD-SCHA linear response formalism:

$$\langle \hat{\mathcal{A}} \rangle_{\rho^{(1)}(\omega)} = \mathbf{p} \mathbf{G}(\omega) \mathbf{q} \mathcal{V}(\omega) \quad (100)$$

Comparing Eq. (100) with the definition of the response function $\chi_{\mathcal{AB}}$ (Eq. 91) we get:

$$\chi_{\mathcal{AB}}(\omega) = \mathbf{p} \mathbf{G}(\omega) \mathbf{q}, \quad (101)$$

where $\mathbf{G}(\omega)$ is defined in Eq. (88), \mathbf{p} in Eq. (96) and \mathbf{q} in Eq. (97).

B. Interacting one-phonon Green function

As a simple illustration, here, we compute the expression for the interacting one-phonon Green function. This is the response function when $\hat{\mathcal{A}} = \sqrt{m_a} \hat{R}_a$ and $\hat{\mathcal{B}} = \sqrt{m_b} \hat{R}_b$.

$$\langle \sqrt{m_a} \hat{R}_a \rangle_{\rho^{(1)}(\omega)} = \tilde{\mathcal{R}}_a^{(1)}(\omega) \quad (102)$$

Thus, the response \mathbf{p} vector (Eq. 96) is:

$$\mathbf{p} = (0 \ 0 \ \delta_a) \quad (103)$$

where we indicate with δ_a the vector with 1 in the a -th atom/Cartesian index and zeros elsewhere.

On the other side, the perturbation vector \mathbf{q} can be obtained substituting $\tilde{\mathcal{B}}$ into Eq. (94):

$$\mathbf{f}_{\mathcal{R}}^{(1)} = 0 \quad \mathbf{f}_{\text{Re}A}^{(1)} = 0 \quad (104)$$

$$f_{\mathcal{R}_c}^{(1)}(\omega) = -\delta_{cb}. \quad (105)$$

Then, from Eq. (97), we get:

$$\mathbf{q} = - \begin{pmatrix} 0 \\ 0 \\ \delta_b \end{pmatrix} \quad (106)$$

From which we get the interacting one-phonon Green function, as the last block of the Green function:

$$\chi_{\sqrt{m_a}R_a, \sqrt{m_b}R_b}(\omega) = \mathcal{G}_{ab}(\omega) = - \begin{pmatrix} 0 & 0 & \delta_a \end{pmatrix} \mathbf{G}(\omega) \begin{pmatrix} 0 \\ 0 \\ \delta_b \end{pmatrix} \quad (107)$$

The one-phonon Green function describes lattice excitations. Its poles are the energy of the physical phonons in the system, and its imaginary part is proportional to the intensity of the fully anharmonic phonon branches probed in X-ray or neutron scattering experiments.

C. Physical phonons when cubic anharmonicity is negligible

The full expressions for the Green function is quite complex. However, it becomes easy if we consider the special case for:

$$D_{abc}^{(3)} = \left\langle \frac{\partial^3 V^{(0)}}{\partial \tilde{R}_a \partial \tilde{R}_b \partial \tilde{R}_c} \right\rangle_{\rho} = 0. \quad (108)$$

This condition is satisfied in some points of the Brillouin zone in highly symmetric crystals[49], or perfectly harmonic systems.

If this is the case, the $\mathcal{R}^{(1)}$ block of the total Green function $\mathbf{G}(\omega)$ is decoupled from the others as $\bar{\mathbf{X}}''$, $\bar{\mathbf{Z}}$ and $\bar{\mathbf{Z}}'$ are all equal to zero (see TABLE I).

Thanks to this block diagonal form of $\mathbf{G}(\omega)$, the inversion needed to compute the one-phonon Green function requires only inverting the $\mathcal{R}^{(1)}$ block. In particular:

$$\mathcal{G}(\omega) = (\omega^2 + \bar{\mathbf{Z}}'')^{-1} \quad (109)$$

If we write this in the basis of polarization modes substituting the expression of $\bar{\mathbf{Z}}''$ (see Appendix F), we get:

$$\mathcal{G}_{\mu\nu}(\omega) = \frac{\delta_{\mu\nu}}{\omega^2 - \omega_{\mu}^2}. \quad (110)$$

This expression resembles the Green function of harmonic phonons. However, this is not true, as the ω_{μ}

frequencies do not coincide with the harmonic result. In particular, ω_{μ} frequencies are the SCHA frequencies, obtained as the average of the second derivative of the BO potential in the equilibrium distribution (Eq. 75). Thanks to this average, the ω_{μ} frequencies are affected

by the $\bar{\mathbf{D}}^{(4)}$ and, thus, they are temperature dependent. Therefore, the static SCHA frequencies ω_{μ} coincides with the poles of the dynamical Green function only if $\bar{\mathbf{D}}^{(3)} = 0$. However, this is not true in the most general case, and to find the poles of the Green function, we must invert Eq. (88).

Notably, this is a general misunderstanding in empirical mean-field methods to deal with strong ionic anharmonicity, as TDEP[50], ALAMODE[51] and the static SCHA[20]. The self-consistent frequencies ω_{μ} extracted from these methods are not the phonon frequencies probed by dynamical experiments. The reason is that the ω_{μ} s extracted from this methods do not coincide with the poles of the interacting one-phonon Green function, unless the cubic anharmonicity is negligible.

D. TD-SCHA self-energy

In Sec. V C, we derived the expression of the one-phonon Green function if $\bar{\mathbf{D}}^{(3)} = 0$. Following the standard many-body approach to Green functions, we define the TD-SCHA self-energy $\Sigma(\omega)$ as:

$$\mathcal{G}^{-1}(\omega) = (\bar{\mathbf{Z}}'' + \omega^2) - \Sigma(\omega), \quad (111)$$

where $(\bar{\mathbf{Z}}'' - \omega^2)$ is the inverse of the one-phonon Green function with $\bar{\mathbf{D}}^{(3)} = 0$ (Eq. 109).

Due to the importance in calculating the interacting one-phonon Green function, the authors of ref.[33] formulated a dynamical *ansatz* for $\Sigma(\omega)$, proposing an analytical continuation at finite frequencies of the static self-energy calculated from equilibrium SCHA. Ref.[33] proved the correctness of this *ansatz* in the limit of small anharmonicity (perturbation theory) and for the static case $\omega = 0$.

In this section, we derive the true expression of the self-energy $\Sigma(\omega)$ within the TD-SCHA, which includes the strong anharmonic regime and high-frequency (as far as BO approximation holds).

The complete one-phonon green function is given by Eq. (107).

$$\mathcal{G}_{\mu\nu}(\omega) = (00\delta_{\mu}) \begin{pmatrix} \bar{\mathbf{X}} + \omega^2 & \bar{\mathbf{Y}} & \bar{\mathbf{Z}} \\ \bar{\mathbf{X}}' & \bar{\mathbf{Y}}' + \omega^2 & \bar{\mathbf{Z}}' \\ \bar{\mathbf{X}}'' & 0 & \bar{\mathbf{Z}}'' + \omega^2 \end{pmatrix}^{-1} \begin{pmatrix} 0 \\ 0 \\ \delta_{\nu} \end{pmatrix}. \quad (112)$$

When $\bar{\mathbf{D}}^{(3)} \neq 0$, $\bar{\mathbf{X}}''$ is non zero and the one-phonon Green function interacts with the rest of the big $\mathbf{G}(\omega)$ matrix through $\bar{\mathbf{X}}''$.

Thus, the self-energy is

$$\Sigma(\omega) = \bar{\mathbf{X}}'' \frac{\partial \tilde{\mathbf{Y}}^{(1)}}{\partial \tilde{\mathbf{R}}^{(1)}}(\omega) \quad (113)$$

and $\bar{\mathbf{X}}''$ is contracted with the indices of $\tilde{\mathbf{Y}}^{(1)}$. In particular, this term indicates how a perturbation in the quantum fluctuations $\tilde{\mathbf{Y}}^{(1)}$ affects the average positions $\tilde{\mathbf{R}}^{(1)}$. If $\bar{\mathbf{D}}^{(3)} \neq 0$, the dynamics in $\tilde{\mathbf{R}}^{(1)}$ affects $\tilde{\mathbf{Y}}^{(1)}$ and $\text{Re}\tilde{\mathbf{A}}^{(1)}$ through $\tilde{\mathbf{Z}}$ and $\tilde{\mathbf{Z}}'$ (Eq. 81a and 81b). They evolve freely (harmonic propagation) and interacting anharmonically through $\bar{\mathbf{D}}^{(4)}$. Finally, $\tilde{\mathbf{Y}}^{(1)}$ affects back $\tilde{\mathbf{R}}^{(1)}$ through $\bar{\mathbf{X}}''$ (Eq. 81c).

To calculate $\Sigma(\omega)$, we need to get an explicit expression from the dependency of $\tilde{\mathbf{Y}}^{(1)}$ and $\tilde{\mathbf{R}}^{(1)}$. It is convenient to remove the $\text{Re}\tilde{\mathbf{A}}^{(1)}(\omega)$ firstly (Eq. 81b):

$$\bar{\mathbf{X}}' \tilde{\mathbf{Y}}^{(1)} + (\bar{\mathbf{Y}}' + \omega^2) \text{Re}\tilde{\mathbf{A}}^{(1)} + \tilde{\mathbf{Z}}' \tilde{\mathbf{R}}^{(1)} = 0 \quad (114)$$

$$\text{Re}\tilde{\mathbf{A}}^{(1)} = -(\bar{\mathbf{Y}}' + \omega^2)^{-1} (\bar{\mathbf{X}}' \tilde{\mathbf{Y}}^{(1)} + \tilde{\mathbf{Z}}' \tilde{\mathbf{R}}^{(1)}). \quad (115)$$

We substitute it in the $\tilde{\mathbf{Y}}^{(1)}(\omega)$ equation (Eq. 81a):

$$\begin{aligned} & [(\bar{\mathbf{X}} + \omega^2) - \bar{\mathbf{Y}}(\bar{\mathbf{Y}}' + \omega^2)^{-1} \bar{\mathbf{X}}'] \tilde{\mathbf{Y}}^{(1)} + \\ & + [\tilde{\mathbf{Z}} - \bar{\mathbf{Y}}(\bar{\mathbf{Y}}' + \omega^2)^{-1} \tilde{\mathbf{Z}}'] \tilde{\mathbf{R}}^{(1)} = 0 \end{aligned} \quad (116)$$

From which we get the relationship between $\tilde{\mathbf{Y}}^{(1)}(\omega)$ and $\tilde{\mathbf{R}}^{(1)}(\omega)$. Here, products between tensors follows the same convention as Eq. (82), where the number of indices to be contracted is determined by the tensor on the left. The inversion of a 4-rank tensor is equivalent of inverting a matrix where we group the first two and last two indices:

$$\bar{X}_{abcd} = \bar{X}_{(ab)(cd)} \quad (117)$$

Now we have all the ingredients to write the interacting one-phonon self-energy:

$$\begin{aligned} \Sigma(\omega) = & -\bar{\mathbf{X}}'' [(\bar{\mathbf{X}} + \omega^2) - \bar{\mathbf{Y}}(\bar{\mathbf{Y}}' + \omega^2)^{-1} \bar{\mathbf{X}}']^{-1} \cdot \\ & \cdot [\tilde{\mathbf{Z}} - \bar{\mathbf{Y}}(\bar{\mathbf{Y}}' + \omega^2)^{-1} \tilde{\mathbf{Z}}'] \end{aligned} \quad (118)$$

Interestingly, $\bar{\mathbf{X}}''$, $\tilde{\mathbf{Z}}$ and $\tilde{\mathbf{Z}}'$ depend on $\bar{\mathbf{D}}^{(3)}$. In Appendix G we prove that this self-energy is equal to the one proposed as dynamical ansatz in ref. [33]:

$$\Sigma(\omega) = \bar{\mathbf{D}} \Lambda(\omega) \left[\mathbb{1} - \bar{\mathbf{D}} \Lambda(\omega) \right]^{-1} \bar{\mathbf{D}} \quad (119)$$

with $\mathbb{1}$ the identity 4-rank tensor and

$$\Lambda(\omega) = -\frac{1}{2} \chi(\omega) \quad (120)$$

With $\chi(\omega)$ the non interacting two-phonon Green function. We calculate it in Eq. (135).

Contemporary to this work, another independent study[52] proved the dynamical *ansatz* of the SCHA, underlying the relevance of the topic.

E. IR and Raman response

In this section, we derive the explicit expression of the IR and Raman response. To compute the general time-correlation function of the two observables $\hat{\mathcal{A}}$ and $\hat{\mathcal{B}}$ in the TD-SCHA formalism, we follow the procedure introduced in Sec. V A: we get the \mathbf{p} and \mathbf{q} vectors of Eq. (96) and (97) from the observables $\hat{\mathcal{A}}$ and $\hat{\mathcal{B}}$, and compute the response $\chi_{AB}(\omega)$ with Eq. (101).

Let us analyze the IR response first. This is related to the ionic dipole-dipole correlation function:

$$\hat{\mathcal{A}} = M_\alpha(\hat{\mathbf{R}}) \quad \hat{\mathcal{B}} = M_{\alpha'}(\hat{\mathbf{R}}) \quad (121)$$

where $M_\alpha(\hat{\mathbf{R}})$ is the α Cartesian component of the net dipole moment when the ions are displaced in the \mathbf{R} position.

To compute the IR response we replace $\mathcal{A} = M_\alpha$ and $\mathcal{B} = M_{\alpha'}$ inside the expressions of vectors \mathbf{p} (Eq. 96) and \mathbf{q} (Eq. 97).

So the quantities we need to compute to obtain \mathbf{p} and \mathbf{q} are the averages of the dipole derivatives:

$$\left\langle \frac{\partial M_\alpha(\mathbf{R})}{\partial R_a} \right\rangle_\rho = \langle \mathcal{Z}_{\alpha a}(\mathbf{R}) \rangle_\rho \quad (122)$$

where $\mathcal{Z}(\mathbf{R})$ is the effective charge of the system when ions are displaced along \mathbf{R} , and, by exploiting integration by parts as introduced in ref.[33],

$$\left\langle \frac{\partial^2 M_\alpha(\mathbf{R})}{\partial R_a \partial R_b} \right\rangle_\rho = \sum_c \Upsilon_{ac} \langle (R_c - \mathcal{R}_c) \mathcal{Z}_{\alpha b}(\mathbf{R}) \rangle_\rho. \quad (123)$$

Both Eq. (122) and Eq. (123) can be computed by averaging the effective charges in a random ensemble extracted according to the equilibrium distribution $\rho(\mathbf{R})$. Since most standard *ab initio* codes calculate effective charges, the full IR response is accessible fully *ab initio*.

In general, the IR response involves the full interacting Green function. A particular case is when effective charges do not depend on the ionic position. In this case, the calculation of IR response is much easier, as Eq. (122) becomes:

$$\langle \mathcal{Z}_{\alpha a}(\mathbf{R}) \rangle_\rho = \mathcal{Z}_{\alpha a}(\mathcal{R}), \quad (124)$$

while Eq. (123):

$$\sum_c \Upsilon_{ac} \langle (R_c - \mathcal{R}_c) \mathcal{Z}_{\alpha b}(\mathbf{R}) \rangle_\rho = 0 \quad (125)$$

In this simple case, only the \mathcal{R} block of \mathbf{p} and \mathbf{q} is different from zero, thus we can link the IR response to the interacting one-phonon Green function:

$$\chi_{M_\alpha M_{\alpha'}}(\omega) = \sum_{ab} \frac{\mathcal{Z}_{\alpha a} \mathcal{Z}_{\alpha' b}}{\sqrt{m_a m_b}} \mathcal{G}_{ab}(\omega) \quad (126)$$

Notably, this equation, that is the standard approximation for IR signal, is only valid for effective charges that do not depend on the ionic displacement. TD-SCHA allows to compute the IR response even in the general scenario.

The same procedure holds also for the Raman response. Here, the \mathcal{A} and \mathcal{B} observables are the polarizability $\alpha_{\alpha\beta}(\hat{\mathbf{R}})$ of the sample along α and β direction (the incoming and outgoing polarization of the light) when ions are displaced in the \mathbf{R} position.

$$\mathcal{A} = \alpha_{\alpha\beta}(\hat{\mathbf{R}}) \quad \mathcal{B} = \alpha_{\alpha'\beta'}(\hat{\mathbf{R}}) \quad (127)$$

The procedure of deriving \mathbf{p} and \mathbf{q} is the same as for the IR. If we define the Raman tensor Ξ as:

$$\Xi_{\alpha\beta a}(\mathbf{R}) = \frac{\partial \alpha_{\alpha\beta}(\mathbf{R})}{\partial R_a} \quad (128)$$

Then we have:

$$\left\langle \frac{\partial \alpha_{\alpha\beta}(\mathbf{R})}{\partial R_a} \right\rangle_{\rho} = \langle \Xi_{\alpha\beta a}(\mathbf{R}) \rangle_{\rho} \quad (129)$$

$$\left\langle \frac{\partial^2 \alpha_{\alpha\beta}(\mathbf{R})}{\partial R_a \partial R_b} \right\rangle_{\rho} = \sum_c \Upsilon_{ac} \langle (R_c - \mathcal{R}_c) \Xi_{\alpha\beta b}(\mathbf{R}) \rangle_{\rho}. \quad (130)$$

Also in this case, the full response function can be obtained by simply calculating the raman tensor Ξ in a randomly distributed ensemble of ionic configurations according to $\rho(\mathbf{R})$. The Raman tensor can be calculated *ab initio* efficiently with the method introduced by ref.[34]. If the Raman tensor depends on nuclear positions, Eq. (130) is different from zero, and we have a contribution to the response function from the complete interacting Green function. However, if we neglect the dependence of Ξ from the nuclear position, we can express the Raman response only from the one-phonon Green function, as we did for the IR:

$$\chi_{\alpha\beta\alpha'\beta'}(\omega) = \sum_{ab} \frac{\Xi_{\alpha\beta a} \Xi_{\alpha'\beta' b}}{\sqrt{m_a m_b}} \mathcal{G}_{ab}(\omega). \quad (131)$$

In next section we give a schematic overview of the processes neglected by considering the response only due to the interacting one-phonon Green function.

F. Mixed one-two and two-phonons Green function

The one-phonon Green function does not provide the response to any general external perturbation $V^{(1)}(\mathbf{R}, t)$, but only to those that depend linearly on the ionic displacements \mathbf{R} , as we show for the specific cases of IR and Raman (Sec. V E). If the perturbation or the observable we probe are nonlinear in \mathbf{R} , then the vectors \mathbf{p} and \mathbf{q} that determine the response function $\chi_{\mathcal{A}\mathcal{B}}(\omega)$ (Eq. 101)

have a non zero contribution also in the $\tilde{\Upsilon}^{(1)}$ and $\text{Re}\tilde{\mathbf{A}}^{(1)}$ sector (Eq. 96 and 97).

This contribution is important if ionic fluctuations are sizable (e.g. in presence of light atoms or close to a second-order phase-transition), or if the linear term in $\mathbf{R} - \mathcal{R}$ of $\mathcal{A}(\hat{\mathbf{R}})$ and $\mathcal{B}(\hat{\mathbf{R}})$ is zero by symmetry. In these conditions, quadratic terms in the coupling between the probe and ionic displacement may become important. It is fundamental to explain IR/Raman spectra of ice VII and X[53] and liquid water[54]. In these works, the authors employed molecular dynamics to go beyond the one-phonon Green function (neglecting quantum fluctuations). Another class of materials with Raman spectra arising from a nonlinear coupling between the probe and the ionic displacement are high-symmetry structures like diamond[55]. Here, the authors calculated the Raman signal within the harmonic approximation. A full treatment with both anharmonicity and quantum fluctuations with a nonlinear probe is missing in the literature.

In FIG. 1 we report a diagrammatic representation of the response function. Let time flow from left to right; when the probe interacts with the sample, it can either excite a single phonon, with the linear term of \mathcal{B} (panels **c,d**) or two phonons with the quadratic dependency of \mathcal{B} on ionic positions (panels **a,b**). Then, the excited phonons evolve interacting through anharmonicity. At the end of the anharmonic evolution, we may either have a single phonon (panels **b,d**) or two phonons (panels **a,c**). Then, the excited phonons give a response in the \mathcal{A} observable; the average of $\mathcal{A}(\hat{\mathbf{R}})$ is affected by two phonons proportionally to its quadratic dependence on ionic displacement (panels **a,c**), while a single phonon affects the \mathcal{A} average proportionally to linear term of $\mathcal{A}(\hat{\mathbf{R}})$ (panels **b,d**). The overall process is divided in (interacting) two-phonon Green functions (**a**), mixed one-two phonon Green functions (**b,c**) and one-phonon Green functions (**d**). Harmonic systems do not have a contribution from mixed Green functions, as phonons cannot decay or scatter during the free propagation (panel **e,f**).

The expression of the IR (Eq. 126) and Raman (Eq. 131) in the approximation of linear coupling with the probe correspond to take only the contribution of the process in panel **d**, neglecting all the others.

Interestingly, also in the pure harmonic case there is an additional contribution due to non-linear couplings between the probe and the system, that is reported in panel **e**. For example, the harmonic two-phonon IR signal is:

$$\chi_{M_{\alpha}M_{\alpha'}}^{(2ph)}(\omega) = \sum_{abcd\mu\nu} \frac{e_{\mu}^a e_{\nu}^b e_{\mu}^c e_{\nu}^d}{\sqrt{m_a m_b m_c m_d}} \frac{dZ_{\alpha a}}{dR_b} \chi_{\mu\nu\mu\nu}(\omega) \frac{dZ_{\alpha' c}}{dR_d} \quad (132)$$

where $\chi_{\mu\nu\mu\nu}(\omega)$ is the harmonic two-phonon Green function. We can compute the expression of the $\chi(\omega)$ tensor as the time correlation between the nuclear quadratic displacements:

$$\hat{\mathbf{A}} = \sqrt{m_a m_b} (\hat{R}_a - \mathcal{R}_a) (\hat{R}_b - \mathcal{R}_b) \quad (133)$$

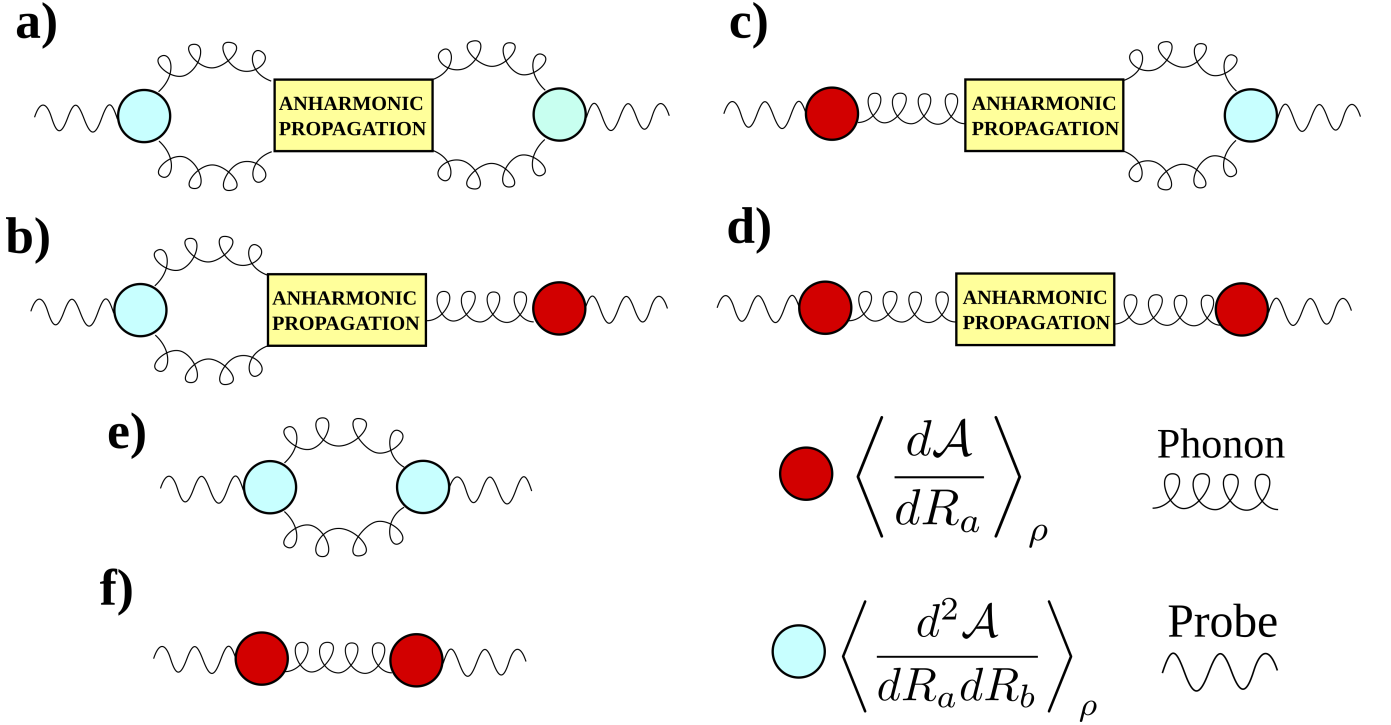


FIG. 1. Schematic representation of all processes captured by the TD-SCHA response function. The circles represent the interaction between the probe and the ionic displacements, that occurs through observable \mathcal{A} . We have two possible interaction, the linear one give rise to a single phonon (dark red), the quadratic one excites two-phonons (light cyan). Panels **a,b,c,d** represent the TD-SCHA processes, where the excited phonons propagate with the full anharmonic interaction. We have a two-phonon signal (panel **a**), mixed one-two phonons (panels **b,c**) and one-phonon (panel **d**). Panels **e,f** show the possible processes with harmonic propagation.

$$\hat{\mathcal{B}} = \sqrt{m_a m_b} (\hat{R}_c - \mathcal{R}_c) (\hat{R}_d - \mathcal{R}_d) \quad (134)$$

Since, in second-quantization formalism, each position operator $\hat{\mathbf{R}}$ is proportional to the creation-annihilation of one phonon, $\hat{\mathcal{A}}$ and $\hat{\mathcal{B}}$ contain creations and annihilations of two phonons; this is the reason why it is called the two-phonon Green function.

We compute the \mathbf{p} and \mathbf{q} vectors (Eq. 96 and 97) from $\hat{\mathcal{A}}$ and $\hat{\mathcal{B}}$ and insert them into Eq. (101) to get the interacting two-phonon Green functions.

The non-interacting (harmonic) two-phonon Green function is obtained when both $\hat{\mathcal{D}}^{(3)}$ and $\hat{\mathcal{D}}^{(4)}$ equal 0. In appendix J we report the details of the calculation. The final result is:

$$\chi_{\mu\nu\mu\nu}(\omega) = \frac{1}{2\omega_\mu\omega_\nu} \left[\frac{(\omega_\mu + \omega_\nu)(n_\mu + n_\nu + 1)}{(\omega_\mu + \omega_\nu)^2 - \omega^2} - \frac{(\omega_\mu - \omega_\nu)(n_\mu - n_\nu)}{(\omega_\mu - \omega_\nu)^2 - \omega^2} \right]. \quad (135)$$

Indeed, Eq. (135) is the well known two-phonon propagator for harmonic systems, and it coincides with the one obtained with the standard many-body approach.

Notably, since usually the non-linear interaction between the probe and the ionic position is small, the diagrams **b,c** in FIG. 1 provide a lower order signal than the harmonic (e) diagram.

Indeed, all the processes represented in panels **a,b,c,d** are automatically included in the response function of the TD-SCHA introduced in Sec. V A. In principle, also higher-order processes exist, where the probe interacts with more than two phonons. However, the Gaussian constrain on the TD-SCHA density matrix does not allow these excitations, but they are accounted for with a mean-field approach affecting the average of the derivatives of \mathcal{A} and \mathcal{B} observables on the ionic probability distribution, providing a temperature dependency for the static SCHA frequencies and vertices in the diagrams reported in FIG. 1.

VI. LANCZOS ALGORITHM TO COMPUTE THE RESPONSE FUNCTION

While a numerical implementation to calculate the dynamical one-phonon Green function has been presented[33], its computational cost diverges quickly for systems with more than 10 atoms, as the self-energy of Eq. (119) requires, for any frequency to probe, the inversion of the matrix

$$\left[\mathbb{1} - \hat{\mathcal{D}}\Lambda(\omega) \right]^{-1}. \quad (136)$$

This matrix has a dimension of $(3N)^2 \times (3N)^2$; its numerical inversion is a heavy computational task. For example, just to store in memory the matrix of Eq. (136) in a system with 100 atoms with 64-bit floating-point precision, more than 60 Gb are needed. The inversion of Eq. (136) requires a LU decomposition of a matrix of size $n = 9N^2$. The LU decomposition scales a n^3 ; the overall scaling for computing the inversion is N^6 , which quickly diverges for realistic systems with more than 10 atoms. For this reason, the application of the full dynamical one-phonon Green function has been performed in realistic systems always under the assumption that $\overset{(4)}{\mathbf{D}} = 0$.

Moreover, as discussed in Sec. VD, the one-phonon Green function does not provide the most general response to the experimental probe, but it is limited to probes interacting linearly with atomic displacements.

In this section, we derive a very efficient algorithm that allows computing the elements of the response function to any general external perturbation, that is computationally achievable in systems of hundreds of atoms even with $\overset{(4)}{\mathbf{D}} \neq 0$.

The response function to any generic probe can be obtained from the total Green function (Eq. 88).

By defining the matrix \mathcal{L} as:

$$\mathcal{L} = - \begin{pmatrix} \bar{\mathbf{X}} & \bar{\mathbf{Y}} & \bar{\mathbf{Z}} \\ \bar{\mathbf{X}}' & \bar{\mathbf{Y}}' & \bar{\mathbf{Z}}' \\ \bar{\mathbf{X}}'' & 0 & \bar{\mathbf{Z}}'' \end{pmatrix}, \quad (137)$$

the full Green function matrix is obtained as:

$$\mathbf{G}(\omega) = (\mathcal{L} - \omega^2)^{-1}. \quad (138)$$

However, we are usually interested only in the response function to two specific observables $\hat{\mathcal{A}}$ and $\hat{\mathcal{B}}$, and not the full Green function in Eq. (138). In this case, instead of fully inverting the big $\mathcal{L} - \omega^2$ matrix, we need just to compute the matrix element:

$$\chi_{AB}(\omega) = \mathbf{p}(\mathcal{L} - \omega^2)^{-1} \mathbf{q} \quad (139)$$

where \mathbf{p} and \mathbf{q} are defined in Eq. (96) and Eq. (97) from $\hat{\mathcal{A}}$ and $\hat{\mathcal{B}}$.

The algorithm we discuss in this section computes only the matrix element of Eq. (139) for any value of ω . This is an easy task if we use a basis where \mathcal{L} is tridiagonal (as we show later). Therefore, the purpose of the algorithm is to find the basis in which \mathcal{L} is tridiagonal.

The bi-conjugate Lanczos algorithm does exactly this job: it builds with an iterative procedure the basis-changing Q matrix (non-singular) so that:

$$Q^{-1} \mathcal{L} Q = \mathcal{T}, \quad (140)$$

where \mathcal{T} is tridiagonal:

$$\mathcal{T} = \begin{pmatrix} \alpha_1 & \gamma_1 & & \cdots & 0 \\ \beta_1 & \alpha_2 & & & \vdots \\ & \ddots & \ddots & & \\ \vdots & & \ddots & \ddots & \gamma_{n-1} \\ 0 & \cdots & & \beta_{n-1} & \alpha_n \end{pmatrix} \quad (141)$$

The basis (non orthonormal) in which \mathcal{L} is tridiagonal is represented by the columns of the Q matrix:

$$Q = (\mathbf{q}_1 \cdots \mathbf{q}_n) \quad (142)$$

The rows of the Q^{-1} matrix defines the conjugate vectors:

$$Q^{-1} = \begin{pmatrix} \mathbf{p}_1 \\ \vdots \\ \mathbf{p}_n \end{pmatrix}. \quad (143)$$

The coefficients of the \mathcal{T} matrix (the α_k , β_k , γ_k), the \mathbf{q} and \mathbf{p} vectors are found with the iterative bi-conjugate Lanczos algorithm[56]:

$$\alpha_k = \mathbf{p}_k \cdot \mathcal{L} \mathbf{q}_k \quad (144a)$$

$$\beta_k \mathbf{q}_{k+1} = \mathbf{r}_k = (\mathcal{L} - \alpha_k) \mathbf{q}_k - \gamma_{k-1} \mathbf{q}_{k-1} \quad (144b)$$

$$\gamma_k \mathbf{p}_{k+1} = \mathbf{s}_k = (\mathcal{L}^\dagger - \alpha_k) \mathbf{p}_k - \beta_{k-1} \mathbf{p}_{k-1} \quad (144c)$$

$$\beta_k = |\mathbf{r}_k| \quad (144d)$$

$$\gamma_k = \frac{\mathbf{s}_k \cdot \mathbf{r}_k}{\beta_k} \quad (144e)$$

This recursion formally ends either when either \mathbf{q}_k or \mathbf{p}_k are linear combinations of the previous vectors or if $\mathbf{p}_k \cdot \mathbf{q}_k = 0$. Unless the system is perfectly harmonic, this condition is usually never reached in practical runs, and the algorithm is truncated after a maximum number of steps N_{\max} .

To facilitate the calculation of the Green function, we initialize the algorithm in the following way:

$$\mathbf{q}_1 = \frac{\mathbf{q}}{|\mathbf{q}|} \quad (145)$$

$$\mathbf{p}_1 = \mathbf{p} \frac{|\mathbf{q}|}{\mathbf{p} \cdot \mathbf{q}} \quad (146)$$

The response function can be rewritten as:

$$\chi_{AB}(\omega) = (\mathbf{p} \cdot \mathbf{q}) \mathbf{p}_1 \cdot (\mathcal{L} - \omega^2)^{-1} \mathbf{q}_1 \quad (147)$$

$$\chi_{AB}(\omega) = (\mathbf{p} \cdot \mathbf{q}) \mathbf{p}_1 Q Q^{-1} \cdot (\mathcal{L} - \omega^2)^{-1} Q Q^{-1} \mathbf{q}_1 \quad (148)$$

Thanks to the definitions in Eq. (142) and (143) we have

$$Q^{-1}\mathbf{q}_1 = \begin{pmatrix} 1 \\ 0 \\ \vdots \\ 0 \end{pmatrix} \quad (149)$$

$$\mathbf{p}_1 Q = (1 \ 0 \ \cdots \ 0) \quad (150)$$

Thus, the response function is the first element of the inverse matrix in the tridiagonal basis:

$$\chi_{AB}(\omega) = (\mathbf{p} \cdot \mathbf{q}) \left[(\mathcal{T} - \omega^2)^{-1} \right]_{11} \quad (151)$$

We can compute the first element of the inverse of a tridiagonal matrix as a continued fraction recursion:

$$\chi_{AB}(\omega) = \frac{(\mathbf{p} \cdot \mathbf{q})}{\alpha_1 - \omega^2 - \frac{\gamma_1 \beta_1}{\alpha_2 - \omega^2 - \frac{\gamma_2 \beta_2}{\ddots}}} \quad (152)$$

Indeed, the application of this method is limited to response function where the perturbation and the response are not orthogonal, i.e. the product $\mathbf{p} \cdot \mathbf{q} \neq 0$. The condition $\mathbf{p} \cdot \mathbf{q} = 0$ is met, for example, by off-diagonal elements of the interacting one-phonon Green function. Luckily, the spectral function depends only on the trace of the interacting one-phonon Green function, so only diagonal elements are required (for which $\mathbf{p} \cdot \mathbf{q} = 1$).

When the recursion is truncated without reaching the stopping condition, we can extend the α, β and γ above N_{\max} by assuming them as constant:

$$k \geq N_{\max} \quad \alpha_k = \alpha_{N_{\max}} \quad \beta_k = \beta_{N_{\max}} \quad \gamma_k = \gamma_{N_{\max}}. \quad (153)$$

Under this hypothesis, the last part of the continued fraction satisfy the self-consistent equation

$$g(\omega) = \frac{1}{\alpha_{N_{\max}} - \omega^2 - \gamma_{N_{\max}} \beta_{N_{\max}} g(\omega)}, \quad (154)$$

that is solved:

$$g(\omega) = \frac{\alpha_{N_{\max}} - \omega^2}{2\gamma_{N_{\max}}\beta_{N_{\max}}} - \frac{\sqrt{(\alpha_{N_{\max}} - \omega^2)^2 - 4\gamma_{N_{\max}}\beta_{N_{\max}}}}{2\gamma_{N_{\max}}\beta_{N_{\max}}}. \quad (155)$$

This introduces an imaginary term to the Green function when the argument inside the square root becomes negative (branch cut). This termination of the recursion is similar to the proposed one for the turbo Lanczos algorithm in TD-DFT[57]. With this method, we compute the response function at any frequency, with a single tridiagonalization procedure: the application of \mathcal{L} to \mathbf{p}_i and \mathbf{q}_i in Eq. (144b) and (144c) is the expensive part of the algorithm. The $\alpha_i, \beta_i, \gamma_i$ coefficients depend on the \mathcal{A} and \mathcal{B} observables (on the vectors \mathbf{p} and \mathbf{q} used to start

the Lanczos algorithm) but not on the frequency ω . The application of \mathcal{L} to a vector does not require any matrix inversion; it is efficient and parallelizable. In particular, \mathcal{L} is a square matrix of dimension $3N(1 + 6N) \sim N^2$ ($3N$ the \mathcal{R} block and $9N^2$ both the \mathcal{Y} and $\text{Re}\mathcal{A}$ blocks). Therefore, the application of the \mathcal{L} matrix to the \mathbf{p}_i and \mathbf{q}_i vectors scales as N^4 , much better than the inversion of Eq. (136) (N^6). To calculate the full response function, we need to apply the \mathcal{L} matrix for each iteration. Thus the overall computational cost scales as $N^4 \cdot N_{\text{steps}}$, where N_{steps} is the number of iterations of the Lanczos algorithm.

The heaviest part of applying \mathcal{L} to a vector is the calculation of the $\overset{(4)}{\mathbf{D}}$ tensor inside $\bar{\mathbf{X}}$ and $\bar{\mathbf{X}}'$. Since $\overset{(4)}{\mathbf{D}}$ is computed as a Monte Carlo integral over randomly displaced ionic configurations, as discussed in ref.[33], its calculation scales as $N^4 \cdot N_{\text{config}}$, where N_{config} is the number of random ionic configurations in which used to evaluate the average of $\overset{(4)}{\mathbf{D}}$ (see Appendix H). The number of configurations needed to converge $\overset{(4)}{\mathbf{D}}$ average depends on the system and on the symmetries; usually N_{config} is of the order of thousands.

On the other side, as we show in Sec. VII B, the Lanczos continued fraction converges quite well already with $N_{\text{steps}} = 40$ iterations. Therefore, the calculation of the $\overset{(4)}{\mathbf{D}}$ matrix has a bigger pre-factor than the full Lanczos procedure, and most of the computational cost goes in the calculation of $\overset{(4)}{\mathbf{D}}$.

However, the memory required to store $\overset{(4)}{\mathbf{D}}$ diverges quickly. In big systems, it may be convenient to recompute $\overset{(4)}{\mathbf{D}}$ on-the-fly for each iteration of the Lanczos, to avoid storing it. In this case the overall computational cost of the Lanczos algorithm scales as $N^4 \cdot N_{\text{steps}} N_{\text{config}}$. Since N_{steps} is small, we can compute the response function for systems of hundreds of atoms even on a standard desktop PC, without requiring a prohibitive amount of RAM to store $\overset{(4)}{\mathbf{D}}$ with a moderate additional computational cost.

VII. APPLICATIONS

We now illustrate two applications of the TD-SCHA. First, as a simple benchmark, we show how the TD-SCHA performs in a toy model composed by a single one-dimensional particle in an external anharmonic potential, comparing the results with the exact (numerical) solution of the problem (Sec. VII A).

Then, we apply the TD-SCHA in linear response regime to a real physical system, the phase III of solid high-pressure hydrogen, and simulate the IR and Raman spectroscopy. This system is challenging for any numerical technique that aims to calculate quantum nuclear time-correlation functions *ab initio*: it is strongly anhar-

monic, quantum effects are important and we have many atoms in the simulation cell ($N = 96$).

A. 1D particle in an external potential

To benchmark the TD-SCHA, we compare it with the numerical solution of the Schroedinger equation. This is possible only for very small systems. In this section, we simulate a one-dimensional particle in a strongly anharmonic external potential. The external potential $V(R)$ plays the role of Born-Oppenheimer energy landscape, its shape is reported in FIG. 2 (panel **a**). In Hartree atomic units it is:

$$V(R) = 3R^4 + \frac{1}{2}R^3 - 3R^2 \quad (156)$$

This example is performed at $T = 0$ K, where the density matrix is a pure state. Our particle has the mass of an electron. We compare the probability distribution of the ground state wave-funciton $|\psi_{GS}\rangle$ (obtained diagonalizing the real Hamiltonian) with the SCHA one in panel **a** of FIG. 2. The SCHA solution is a Gaussian, while the exact ground state is a complex function. In panel **b** of the same figure, we present the linear response to a dynamical perturbation. We plot the one-phonon spectral function multiplied by ω , defined as:

$$S(\omega) = -\frac{\omega}{\pi} \text{Im}\mathcal{G}(\omega). \quad (157)$$

In this way, $S(\omega)$ satisfy the sum rule that its integral is proportional to the number of phonons[22] (the intensity of a peak does not depend on the phonon frequency). We compare the results computed with the harmonic approximation and the TD-SCHA to the exact (numerical) solution.

The exact solution is calculated with the Lehmann representation of the Green function, where we performed the full diagonalization on the Hamiltonian \hat{H} to obtain the excited sates $|\psi_i\rangle$:

$$\mathcal{G}(\omega) = \sum_{i=1}^{\infty} \frac{|\langle \psi_i | \sqrt{m}(\hat{R} - \mathcal{R}) | \psi_{GS} \rangle|^2}{\hbar\omega - E_i + E_{GS} + i0^+} + \sum_{i=1}^{\infty} \frac{|\langle \psi_i | \sqrt{m}(\hat{R} - \mathcal{R}) | \psi_{GS} \rangle|^2}{\hbar\omega + E_i - E_{GS} + i0^+} \quad (158)$$

$$\mathcal{R} = \langle \psi_{GS} | \hat{R} | \psi_{GS} \rangle \quad (159)$$

Since we have a 1D system, we can calculate the TD-SCHA response analytically. In particular, we can write the \mathcal{L} matrix explicitly (Eq. 137):

$$\mathcal{L} = \begin{pmatrix} -\frac{(4)}{2\omega_s} - 2\omega_s^2 & 4\omega_s^2 & 4\omega_s D^{(3)} \\ 0 & 0 & 0 \\ \frac{(3)}{8\omega_s^2} & 0 & -\omega_s^2 \end{pmatrix} \quad (160)$$

where ω_s is the frequency of the self-consistent harmonic Hamiltonian of the equilibrium SCHA. Since we are at $T = 0$ K the line of \mathcal{L} that represent the evolution of $\text{Re}A^{(1)}$ is zero, as the system is in a pure state. Therefore, $\text{Re}A$ does not affect the dynamics and we can remove it:

$$\mathcal{L} = \begin{pmatrix} -\frac{(4)}{2\omega_s} - 2\omega_s^2 & 4\omega_s D^{(3)} \\ \frac{(3)}{8\omega_s^2} & -\omega_s^2 \end{pmatrix} \quad (161)$$

The full anharmonic Green function is:

$$\mathcal{G}(\omega) = -(\mathcal{L} - \omega^2)^{-1} \quad (162)$$

The one-phonon Green function $\mathcal{G}(\omega)$ is the element in the \mathcal{R} block (the last) of the full Green function $\mathcal{G}(\omega)$. Performing the inversion analytically we can compute the self-energy:

$$\mathcal{G}(\omega)^{-1} = \omega^2 - \omega_s^2 - \Sigma(\omega) \quad (163)$$

$$\Sigma(\omega) = -\frac{D^{(3)2}/(2\omega_s)}{\omega^2 - 4\omega_s^2 - D^{(4)}/(2\omega_s)} \quad (164)$$

As we proved for the general case in Sec. V D, this self-energy is the same as the one obtained by exploiting the dynamical ansatz formulated in ref.[33]:

$$\Sigma(\omega) = D^{(3)}\Lambda(\omega) \left[1 - D^{(4)}\Lambda(\omega) \right]^{-1} D^{(3)} \quad (165)$$

where in 1D at $T = 0$ K we have:

$$\Lambda(\omega) = -\frac{1}{4\omega_s^2} \frac{1}{4\omega_s^2 - \omega^2} \quad (166)$$

As shown in FIG. 2, the strong anharmonicity downshifts the energy of the peak by 50 % of the harmonic result. Here, the TD-SCHA displays a relative error with the exact solution on the phonon energy of 5 %; an important improvement from the 100 % of the harmonic approximation. The TD-SCHA still slightly overestimates the vibrational energy. This is a general feature of the method, as the TD-SCHA wave-function is more rigid than the real one, as we constrained its Gaussian form.

Moreover, the TD-SCHA spectral function displays an overtone, that arises from the anharmonic coupling between the oscillations of the average position and the fluctuations. This overtone is produced by the pole of the self-energy in Eq. (164). We plot, in FIG. 3, the spectral function zoomed in the energy region where the overtone appears. In this example, it is 100 times smaller than the principal peak. This is a consequence that the overtone is off-resonant: there is not a one-phonon excitation close to its frequency triggering a Fermi resonance. The TD-SCHA correctly reproduces the overtone intensity but with a relative error on its energy of a 60%. Interestingly, the energy of the overtone is not twice the

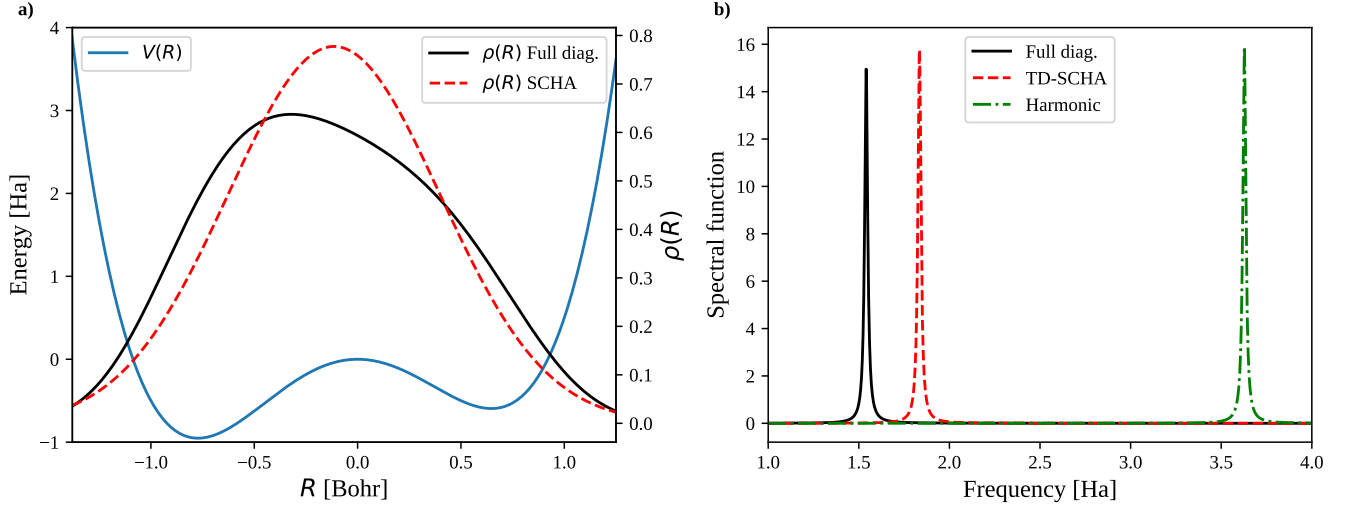


FIG. 2. One dimensional anharmonic model. Panel **a**: The Born-Oppenheimer energy landscape $V(R)$ is plotted with the exact ground state $\psi(R)$ probability density (full diagonalization) and the SCHA equilibrium distribution $\rho(R)$. Panel **b**: the dynamical spectral function of the model. Comparison between the exact result (full diagonalization), the linear response from TD-SCHA, and the Harmonic approximation. The finite line-width arise from a smearing we introduced for presentation purposes.

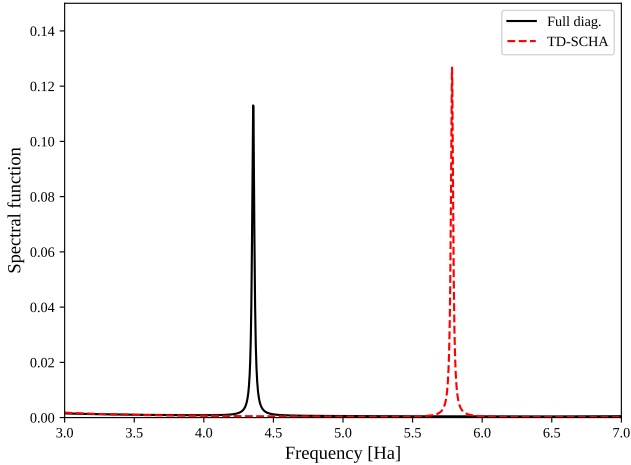


FIG. 3. Zoom in the spectral function at high frequencies. We plot the comparison between the exact overtone and the TD-SCHA overtone.

energy of the fundamental phonon mode, as there is a very strong anharmonicity. The TD-SCHA is unable to simulate third or higher overtones, as we have only two poles from the Green function that are the zeros of the determinant of the inverse of $\mathbf{G}(\omega)$.

Finally, we can simulate the wave-function dynamics adding a time-dependent external potential in a nonlinear regime. For this purpose, we integrate the TD-SCHA equation of motion comparing the result with the exact evolution. We introduce, at $t_0 = 0$, a perturbation of the

form:

$$V^{(1)}(R, t) = E_0 R \sin(\omega_0 t) \quad (167)$$

where $E_0 = 1 \text{ Ha/Bohr}$, and $\omega_0 = 1 \text{ Ha}$. The results are shown in FIG. 4.

The TD-SCHA time evolution is very close to the exact dynamics in the first oscillations, where the wave-function is well localized. The two solutions deviate when the exact wave-function becomes delocalized: The TD-SCHA probability distribution is more localized during the whole dynamics, as shown by the mean square displacement reported in panel **d**. However, the average position of the particle matches very nicely the exact result (panel **c**). The TD-SCHA can reproduce well the nuclear dynamics even in the nonlinear regime.

B. High-pressure hydrogen

In this section, we employ the linear response theory of the TD-SCHA to calculate the Raman and spectra of high-pressure hydrogen phase III. The simulation of vibrational spectra in high-pressure phases of molecular hydrogen is very important to dissect the crystal geometry, as it is the only experimental signature directly related to the lattice. In fact, both X-ray spectroscopy and neutron scattering are extremely challenging for the small samples of hydrogen available. Thus, the structure identification is possible only by comparing results from *ab initio* simulations with experimental data. The physical interpretation of the results and their comparison with experimental data has been presented in ref.[26]. Here,

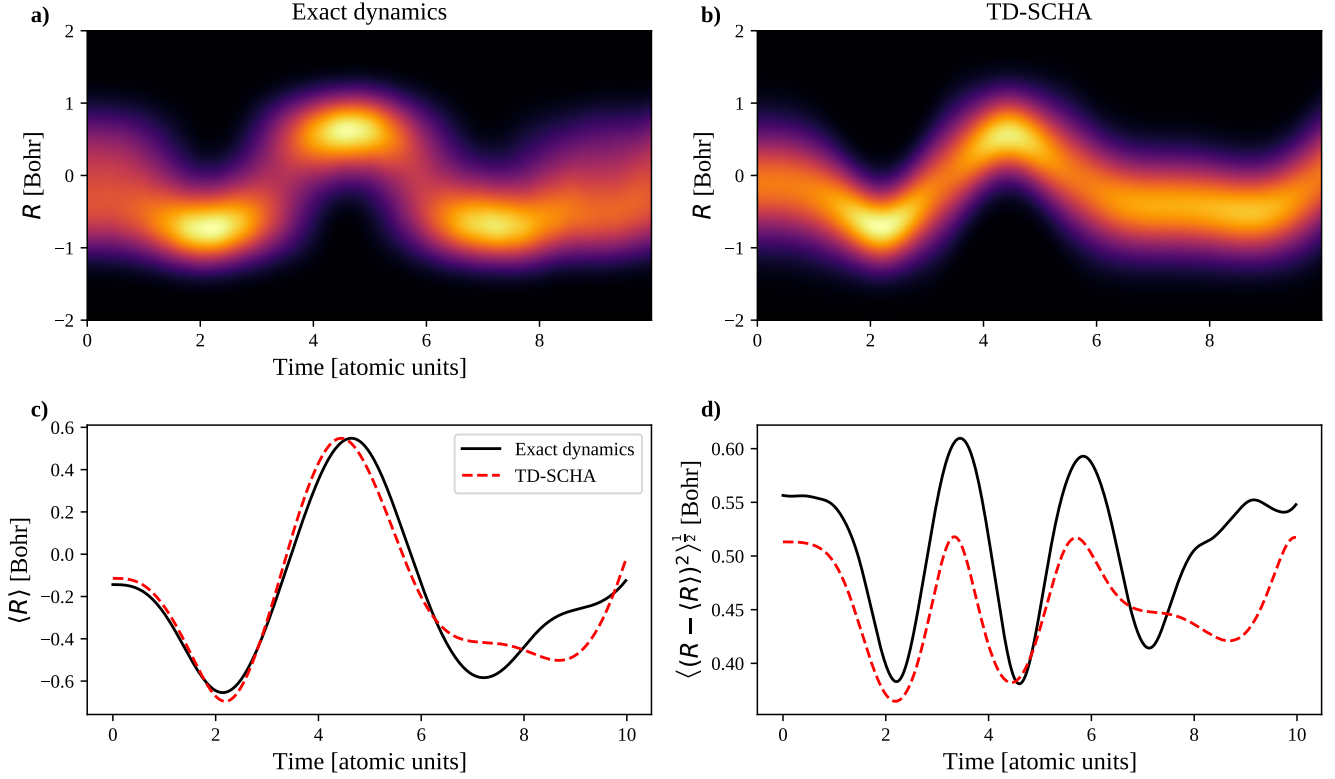


FIG. 4. Time evolution of the wave-function in a time-dependent external potential. The simulation starts from the equilibrium configuration of FIG. 2. Panel **a**: time evolution of the modulus square of the exact wave-function. Panel **b**: Time evolution of the TD-SCHA Gaussian distribution. Panel **c**: average position of the particle as a function of time. Panel **d**: quantum dispersion (mean square displacement).

instead, we focus on the details of the calculation of the Raman response at 260 GPa ($T = 0$ K). Hydrogen phase III is a monoclinic crystal of symmetry group $C2/c$, with 24 atoms in the primitive cell.

We computed only the one-phonon contribution to the full response function: we approximate the Raman tensor as independent from the ionic displacement equal to the value on the SCHA equilibrium positions, as described in Sec. V E and V F.

The Lanczos algorithm introduced in Sec. VI enables the calculation of the dynamical response accounting also for the contribution from 4-phonon scattering processes non perturbatively ($\bar{D}^{(4)}$). In FIG. 5 we report the result of the Raman spectra by progressively switching on anharmonicity. In panel **a**, we report the harmonic Raman spectra, computed within perturbation theory. As an illustration, we report in panel **b** the Raman spectra from the SCHA equilibrium self-consistent harmonic Hamiltonian (Eq. 31). Here, phonons have an infinite lifetime, as in the harmonic case. However, the peak positions and intensities are already strongly affected by anharmonicity through the equilibrium SCHA self-consistency. This response is what we would obtain when cubic anharmonicity is negligible as discussed in Sec. V C, and is equivalent

to the phonon spectra presented in the original derivation of the static SCHA[20, 58, 59].

Indeed, phonons defined from the static SCHA self-consistent harmonic Hamiltonian are not the true dynamical response. To get the real Raman spectrum, one has to calculate the dynamical response function, as introduced in Sec. V A. In panel **c,d**, we report the anharmonic Raman spectrum calculated within TD-SCHA and the Lanczos algorithm introduced in Sec. VI. Panel **c** presents the results with $\bar{D}^{(4)} = 0$, which is equivalent to add a “bubble diagram” to the interacting one-phonon self-energy applied to the equilibrium SCHA Green function. This approximation has been employed for the dynamical response within the SCHA in most studies[22, 30, 31, 33]. In panel **d**, we report the full anharmonic Raman spectra, also accounting for the full expression of the self-energy, including also the four-phonon scattering process explicitly $\bar{D}^{(4)}$. Notice that nonperturbative quartic anharmonicity is also accounted for within the self-consistency of the SCHA Hamiltonian in panels **b,c**.

The downshift of the vibron peak (the strongest peak in the spectrum at high frequencies) from the Harmonic (panel **a**) to the full anharmonic spectrum (panel **d**) oc-

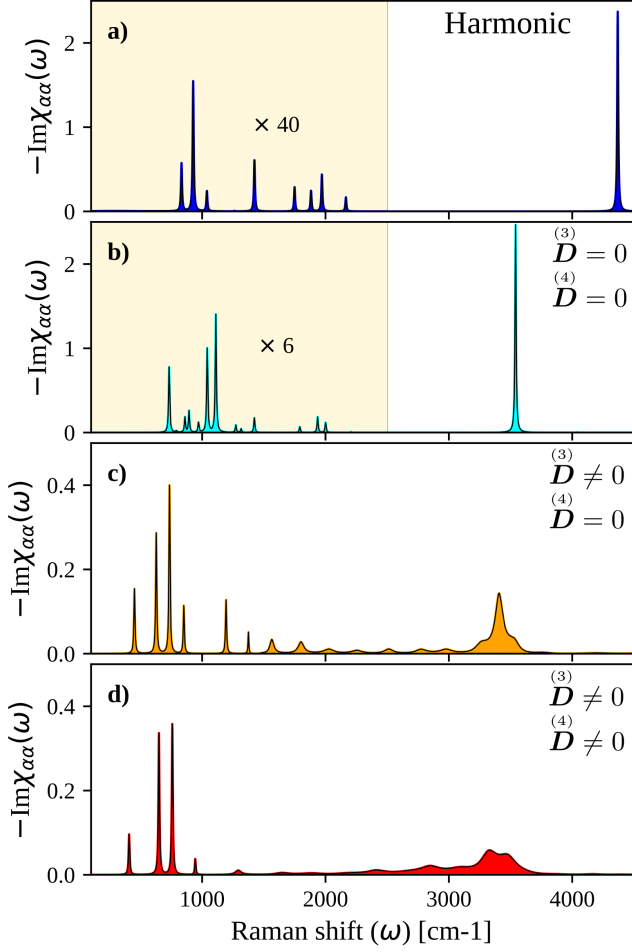


FIG. 5. Raman spectra of high-pressure hydrogen phase III (260 GPa, 0 K). **a**: Harmonic spectra. **b**: Anharmonic spectra of static SCHA quasi-particles. It is obtained neglecting $\bar{D}^{(3)}$ and $\bar{D}^{(4)}$ in the TD-SCHA response function (Sec. V C) **c**: Anharmonic spectra within TD-SCHA, where we set $\bar{D}^{(4)} = 0$ in the calculation of the response function Eq. (101). **d**: Full anharmonic spectra within TD-SCHA. Here, the full response function was computed with $\bar{D}^{(4)} \neq 0$.

curs already when considering equilibrium SCHA auxiliary phonons. The vibron acquires a broad shape and a finite lifetime when we calculate the response function with the Lanczos considering $\bar{D}^{(3)} \neq 0$. The contribution of $\bar{D}^{(4)}$ here is not negligible, as it further reduces the lifetime, deviating from the Lorentzian shape.

In FIG. 6 we report how the Raman spectrum depends on the number of iterations in the Lanczos algorithm, showing the convergence of the algorithm.

From the comparison between FIG. 6, we show how the spectrum becomes more refined as we increase the number of Lanczos iterations. Most of the changes in the spectra occur in the low-frequency region. On the other

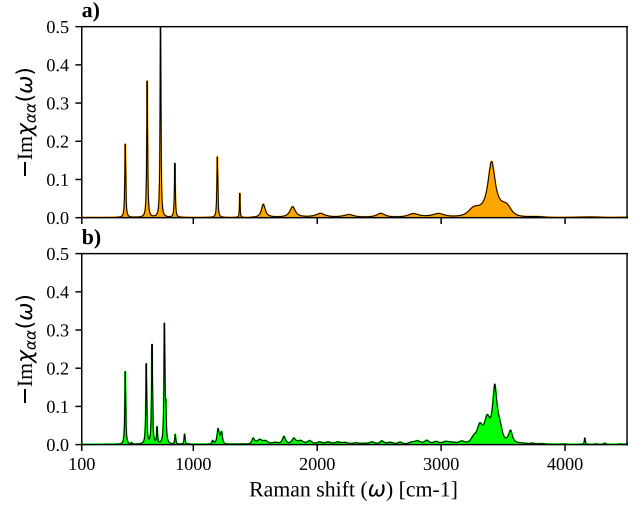


FIG. 6. Convergence of the Raman signal with the number of steps in the Lanczos chain. In panel **a** we report the Raman signal with $\bar{D}^{(4)} = 0$ and 41 Lanczos iterations. In panel **b**, we report the same signal after 200 iterations.

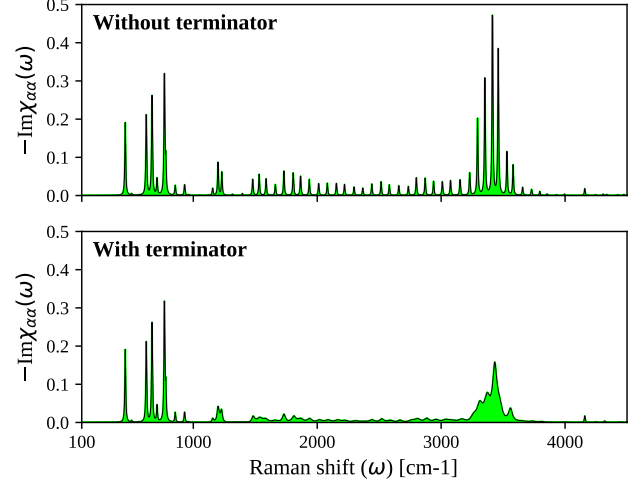


FIG. 7. Raman signal computed within the TD-SCHA Lanczos algorithm and $\bar{D}^{(4)} = 0$ after 200 iterations, with and without the terminator of Eq. (155).

side, the algorithm describes the vibron shape very well already with few iterations. The good convergence with a limited number of iteration of the algorithm is mainly due to the use of a terminator, as discussed in Sec. VI and Appendix H. In FIG. 7, we report the spectra obtained with 200 iterations with and without the terminator, displaying how it improves the convergence of the algorithm. Further details are reported in Appendix H.

Since the energy of the vibron is more than 3000 cm^{-1} , the temperature needed to populate excited states is above 4000 K. For this reason, there is no hope to sim-

ulate this lattice vibration with standard AIMD, that neglects quantum fluctuations. For this reason, previous studies on high-pressure hydrogen that neglected quantum effects reported a much more modest anharmonicity in the Raman signal[60, 61].

These results indicate that linear response of TD-SCHA can tackle complex open physical problems from first principles, providing an unprecedented precision on the evaluation of dynamical correlation functions that is sufficient to compare with experimental results[26].

VIII. CONCLUSIONS

In this work, we introduced a new time-dependent theory for lattice dynamics based on the self-consistent harmonic approximation that can be applied to real systems with a first-principle treatment of the electrons. We discussed the linear response on the static SCHA equilibrium solution of the new equations and derived an efficient algorithm that computes the response function at any frequency with a single calculation. This algorithm, with the simple knowledge of two observables of ionic positions, can compute efficiently time-correlation function, with the inclusion of thermal and quantum effects. Notably, this result is not empirical but derived from a grounded basis: the least action principle. We benchmark the theory both in a simple strongly anharmonic one-dimensional case and on phase III of solid hydrogen, a real complex molecular crystal, with *ab initio* treatment of electrons.

The theory proved to be able to accurately reproduce complex phonon line-width that arises from strong anharmonic coupling. The TD-SCHA theory paves the way to predict from first-principles the outcome of most experiments that probe the lattice dynamics, like IR and Raman spectroscopy, Neutron, and X-Ray scattering. The theory can be employed in strongly anharmonic regimes, even when quantum fluctuations are dominant and where perturbative approach fails, as in cryogenic conditions, when light ions are present, or in systems close to a second order structural phase transition, as multiferroics, charge density waves, ferroelectrics and thermoelectric materials. Moreover, TD-SCHA describes also out-of-equilibrium dynamics, enabling the study of chemical reactions with light atoms, as the proton transfer in biomolecules, and the simulation of pump-probe spectroscopies.

Appendices

A. EQUATIONS OF MOTION

In this section, we report the details of the derivation of the dynamical equation of motion in Eq. (54).

We need to cast the density matrix definition Eq. (48) into the TD-SCHA equation (Eq. 46).

First, we compute the left-hand side of the dynamical equation of motion:

$$i\hbar \frac{d}{dt} \hat{\rho}$$

where $\hat{\rho}$ is the general Gaussian density matrix defined in Eq. (48). We write the density matrix in real space $\rho(\mathbf{R}, \mathbf{R}')$.

$$\begin{aligned} \frac{1}{\rho} \frac{d\rho}{dt} = & \sum_{ab} (R_a - \mathcal{R}_a)(R_b - \mathcal{R}_b) \left[i \frac{d}{dt} C_{ab} - \frac{1}{4} \frac{d}{dt} \Theta_{ab} \right] + \\ & + \sum_{ab} (R'_a - \mathcal{R}_a)(R'_b - \mathcal{R}_b) \left[-i \frac{d}{dt} C_{ab} - \frac{1}{4} \frac{d}{dt} \Theta_{ab} \right] + \\ & + \sum_{ab} (R'_a - \mathcal{R}_a)(R_b - \mathcal{R}_b) \frac{d}{dt} A_{ab} + \\ & - \sum_{ab} (R - \mathcal{R}_a) \left[2i C_{ab} - \frac{1}{2} \Theta_{ab} + A_{ab} \right] \frac{d}{dt} \mathcal{R}_b + \\ & - \sum_{ab} (R' - \mathcal{R}_a) \left[-2i C_{ab} - \frac{1}{2} \Theta_{ab} + A_{ab} \right] \frac{d}{dt} \mathcal{R}_b + \\ & - i \sum_a (R_a - \mathcal{R}_a) \frac{dQ_a}{dt} + i \sum_a (R'_a - \mathcal{R}_a) \frac{dQ_a}{dt} + \frac{1}{N} \frac{dN}{dt} \end{aligned} \quad (168)$$

This is a polynomial in $(\mathbf{R} - \mathbf{\mathcal{R}})$ and $(\mathbf{R}' - \mathbf{\mathcal{R}})$. On the right-hand side of the TD-SCHA equation (Eq. 46) we have the Liouville operator:

$$\hat{\mathcal{H}}[\rho] \hat{\rho} - \hat{\rho} \hat{\mathcal{H}}[\rho], \quad (169)$$

where the Hamiltonian is:

$$\begin{aligned} \hat{\mathcal{H}}[\rho] = & \frac{1}{2} \sum_{ab} (R_a - \mathcal{R}_a) \left\langle \frac{d^2 V^{(\text{tot})}}{dR_a dR_b} \right\rangle_{\rho(t)} (R_b - \mathcal{R}_b) + \\ & - \sum_a \langle f_a \rangle_{\rho(t)} (R_a - \mathcal{R}_a) + \sum_a \frac{p_a^2}{2m_a}. \end{aligned} \quad (170)$$

We compute first the commutator with the kinetic operator:

$$p_a^2 \rightarrow -\hbar^2 \frac{\partial^2}{\partial R_a^2}$$

We start computing the first derivative of the R_a variable:

$$\begin{aligned} \frac{1}{\rho} \frac{d\rho}{dR_a} = & \sum_b (R_b - \mathcal{R}_b) \left[2i C_{ab} - \frac{\Theta_{ab}}{2} \right] + \\ & + \sum_b (R'_b - \mathcal{R}_b) A_{ab} - i Q_a \end{aligned} \quad (171)$$

Then, we perform the second derivative:

$$\begin{aligned}
\frac{1}{\rho} \frac{d^2 \rho}{dR_a^2} &= \sum_{bc} (R_b - \mathcal{R}_b)(R_c - \mathcal{R}_c) \left[-4C_{ab}C_{ac} + \frac{\Theta_{ab}\Theta_{ac}}{4} - iC_{ab}\Theta_{ac} - iC_{ac}\Theta_{ab} \right] + \\
&+ \sum_{bc} (R'_b - \mathcal{R}_b)(R'_c - \mathcal{R}_c) A_{ab}A_{ac} + \sum_{bc} (R_b - \mathcal{R}_b)(R'_c - \mathcal{R}_c) (4iC_{ab}A_{ac} - \Theta_{ab}A_{ac}) + \\
&+ \sum_b (R_b - \mathcal{R}_b)(4C_{ab}Q_a + iQ_a\Theta_{ab}) - \sum_b (R'_b - \mathcal{R}_b)2iA_{ab}Q_a - Q_a^2 + 2iC_{aa} - \frac{1}{2}\Theta_{aa} \quad (172)
\end{aligned}$$

If we change the derivative of R with R' (that is obtained from $\hat{\rho}\hat{\mathcal{H}}[\rho]$), we get the complex conjugate of Eq. (172) where R and R' variables exchanged.

Therefore, we collect all the terms in Eq. (168) and Eq. (169) quadratic in \mathbf{R} , i.e. the coefficients of $\sum_{ab}(R_a - \mathcal{R}_a)(R_b - \mathcal{R}_b)$.

$$\begin{aligned}
i\hbar \left(i \frac{dC_{ab}}{dt} - \frac{1}{4} \frac{d\Theta_{ab}}{dt} \right) &= -\frac{1}{2} \left\langle \frac{d^2 V^{(\text{tot})}}{dR_a dR_b} \right\rangle_\rho + \\
&- \sum_c \frac{\hbar^2}{2m_c} \left[4C_{ac}C_{cb} - \frac{1}{4}\Theta_{ac}\Theta_{cb} + \right. \\
&\left. + 2iC_{ac}\Theta_{cb} + A_{ac}A_{bc} \right] \quad (173)
\end{aligned}$$

We can split the imaginary and real part to get the first two equation of motion for \mathbf{C} and $\mathbf{\Theta}$:

$$\begin{aligned}
\frac{dC_{ab}}{dt} &= \frac{1}{2\hbar} \left\langle \frac{d^2 V}{dR_a dR_b} \right\rangle_\rho + \sum_c \frac{\hbar}{2m_c} \left[4C_{ac}C_{cb} + \right. \\
&\left. - \frac{1}{4}\Theta_{ac}\Theta_{cb} + \text{Re}[A_{ac}A_{bc}] \right] \quad (174)
\end{aligned}$$

$$\begin{aligned}
\frac{d\Theta_{ab}}{dt} &= \sum_c \frac{2\hbar}{m_c} (C_{ac}\Theta_{cb} + C_{bc}\Theta_{ca} + \text{Im}[A_{ac}A_{bc}]) \\
&\quad (175)
\end{aligned}$$

We now consider the equality between Eq. (168) and (169) of the coefficient that multiplies $(\mathbf{R} - \mathcal{R})(\mathbf{R}' - \mathcal{R})$.

$$\begin{aligned}
i\hbar \frac{dA_{ab}}{dt} &= \sum_c \frac{\hbar^2}{2m_c} [4iC_{ac}A_{cb} + 4iC_{bc}A_{ac} + \\
&- \Theta_{ac}A_{cb} + \Theta_{bc}A_{ac}] \quad (176)
\end{aligned}$$

We can split also this equation in real and imaginary part:

$$\begin{aligned}
\text{Re} \frac{dA_{ab}}{dt} &= \sum_c \frac{\hbar}{2m_c} (4C_{ac}\text{Re}A_{cb} + 4C_{bc}\text{Re}A_{ca} + \\
&- \Theta_{ac}\text{Im}A_{cb} + \Theta_{bc}\text{Im}A_{ac}) \quad (177)
\end{aligned}$$

$$\begin{aligned}
\text{Im} \frac{dA_{ab}}{dt} &= \sum_c \frac{\hbar}{2m_c} [4C_{ac}\text{Im}A_{cb} + 4C_{bc}\text{Im}A_{ac} + \\
&+ \Theta_{ac}\text{Re}A_{cb} - \Theta_{bc}\text{Re}A_{ac}] \quad (178)
\end{aligned}$$

The last two equations for \mathbf{Q} and \mathcal{R} are obtained from the real and imaginary part of the terms linear in \mathbf{R}

$$\begin{aligned}
-i\hbar \sum_b \left(2iC_{ab} - \frac{1}{2}\Theta_{ab} + A_{ab} \right) \frac{d\mathcal{R}_b}{dt} - \hbar \frac{dQ_a}{dt} &= \\
= \sum_c \frac{\hbar^2}{2m_c} (4C_{ca}Q_c + iQ_c\Theta_{ca} - 2iA_{ca}Q_c) - \langle f_a^{(\text{tot})} \rangle \quad (179)
\end{aligned}$$

Separating real and imaginary parts we get:

$$\begin{aligned}
\sum_b (2C_{ab} + \text{Im}A_{ab}) \frac{d\mathcal{R}_b}{dt} - \frac{dQ_a}{dt} &= \\
= \sum_b \frac{\hbar}{m_b} (2C_{ab} + \text{Im}A_{ab}) Q_b - \frac{\langle f_a^{(\text{tot})} \rangle}{\hbar} \quad (180)
\end{aligned}$$

$$\begin{aligned}
\sum_b \hbar \left(\frac{1}{2}\Theta_{ab} - \text{Re}A_{ab} \right) \frac{d\mathcal{R}_b}{dt} &= \\
= \sum_b \frac{\hbar^2}{2m_b} (\Theta_{ab} - 2\text{Re}A_{ab}) Q_b \quad (181)
\end{aligned}$$

Simplifying we get the last equations:

$$\frac{d\mathcal{R}_a}{dt} = \frac{\hbar Q_a}{m_a} \quad (182)$$

$$\frac{dQ_a}{dt} = \frac{\langle f_a \rangle}{\hbar} \quad (183)$$

The last term of the equivalence between Eq. (168) and (169) is the term that does depend in neither $(\mathbf{R} - \mathcal{R})$ nor $(\mathbf{R}' - \mathcal{R})$. This last equation expresses the time evolution for the norm $N(t)$, and it is just the conservation of the density matrix normalization.

The final equations of motion are obtained substituting the expression of $\mathbf{\Upsilon}$ (Eq. 50) and dividing for the masses to obtain the mass-rescaled matrices (Eq. 53). The convenience of rescaling the masses is that we can express all the summations as standard rows-by-columns products.

B. ENERGY CONSERVATION

Here, we calculate the time derivative of the average potential (Eq. 66), showing that it balances the time derivative of the average kinetic energy, proving that the total energy is conserved by the equation of motions.

For this purpose, we use formalism introduced by Bianco et al[33] (appendix C, Eq. C1): given an observable $O(\mathbf{R})$, the average of its derivative can be written as:

$$\left\langle \frac{dO}{dR_a} \right\rangle_\rho = \sum_b \Upsilon_{ab} \langle (R_b - \mathcal{R}_b) O \rangle_\rho \quad (184)$$

For this reason, we can write:

$$\sum_{ab} \frac{d\mathcal{R}_b}{dt} \Upsilon_{ab} \langle (R_a - \mathcal{R}_a) V \rangle_\rho = - \sum_b \frac{d\mathcal{R}_b}{dt} \langle f_a(\mathbf{R}) \rangle_\rho \quad (185)$$

For simplicity, we define $\mathbf{u} = (\mathbf{R} - \mathcal{R})$. The other term of Eq. (66) is

$$\begin{aligned} \sum_{ab} \langle u_a u_b V \rangle_\rho \frac{1}{2} \frac{d\Upsilon_{ab}}{dt} &= \sum_{abcd} \langle u_c u_b V \rangle_\rho \Upsilon_{cd} \Upsilon_{da}^{-1} \frac{1}{2} \frac{d\Upsilon_{ab}}{dt} \\ &= \sum_{abd} \left\langle \frac{d(u_b V)}{dR_d} \right\rangle_\rho \Upsilon_{da}^{-1} \frac{1}{2} \frac{d\Upsilon_{ab}}{dt} \end{aligned} \quad (186)$$

The derivative gives:

$$\begin{aligned} \sum_{ab} \langle u_a u_b V \rangle_\rho \frac{1}{2} \frac{d\Upsilon_{ab}}{dt} &= \sum_{ab} \langle V \rangle_\rho \Upsilon_{ba}^{-1} \frac{1}{2} \frac{d\Upsilon_{ab}}{dt} + \\ &+ \sum_{abd} \left\langle u_b \frac{dV}{dR_d} \right\rangle_\rho \Upsilon_{da}^{-1} \frac{1}{2} \frac{d\Upsilon_{ab}}{dt} \end{aligned} \quad (187)$$

The first term is zero, because:

$$\sum_{ab} \Upsilon_{ba}^{-1} \frac{d\Upsilon_{ab}}{dt} = \frac{1}{2} \frac{d}{dt} \text{Tr} [\Upsilon^{-1} \Upsilon] = 0 \quad (188)$$

While for the second term we can proceed again:

$$\sum_{ab} \langle u_a u_b V \rangle_\rho \frac{1}{2} \frac{d\Upsilon_{ab}}{dt} = \sum_{abcde} \left\langle u_e \frac{dV}{dR_d} \right\rangle_\rho \Upsilon_{ec} \Upsilon_{cb}^{-1} \Upsilon_{da}^{-1} \frac{1}{2} \frac{d\Upsilon_{ab}}{dt} \quad (189)$$

$$\sum_{ab} \langle u_a u_b V \rangle_\rho \frac{1}{2} \frac{d\Upsilon_{ab}}{dt} = \sum_{abcd} \left\langle \frac{d^2 V}{dR_c dR_d} \right\rangle_\rho \Upsilon_{cb}^{-1} \Upsilon_{da}^{-1} \frac{1}{2} \frac{d\Upsilon_{ab}}{dt} \quad (190)$$

Introducing the mass re-scaled for Υ^{-1} :

$$\tilde{\Upsilon}_{ab}^{-1} = \sqrt{m_a m_b} \Upsilon_{ab}^{-1}, \quad (191)$$

we get the final equivalence:

$$\frac{1}{2} \text{Tr} \left[\langle \mathbf{u} \otimes \mathbf{u} V \rangle_\rho \frac{d\Upsilon}{dt} \right] = \frac{1}{2} \text{Tr} \left[\left\langle \frac{d^2 V}{d\tilde{\mathbf{R}} d\tilde{\mathbf{R}}} \right\rangle_\rho \tilde{\Upsilon}^{-1} \tilde{\Upsilon}^{-1} \frac{d\tilde{\Upsilon}}{dt} \right]. \quad (192)$$

Substituting Eq. (185) and (192) into Eq. (66), and substituting the equation of motion, it is easy to show that

$$\frac{d}{dt} \langle \hat{K} \rangle_{\rho(t)} = - \frac{d}{dt} \langle \hat{V} \rangle_{\rho(t)}$$

C. LEAST ACTION

Here, we prove that for a Gaussian pure state expressed in Eq. (40), the action (Eq. 41) with the TD-SCHA dynamics is stationary.

First we break the action in three parts: kinetic, potential, and time:

$$A_1 = \frac{1}{t_2 - t_1} \int_{t_1}^{t_2} dt \langle \psi(t) | \hat{K} | \psi(t) \rangle \quad (193)$$

$$A_2 = \frac{1}{t_2 - t_1} \int_{t_1}^{t_2} dt \langle \psi(t) | V(\hat{\mathbf{r}}^{\text{tot}}) | \psi(t) \rangle \quad (194)$$

$$A_3 = - \frac{i}{\hbar} \frac{1}{t_2 - t_1} \int_{t_1}^{t_2} dt \langle \psi(t) | \frac{d}{dt} | \psi(t) \rangle \quad (195)$$

by substituting Eq. (40) in Eq. (193), (194) and (195), we get:

$$A_1 = \frac{\hbar^2}{t_2 - t_1} \int_{t_1}^{t_2} dt \left\{ \sum_a \frac{Q_a^2}{2m_a} + \text{Tr} \left[\frac{\tilde{\Upsilon}}{8} + 2\tilde{C}_{ab} \tilde{\Upsilon}^{-1} \tilde{C} \right] \right\} \quad (196)$$

From which the derivatives of the action are:

$$\frac{\delta A_1}{\delta \tilde{C}} = 2\hbar^2 \tilde{\Upsilon}^{-1} \tilde{C} + 2\hbar^2 \tilde{C} \tilde{\Upsilon}^{-1} \quad (197)$$

$$\frac{\delta A_1}{\delta Q_a} = \frac{\hbar^2 Q_a}{m_a} \quad \frac{\delta A_1}{\delta \mathcal{R}} = 0 \quad (198)$$

$$\frac{\delta A_1}{\delta \tilde{\Upsilon}_{ab}} = - \frac{\hbar^2}{8} \sum_{hk} \tilde{\Upsilon}_{ch} \tilde{\Upsilon}_{ck} \frac{\partial \tilde{\Upsilon}_{hk}^{-1}}{\partial \tilde{\Upsilon}_{ab}} + 2\hbar^2 \sum_{cde} \tilde{C}_{cd} \frac{\partial \tilde{\Upsilon}_{de}^{-1}}{\partial \tilde{\Upsilon}_{ab}} \tilde{C}_{ec} \quad (199)$$

In the same way A_2 :

$$\frac{\delta A_2}{\delta \Upsilon_{ab}} = \frac{1}{2} \sum_{cd} \frac{\partial \Upsilon_{cd}^{-1}}{\partial \Upsilon_{ab}} \left\langle \frac{\partial^2 V^{(\text{tot})}}{\partial R_c \partial R_d} \right\rangle_\rho \quad (200)$$

$$\frac{\delta A_2}{\delta \mathcal{R}_a} = - \left\langle f_a^{(\text{tot})} \right\rangle_\rho \quad (201)$$

$$\frac{\delta A_2}{\delta Q_a} = \frac{\delta A_2}{\delta C_{ab}} = 0 \quad (202)$$

And for A_3 :

$$\frac{\delta A_3}{\delta Q_a} = \hbar \frac{d\mathcal{R}_a}{dt} \quad (203)$$

$$\frac{\delta A_3}{\delta \mathcal{R}_a} = -\hbar \frac{dQ_a}{dt} \quad (204)$$

$$\frac{\delta A_3}{\delta C_{ab}} = -\hbar \sum_{cd} \frac{\partial \Upsilon_{ab}^{-1}}{\partial \Upsilon_{cd}} \frac{d\Upsilon_{cd}}{dt} \quad (205)$$

$$\frac{\delta A_3}{\delta \Upsilon_{ab}} = \hbar \sum_{cd} \frac{\partial \Upsilon_{cd}^{-1}}{\partial \Upsilon_{ab}} \frac{dC_{cd}}{dt} \quad (206)$$

By imposing that:

$$\delta A = \delta A_1 + \delta A_2 + \delta A_3 = 0$$

we get the equation of motion.

$$\begin{aligned} \frac{\delta A}{\delta Q} &= 0 \\ \frac{d\mathcal{R}_a}{dt} &= \frac{\hbar Q_a}{m_a} \end{aligned} \quad (207)$$

$$\begin{aligned} \frac{\delta A}{\delta \mathcal{R}} &= 0 \\ \frac{dQ_a}{dt} &= \frac{1}{\hbar} \left\langle f_a^{(tot)} \right\rangle_{\rho(t)} \end{aligned} \quad (208)$$

Indeed, Eq. (208) is equal to Eq. (54a). We can proceed to get the equations for \mathbf{C} and $\mathbf{\Upsilon}$. To proceed, we need to remove the $\partial \Upsilon^{-1} / \partial \Upsilon$ tensor:

$$\frac{\partial \Upsilon_{cd}^{-1}}{\partial \Upsilon_{ab}} = -\frac{1}{2} \Upsilon_{ac}^{-1} \Upsilon_{bd}^{-1} - \frac{1}{2} \Upsilon_{cb}^{-1} \Upsilon_{ad}^{-1} \quad (209)$$

$$\frac{\delta A}{\delta C_{ab}} = 0$$

$$\frac{d\tilde{\mathbf{\Upsilon}}}{dt} = 2\hbar (\tilde{\mathbf{\Upsilon}}\tilde{\mathbf{C}} + \tilde{\mathbf{C}}\tilde{\mathbf{\Upsilon}}) \quad (210)$$

Eq. (210) is equal to Eq. (54b) if we set $\mathbf{A} = 0$.

Lastly,

$$\begin{aligned} \frac{\delta A}{\delta \Upsilon_{ab}} &= 0 \\ \frac{d\tilde{\mathbf{C}}}{dt} &= \frac{1}{2\hbar} \left\langle \frac{\partial^2 V}{\partial \tilde{\mathbf{R}} \partial \tilde{\mathbf{R}}} \right\rangle_{\rho} - \frac{\hbar}{8} \tilde{\mathbf{\Upsilon}}\tilde{\mathbf{\Upsilon}} + 2\hbar \tilde{\mathbf{C}}\tilde{\mathbf{C}} \end{aligned} \quad (211)$$

Indeed, also in this case, Eq. (211) is equal to Eq. (54e) if we set $\mathbf{A} = 0$.

Therefore, we found that the dynamical equations for obtained with the least action principle coincides with those obtained from the TD-SCHA.

D. EQUILIBRIUM

Here we show that, among all possible stationary solutions, the one that minimizes the functional:

$$F = E - TS$$

is the SCHA solution, i.e. the one where temperature is uniform on all the degrees of freedom.

Since we are in a stationary solution, we can write everything in the basis of \mathbf{e}_{μ} vectors that diagonalizes the $\mathbf{\Upsilon}$, \mathbf{A} and $\left\langle \partial^2 V / \partial \tilde{\mathbf{R}}^2 \right\rangle_{\rho}$.

The F functional is:

$$F[\hat{\rho}] = \left\langle \hat{K} + \hat{V} \right\rangle_{\hat{\rho}} - TS[\hat{\rho}] \quad (212)$$

The average of the kinetic energy (Eq. 63) is:

$$\left\langle \hat{K} \right\rangle_{\hat{\rho}} = \frac{\hbar^2}{2} \sum_{\mu} \left(\frac{\tilde{\Upsilon}_{\mu}}{4} + \tilde{A}_{\mu} \right) \quad (213)$$

Substituting Eq. (77), we get:

$$\left\langle \hat{K} \right\rangle_{\hat{\rho}} = \sum_{\mu} \frac{\hbar \omega_{\mu} (2n_{\mu} + 1)}{4} \quad (214)$$

The entropy $S[\hat{\rho}]$ can be obtained as the sum of the entropies of the Harmonic oscillators on the μ modes:

$$S = \frac{k_b}{2} \sum_{\mu} \left[\frac{\beta_{\mu} \hbar \omega_{\mu}}{\tanh \frac{\beta_{\mu} \hbar \omega_{\mu}}{2}} - 2 \log \left(\sinh \frac{\beta_{\mu} \hbar \omega_{\mu}}{2} \right) \right] \quad (215)$$

We must impose that

$$\frac{\partial F}{\partial \beta_{\mu}} = 0 \quad (216)$$

$$\frac{\partial \langle \hat{K} \rangle}{\partial \beta_{\mu}} + \frac{\partial \langle \hat{V} \rangle}{\partial \beta_{\mu}} - T \frac{\partial S}{\partial \beta_{\mu}} = 0 \quad (217)$$

$$\frac{\partial \langle \hat{K} \rangle}{\partial \beta_{\mu}} = -\frac{\hbar^2 \omega_{\mu}^2}{8 \sinh^2 \left(\frac{\beta_{\mu} \hbar \omega_{\mu}}{2} \right)} \quad (218)$$

The derivative of the average of the potential can be computed exploiting the formalism introduced by Bianco et al.[33]. In particular, they showed that the derivative of any observable with respect to a the quantum fluctuations is:

$$\frac{\partial \langle V(\mathbf{R}) \rangle_{\rho}}{\partial \Upsilon_{\mu}} = \frac{1}{2} \sum_{ab} \frac{\partial \Upsilon_{ab}^{-1}}{\partial \Upsilon_{\mu}} \left\langle \frac{\partial^2 V}{\partial \tilde{R}_a \partial \tilde{R}_b} \right\rangle_{\rho} \quad (219)$$

We can write it in the polarization basis (exploiting Eq. (77):

$$\frac{\partial \langle V(\mathbf{R}) \rangle_{\rho}}{\partial \Upsilon_{\mu}} = -\frac{1}{2} \tilde{\Upsilon}_{\mu}^{-2} \omega_{\mu}^2 \quad (220)$$

From which we get the average of the potential:

$$\frac{\partial \langle V(\mathbf{R}) \rangle_\rho}{\partial \beta_\mu} = - \frac{\hbar^2 \omega_\mu^2}{8 \sinh^2 \left(\frac{\beta_\mu \hbar \omega_\mu}{2} \right)} \quad (221)$$

While the derivative of the entropy is:

$$\frac{\partial S}{\partial \beta_\mu} = - \frac{\beta_\mu \hbar^2 \omega_\mu^2 k_b}{4 \sinh^2 \left(\frac{\beta_\mu \hbar \omega_\mu}{2} \right)} \quad (222)$$

Putting all together we get:

$$\frac{2\hbar^2 \omega_\mu^2 - k_b T 2\beta_\mu \hbar^2 \omega_\mu^2}{8 \sinh^2 \left(\frac{\beta_\mu \hbar \omega_\mu}{2} \right)} = 0 \quad (223)$$

And we get the condition that β_μ must satisfy to minimize the free energy:

$$\beta_\mu = \frac{1}{k_b T} \quad (224)$$

E. DERIVATION OF THE LINEAR RESPONSE SYSTEM

Here, we apply perturbation theory on the TD-SCHA equations for small perturbations. Since we are expanding around equilibrium solutions, we have:

$$\mathbf{C} = 0 \quad \mathbf{Q} = 0 \quad \text{Im}\mathbf{A} = 0 \quad (225)$$

When $t \geq t_0$, we add an external time dependent perturbation to the non interacting potential:

$$V(\mathbf{R}, t) = V^{(0)}(\mathbf{R}) + V^{(1)}(\mathbf{R}, t) \quad (226)$$

And we want to study the dynamics of the system close to equilibrium. This perturbation affects the dynamics (Eq. 54) only in the two averages:

$$\langle f_a \rangle_\rho \quad \left\langle \frac{d^2 V}{dR_a dR_b} \right\rangle_\rho \quad (227)$$

We indicate with $^{(1)}$ the perturbed quantities. If omitted, we refer to static quantities.

Since the perturbation changes the parameters of the density matrix, they also change the ionic probability distribution:

$$\rho(\mathbf{R}, t) = \rho(\mathbf{R}) + \rho^{(1)}(\mathbf{R}, t) \quad (228)$$

This affect also the generic average over an observable:

$$\langle O(\mathbf{R}) \rangle_{\rho(t)} = \langle O(\mathbf{R}) \rangle_\rho + \left\langle O^{(0)}(\mathbf{R}) \right\rangle_{\rho^{(1)}} \quad (229)$$

By expanding the probability distribution $\rho^{(1)}(\mathbf{R}, t)$ as a function of the perturbed centroid position $\mathbf{R}^{(1)}$ and

the perturbed fluctuations $\Upsilon^{(1)}$, we get:

$$\langle O \rangle_{\rho^{(1)}} = \frac{1}{2} \sum_{ab} \left[\Upsilon_{ab} \left(\langle O u_a \rangle_\rho \mathcal{R}_b^{(1)} + \mathcal{R}_a^{(1)} \langle O u_b \rangle_\rho \right) + \right. \\ \left. - \Upsilon_{ab}^{(1)} \langle u_a u_b O \rangle_\rho \right] \quad (230)$$

where u is the displacement with respect to the equilibrium centroid. In particular, we are interested in the averages of forces and second derivative of the BO potential:

$$\left\langle \frac{dV}{dR_a} \right\rangle_{\rho^{(1)}} = \frac{1}{2} \sum_{hk} \left[\Upsilon_{hk} \left\langle \frac{dV}{dR_a} u_h \right\rangle_\rho \mathcal{R}_k^{(1)} + \right. \\ \left. + \Upsilon_{hk} \mathcal{R}_h^{(1)} \left\langle \frac{dV}{dR_a} u_k \right\rangle_\rho - \Upsilon_{hk}^{(1)} \left\langle u_h u_k \frac{dV}{dR_a} \right\rangle_\rho \right] \quad (231)$$

Using the definition of the 3 and 4 phonon scattering tensor $\Phi^{(3)}$ and $\Phi^{(4)}$ (ref.[33]), we have:

$$\Phi_{ab} = \sum_p \Upsilon_{ap} \left\langle u_p \frac{dV}{dR_b} \right\rangle_\rho \quad (232)$$

$$\Phi_{abc}^{(3)} = \sum_{pq} \Upsilon_{ap} \Upsilon_{bq} \left\langle u_p u_q \frac{dV}{dR_c} \right\rangle_\rho \quad (233)$$

$$\Phi_{abcd}^{(4)} = \sum_{pqr} \Upsilon_{ap} \Upsilon_{bq} \Upsilon_{cr} \left\langle u_p u_q u_r \frac{dV}{dR_d} \right\rangle_\rho \quad (234)$$

Thus we have:

$$\left\langle \frac{dV}{dR_a} \right\rangle_{\rho^{(1)}} = -\frac{1}{2} \sum_{hkpqrs} \Upsilon_{hk}^{(1)} \Upsilon_{kp}^{-1} \Upsilon_{ps} \Upsilon_{hq}^{-1} \Upsilon_{qr} \left\langle u_r u_s \frac{dV}{dR_a} \right\rangle_\rho + \\ + \sum_h \Phi_{ah} \mathcal{R}_h^{(1)} \quad (235)$$

$$\left\langle \frac{d^2 V}{dR_a dR_b} \right\rangle_{\rho^{(1)}} = \sum_h \Phi_{ah} \mathcal{R}_h^{(1)} - \frac{1}{2} \sum_{hkpq} \Upsilon_{hk}^{(1)} \Upsilon_{kp}^{-1} \Upsilon_{hq}^{-1} \Phi_{qpa}^{(3)} \quad (236)$$

To simplify notation, in the rest of this section we use the convention:

$$\langle \cdot \rangle = \langle \cdot \rangle_\rho$$

in an analogous way we can get the other term of the perturbation:

$$\left\langle \frac{d^2 V}{dR_a dR_b} \right\rangle_{\rho^{(1)}} = \frac{1}{2} \sum_{hk} \left[\Upsilon_{hk} \left\langle \frac{d^2 V}{dR_a dR_b} u_h \right\rangle_\rho \mathcal{R}_k^{(1)} + \right. \\ \left. + \Upsilon_{hk} \mathcal{R}_h^{(1)} \left\langle \frac{d^2 V}{dR_a dR_b} u_k \right\rangle_\rho + \right. \\ \left. - \Upsilon_{hk}^{(1)} \left\langle u_h u_k \frac{d^2 V}{dR_a dR_b} \right\rangle_\rho \right] \quad (237)$$

Using the Bianco formalism introduced in Eq. (184), we get:

$$\left\langle \frac{d^2 V}{dR_a dR_b} \right\rangle_{\rho^{(1)}} = -\frac{1}{2} \sum_{hkpq} \Upsilon_{kp}^{-1} \Upsilon_{hq}^{-1} \Phi_{abpq}^{(4)} \Upsilon_{hk}^{(1)} + \sum_h \Phi_{abh}^{(3)} \mathcal{R}_h^{(1)} \quad (238)$$

We can derive now the explicit expression of all the perturbed equation of motion:

$$m_a \ddot{\mathcal{R}}_a^{(1)} = \langle f_a^{(1)} \rangle - \sum_h \Phi_{ah} \mathcal{R}_h^{(1)} + \frac{1}{2} \sum_{hkpq} \Upsilon_{hk}^{(1)} \Upsilon_{kp}^{-1} \Upsilon_{hq}^{-1} \Phi_{qpa}^{(3)} \quad (239)$$

$$\begin{aligned} \dot{\Upsilon}_{ab}^{(1)} = \sum_c \frac{\hbar}{m_c} \left[\Upsilon_{cb} (2C_{ac}^{(1)} - \text{Im}A_{ac}^{(1)}) + \Upsilon_{ac} (2C_{cb}^{(1)} + \right. \\ \left. + \text{Im}A_{cb}^{(1)}) + \text{Im}A_{cb}^{(1)} \text{Re}A_{ac} - \text{Im}A_{ac}^{(1)} \text{Re}A_{cb} \right] \quad (240) \end{aligned}$$

$$\begin{aligned} \text{Im}A_{ab}^{(1)} = \sum_c \frac{\hbar}{2m_c} \left(\Theta_{ac}^{(1)} \text{Re}A_{cb} + \right. \\ \left. - \Theta_{bc}^{(1)} \text{Re}A_{ac} + \Theta_{ac} \text{Re}A_{cb}^{(1)} - \Theta_{bc} \text{Re}A_{ac}^{(1)} \right) \quad (241) \end{aligned}$$

$$\begin{aligned} \text{Re}A_{ab}^{(1)} = \sum_c \frac{\hbar}{2m_c} \left(4C_{ac}^{(1)} \text{Re}A_{cb} + 4C_{bc}^{(1)} \text{Re}A_{ca} + \right. \\ \left. - \Theta_{ac} \text{Im}A_{cb}^{(1)} + \Theta_{bc} \text{Im}A_{ac}^{(1)} \right) \quad (242) \end{aligned}$$

$$\begin{aligned} \dot{C}_{ab}^{(1)} = \frac{1}{2\hbar} \left\langle \frac{d^2 V^{(1)}}{dR_a dR_b} \right\rangle + \frac{1}{2\hbar} \sum_h \Phi_{abh}^{(3)} \mathcal{R}_h^{(1)} + \\ - \frac{1}{4\hbar} \sum_{hkpq} \Upsilon_{kp}^{-1} \Upsilon_{hq}^{-1} \Phi_{abpq}^{(4)} \Upsilon_{hk}^{(1)} + \\ + \sum_c \frac{\hbar}{2m_c} \left(-\frac{1}{4} \Theta_{ac}^{(1)} \Theta_{cb} - \frac{1}{4} \Theta_{ac} \Theta_{cb}^{(1)} + \right. \\ \left. + \text{Re}A_{ac} \text{Re}A_{bc}^{(1)} + \text{Re}A_{ac}^{(1)} \text{Re}A_{bc} \right) \quad (243) \end{aligned}$$

$$\Theta_{ab}^{(1)} = \Upsilon_{ab}^{(1)} + 2\text{Re}A_{ab}^{(1)} \quad (244)$$

We can remove the theta dependence on $\text{Im}\dot{\mathbf{A}}$ and $\dot{\mathbf{C}}$:

$$\begin{aligned} \text{Im}A_{ab}^{(1)} = \sum_c \frac{\hbar}{2m_c} \left(\text{Re}A_{cb} \Upsilon_{ac}^{(1)} - \text{Re}A_{ac} \Upsilon_{bc}^{(1)} + \right. \\ \left. + \text{Re}A_{cb}^{(1)} \Upsilon_{ac} - \text{Re}A_{ac}^{(1)} \Upsilon_{bc} \right) \quad (245) \end{aligned}$$

$$\begin{aligned} \dot{C}_{ab}^{(1)} = \frac{1}{2\hbar} \left\langle \frac{d^2 V^{(1)}}{dR_a dR_b} \right\rangle + \frac{1}{2\hbar} \sum_h \Phi_{abh}^{(3)} \mathcal{R}_h^{(1)} + \\ - \frac{1}{4\hbar} \sum_{hkpq} \Upsilon_{kp}^{-1} \Upsilon_{hq}^{-1} \Phi_{abpq}^{(4)} \Upsilon_{hk}^{(1)} + \\ + \sum_c \frac{\hbar}{8m_c} \left(2\text{Re}A_{ac} \Upsilon_{cb}^{(1)} + 2\text{Re}A_{cb} \Upsilon_{ac}^{(1)} + \right. \\ \left. + 2\text{Re}A_{ac}^{(1)} \Upsilon_{cb} + 2\text{Re}A_{cb}^{(1)} \Upsilon_{ac} - \Upsilon_{ac} \Upsilon_{cb}^{(1)} - \Upsilon_{cb} \Upsilon_{ac}^{(1)} \right) \quad (246) \end{aligned}$$

By further deriving $\dot{\Upsilon}^{(1)}$ and $\text{Re}\dot{\mathbf{A}}^{(1)}$ we delete two variables from the equations (\mathbf{C} and $\text{Im}\mathbf{A}$). And arrive to the final system of Eq. (81).

The $\overset{(3)}{\mathbf{D}}$ and $\overset{(4)}{\mathbf{D}}$ terms are obtained from the $\overset{(3)}{\Phi}$ and $\overset{(4)}{\Phi}$ when transforming in the mass-rescaled variables.

$$\overset{(3)}{D}_{abc} = \frac{\overset{(3)}{\Phi}_{abc}}{\sqrt{m_a m_b m_c}} \quad (247)$$

$$\overset{(4)}{D}_{abcd} = \frac{\overset{(4)}{\Phi}_{abcd}}{\sqrt{m_a m_b m_c m_d}} \quad (248)$$

F. FULL EXPRESSION OF THE LINEAR PERTURBATION SYSTEM

Here we report the full expressions of the 2,3,4-rank tensors that define the linear response system of the TD-SCHA. These are obtained writing the full expression of the system as derived in appendix E. These are expressed in the polarization basis, i.e. the basis that diagonalizes the SCHA dynamical matrix at equilibrium:

$$\bar{X}_{\mu\nu\eta\lambda} = -\frac{\hbar(2n_\eta+1)(2n_\lambda+1)(2\omega_\mu n_\nu+2\omega_\nu n_\mu+\omega_\mu+\omega_\nu)^{(4)}}{4(2n_\mu+1)(2n_\nu+1)\omega_\eta\omega_\lambda} D_{\mu\nu\eta\lambda} - \frac{\delta_{\mu\eta}\delta_{\nu\lambda}+\delta_{\mu\lambda}\delta_{\nu\eta}}{2} \left(\omega_\mu^2 + \omega_\nu^2 + \frac{2\omega_\mu\omega_\nu}{(2n_\mu+1)(2n_\nu+1)} \right) \quad (249)$$

$$\begin{aligned} \bar{X}'_{\mu\nu\eta\lambda} = & -\frac{\hbar[\omega_\mu n_\mu(n_\mu+1)(2n_\nu+1)+\omega_\nu n_\nu(n_\nu+1)(2n_\mu+1)](2n_\eta+1)(2n_\lambda+1)^{(4)}}{4(2n_\mu+1)(2n_\nu+1)\omega_\eta\omega_\lambda} D_{\mu\nu\eta\lambda} + \\ & -\left(\frac{\delta_{\mu\eta}\delta_{\nu\lambda}+\delta_{\mu\lambda}\delta_{\nu\eta}}{2} \right) \frac{(2n_\mu n_\nu+n_\mu+n_\nu)(2n_\mu n_\nu+n_\mu+n_\nu+1)2\omega_\mu\omega_\nu}{(2n_\mu+1)(2n_\nu+1)} \end{aligned} \quad (250)$$

$$\bar{Y}_{\mu\nu\eta\lambda} = -\frac{4(\delta_{\mu\eta}\delta_{\nu\lambda}+\delta_{\mu\lambda}\delta_{\nu\eta})\omega_\mu\omega_\nu}{(2n_\mu+1)(2n_\nu+1)} \quad (251)$$

$$\begin{aligned} \bar{Y}'_{\mu\nu\eta\lambda} = & \frac{\delta_{\mu\eta}\delta_{\nu\lambda}+\delta_{\mu\lambda}\delta_{\nu\eta}}{2} \cdot \\ & \cdot \left(\frac{2\omega_\mu\omega_\nu}{(2n_\mu+1)(2n_\nu+1)} - \omega_\mu^2 - \omega_\nu^2 \right) \end{aligned} \quad (252)$$

$$\bar{Z}_{\mu\nu\eta} = \frac{2[(2n_\mu+1)\omega_\nu+(2n_\nu+1)\omega_\mu]^{(3)}}{\hbar(2n_\mu+1)(2n_\nu+1)} D_{\mu\nu\eta} \quad (253)$$

$$\begin{aligned} \bar{Z}'_{\mu\nu\eta} = & \frac{2\omega_\mu n_\mu(n_\mu+1)(2n_\nu+1)^{(3)}}{\hbar(2n_\mu+1)(2n_\nu+1)} D_{\mu\nu\eta} + \\ & + \frac{2\omega_\nu n_\nu(n_\nu+1)(2n_\mu+1)^{(3)}}{\hbar(2n_\mu+1)(2n_\nu+1)} D_{\mu\nu\eta} \end{aligned} \quad (254)$$

$$\bar{X}''_{\mu\nu\eta} = \frac{\hbar^2(2n_\nu+1)(2n_\eta+1)^{(3)}}{8\omega_\nu\omega_\eta} D_{\mu\nu\eta} \quad (255)$$

$$\bar{Z}''_{\mu\nu} = -\delta_{\mu\nu}\omega_\mu^2 \quad (256)$$

G. PROOF OF THE DYNAMICAL ANSATZ

In this appendix we proof that the self-energy calculated from the TD-SCHA in Eq. (118) correspond to the dynamical *ansatz* proposed by Bianco et al.[33], reported in Eq. (119).

Our expression for the self-energy is:

$$\begin{aligned} \Sigma(\omega) = & -\bar{X}''[(\bar{X}+\omega^2)-\bar{Y}(\bar{Y}'+\omega^2)^{-1}\bar{X}']^{-1} \cdot \\ & \cdot [\bar{Z}-\bar{Y}(\bar{Y}'+\omega^2)^{-1}\bar{Z}'] \end{aligned} \quad (257)$$

To simplify the expression, we define the tensor \mathbf{U} , \mathbf{P} and \mathbf{T} , that in the polarization basis are:

$$\bar{X}''_{\alpha\beta\gamma} = U_{\alpha\beta} D_{\alpha\beta\gamma}^{(3)} \quad (258)$$

$$\mathbf{P} = (\bar{X}+\omega^2) - \bar{Y}(\bar{Y}'+\omega^2)^{-1}\bar{X}' \quad (259)$$

$$T_{\alpha\beta} = \frac{\bar{Z}_{\alpha\beta\gamma}}{D_{\alpha\beta\gamma}^{(3)}} - \bar{Y}_{\alpha\beta}(\bar{Y}'_{\alpha\beta}+\omega^2)^{-1} \frac{Z'_{\alpha\beta\gamma}}{D_{\alpha\beta\gamma}^{(3)}} \quad (260)$$

Both \mathbf{U} and \mathbf{T} are 2-rank tensors, while \mathbf{P} is in general a 4-rank tensor. However, if $\mathbf{D}^{(4)} = 0$ also \mathbf{P} becomes a 2-rank tensor. For this reason it is easier to split \mathbf{P} in two contribution:

$$\mathbf{P} = \mathbf{P}^{(0)} + \mathbf{P}^{(1)} \quad (261)$$

where $\mathbf{P}^{(0)} = \mathbf{P}$ if $\mathbf{D}^{(4)} = 0$.

With this expression, the self-energy becomes:

$$\Sigma(\omega) = \mathbf{D}^{(3)} \mathbf{U} \mathbf{P}^{-1} \mathbf{T} \mathbf{D}^{(3)} \quad (262)$$

Here, the inversion of the 4-rank \mathbf{P} tensor is equal to the inversion of a big rank 2 tensor in which the first two and last two indices are grouped together. Moreover, \mathbf{T} has only two indices even if in the right-hand expression of Eq. (260) three indices appears, as both $\bar{Z}_{\alpha\beta\gamma}$ and $\bar{Z}'_{\alpha\beta\gamma}$ loose the dependence on the γ index if divided by $D_{\alpha\beta\gamma}^{(3)}$.

First of all, lets consider the simple case for which $\mathbf{D}^{(4)} = 0$ but $\mathbf{D}^{(3)} \neq 0$. In this case the Bianco self-energy reduces to the bubble diagram:

$$\Sigma(\omega) = \mathbf{D}^{(3)} \Lambda(\omega) \mathbf{D}^{(3)} \quad (263)$$

If we set $\mathbf{D}^{(4)} = 0$ in our Eq. (262) we get:

$$\Sigma(\omega) = \mathbf{D}^{(3)} \mathbf{U} \mathbf{P}^{(0)-1} \mathbf{T} \mathbf{D}^{(3)} \quad (264)$$

The two equations are equal if:

$$\Lambda(\omega) = \mathbf{U} \mathbf{P}^{(0)-1} \mathbf{T} \quad (265)$$

This equality can be proved by a simple algebraic calculations. In fact, $\mathbf{P}^{(0)}$ is a diagonal 4-rank tensor in the polarization basis, and can be inverted by inverting its elements.

The explicit expression in the polarization basis of the \mathbf{T} , $\mathbf{P}^{(0)}$ and \mathbf{U} are:

$$U_{\alpha\beta} = -\hbar^2 \frac{(2n_\alpha+1)(2n_\beta+1)}{8\omega_\alpha\omega_\beta} \quad (266)$$

$$T_{\gamma\delta} = \left[\frac{(4n_\gamma + 2)\omega_\delta + (4n_\delta + 2)\omega_\gamma}{\hbar(2n_\gamma + 1)(2n_\delta + 1)} + \frac{8\omega_\gamma\omega_\delta}{(2n_\gamma + 1)(2n_\delta + 1)} \frac{(2n_\gamma + 1)(2n_\delta + 1)}{(\omega^2 - \omega_\gamma^2 - \omega_\delta^2)(2n_\gamma + 1)(2n_\delta + 1) + 2\omega_\gamma\omega_\delta} \cdot \left(\frac{2\omega_\gamma n_\gamma(n_\gamma + 1)}{\hbar(2n_\gamma + 1)} + \frac{2\omega_\delta n_\delta(n_\delta + 1)}{\hbar(2n_\delta + 1)} \right) \right] \quad (267)$$

$$T_{\gamma\delta} = \left[\frac{(4n_\gamma + 2)\omega_\delta + (4n_\delta + 2)\omega_\gamma}{\hbar(2n_\gamma + 1)(2n_\delta + 1)} + \frac{8\omega_\gamma\omega_\delta}{(\omega^2 - \omega_\gamma^2 - \omega_\delta^2)(2n_\gamma + 1)(2n_\delta + 1) + 2\omega_\gamma\omega_\delta} \left(\frac{2\omega_\gamma n_\gamma(n_\gamma + 1)}{\hbar(2n_\gamma + 1)} + \frac{2\omega_\delta n_\delta(n_\delta + 1)}{\hbar(2n_\delta + 1)} \right) \right] \quad (268)$$

$$P_{\alpha\beta}^{(0)} = \omega^2 - \omega_\alpha^2 - \omega_\beta^2 - \frac{2\omega_\alpha\omega_\beta}{(2n_\alpha + 1)(2n_\beta + 1)} - \frac{8\omega_\alpha\omega_\beta}{(\omega^2 - \omega_\alpha^2 - \omega_\beta^2)(2n_\alpha + 1)(2n_\beta + 1) + 2\omega_\alpha\omega_\beta} \cdot \frac{2\omega_\alpha\omega_\beta(2n_\alpha n_\beta + n_\alpha + n_\beta)(2n_\alpha n_\beta + n_\alpha + n_\beta + 1)}{(2n_\alpha + 1)(2n_\beta + 1)} \quad (269)$$

$$P_{\alpha\beta}^{(0)} = \omega^2 - \omega_\alpha^2 - \omega_\beta^2 - \frac{2\omega_\alpha\omega_\beta}{(2n_\alpha + 1)(2n_\beta + 1)} \left[1 + \frac{8\omega_\alpha\omega_\beta(2n_\alpha n_\beta + n_\alpha + n_\beta)(2n_\alpha n_\beta + n_\alpha + n_\beta + 1)}{(\omega^2 - \omega_\alpha^2 - \omega_\beta^2)(2n_\alpha + 1)(2n_\beta + 1) + 2\omega_\alpha\omega_\beta} \right] \quad (270)$$

With some algebraic manipulation, it is straightfoward to show that

$$\frac{U_{\alpha\beta}T_{\alpha\beta}}{P_{\alpha\beta}^{(0)}} = -\frac{\hbar^2}{4\omega_\alpha\omega_\beta} \left[\frac{(\omega_\alpha + \omega_\beta)(n_\alpha + n_\beta + 1)}{(\omega_\alpha + \omega_\beta)^2 - \omega^2} + \frac{(\omega_\alpha - \omega_\beta)(n_\alpha - n_\beta)}{(\omega_\alpha - \omega_\beta)^2 - \omega^2} \right] \quad (271)$$

That is exactly the expression in the polarization basis of the $\mathbf{\Lambda}(\omega)$ tensor. Therefore we proved Eq. (265), and the dynamical ansatz of Bianco in the case $\mathbf{D}^{(4)} = 0$. To proceed with the case $\mathbf{D}^{(4)} \neq 0$ we must add the $\mathbf{P}^{(1)}$.

$$\Sigma(\omega) = \mathbf{D}\mathbf{U} \left[\mathbf{P}^{(0)} + \mathbf{P}^{(1)} \right]^{-1} \mathbf{T}\mathbf{D} \quad (272)$$

$$\Sigma(\omega) = \mathbf{D}\mathbf{U} \left[\mathbb{1} + \mathbf{P}^{(0)-1} \mathbf{P}^{(1)} \right]^{-1} \mathbf{P}^{(0)-1} \mathbf{T}\mathbf{D} \quad (273)$$

We already proved that

$$\mathbf{\Lambda}(\omega) = \mathbf{U}\mathbf{P}^{(0)-1}\mathbf{T} \quad (274)$$

Therefore, it is trivial to show that Eq. (273) is the Bianco self-energy (Eq. 119) if we prove that:

$$\mathbf{P}^{(0)-1} \mathbf{P}^{(1)} = \mathbf{P}^{(0)-1} \mathbf{T}\mathbf{D}\mathbf{U}. \quad (275)$$

In fact, if we substitute Eq. (275) into Eq. (273), and we perform the Taylor expansion for small $\mathbf{D}^{(4)}$, we get:

$$\Sigma(\omega) = \mathbf{D}\mathbf{U}\mathbf{P}^{(0)-1} \mathbf{T}\mathbf{D} + \mathbf{D}\mathbf{U}\mathbf{P}^{(0)-1} \mathbf{T}\mathbf{D}\mathbf{U}\mathbf{P}^{(0)-1} \mathbf{T}\mathbf{D} + \dots$$

$$\Sigma(\omega) = \mathbf{D}\mathbf{\Lambda}(\omega)\mathbf{D} + \mathbf{D}\mathbf{\Lambda}(\omega)\mathbf{D}\mathbf{\Lambda}(\omega)\mathbf{D} + \dots \quad (276)$$

That is the correct diagrammatic expansion of the self-energy, as defined in ref.[33].

We give here the explicit expression of the $\mathbf{P}^{(1)}$ 4-rank tensor.

$$P_{\alpha\beta\gamma\delta}^{(1)} = -\frac{\hbar(2n_\gamma + 1)(2n_\delta + 1)(2\omega_\alpha n_\beta + 2\omega_\beta n_\alpha + \omega_\alpha + \omega_\beta)}{4(2n_\alpha + 1)(2n_\beta + 1)\omega_\gamma\omega_\delta} \mathbf{D}_{\alpha\beta\gamma\delta}^{(4)} - \frac{8\omega_\alpha\omega_\beta}{(\omega^2 - \omega_\alpha^2 - \omega_\beta^2)(2n_\alpha + 1)(2n_\beta + 1) + 2\omega_\alpha\omega_\beta} \cdot \frac{\hbar[\omega_\alpha n_\alpha(n_\alpha + 1)(2n_\beta + 1) + \omega_\beta n_\beta(n_\beta + 1)(2n_\alpha + 1)]}{4(2n_\alpha + 1)(2n_\beta + 1)\omega_\gamma\omega_\delta} \mathbf{D}_{\alpha\beta\gamma\delta}^{(4)} \quad (277)$$

$$P_{\alpha\beta\gamma\delta}^{(1)} = -\frac{\hbar(2n_\gamma+1)(2n_\delta+1)D_{\alpha\beta\gamma\delta}^{(4)}}{4(2n_\alpha+1)(2n_\beta+1)\omega_\gamma\omega_\delta} \left[2\omega_\alpha n_\beta + 2\omega_\beta n_\alpha + \omega_\alpha + \omega_\beta + \frac{8\omega_\alpha\omega_\beta[\omega_\alpha n_\alpha(n_\alpha+1)(2n_\beta+1) + \omega_\beta n_\beta(n_\beta+1)(2n_\alpha+1)]}{(\omega^2 - \omega_\alpha^2 - \omega_\beta^2)(2n_\alpha+1)(2n_\beta+1) + 2\omega_\alpha\omega_\beta} \right] \quad (278)$$

Again, with straightfoward algebra we can prove that:

$$\frac{P_{\alpha\beta\gamma\delta}^{(1)}}{P_{\alpha\beta}^{(0)}} = \frac{T_{\alpha\beta}^{(4)} D_{\alpha\beta\gamma\delta} U_{\gamma\delta}}{P_{\alpha\beta}^{(0)}} \quad (279)$$

This concludes the proof that the one-phonon self-energy proposed as *ansatz* by Bianco et al.[33] can be formally derived in a full dynamical context within the TD-SCHA theory.

H. ADDITIONAL DETAILS ON THE LANCZOS ALGORITHM

The Lanczos matrix \mathcal{L} depends on the static SCHA self-consistent frequencies ω_μ that appears in the expressions of the Lanczos matrix \mathcal{L} (Eq. 137, 249, 250, 251, 252, 253, 254, 255, 256) and on the anharmonic scattering tensors $\mathbf{D}^{(3)}$ and $\mathbf{D}^{(4)}$ defined in Eq. (84) and (85). The frequencies ω_μ are obtained through the SCHA minimization[20, 37], while $\mathbf{D}^{(3)}$ and $\mathbf{D}^{(4)}$ are computed using only first derivatives of the BO potential (i.e. *ab initio* forces) with the method described in ref.[33].

In particular they are evaluated with a Monte Carlo average on an ensemble of N_{conf} configurations (see Appendix F and ref.[33]).

For the simulation of hydrogen reported in Sec. VII B, we employed an ensemble of 40000 configurations.

The Lanczos algorithm works computing the tri-diagonal elements of the \mathcal{T} matrix $(\alpha_i, \beta_i, \gamma_i)$. Each step we apply the \mathcal{L} matrix (Eq. 137) to a vector, and we obtain the next values of α_i, β_i and γ_i . These values are used to obtain the Green function with Eq. (152). As can be seen from the expression of the Green function, each new iteration introduces a new pole in the Green function. This is well represented in FIG. 6 of the main text.

To see the signal coming from the poles of the spectral function, we need to introduce an imaginary part on the Green function. This is done in two ways. The standard way is introducing a finite smearing η by changing $\omega \rightarrow \omega + i\eta$. Also, we can employ the “terminator” of Eq. (155). It introduces a branch cut in the Green function that smooth the overall result non uniformly, allowing to converge with a much lower number of iterations.

We present in FIG. 7 the result of the Raman signal of high-pressure hydrogen presented in Sec. VII B, with and without the terminator ($N_{\text{steps}} = 200$, $\mathbf{D}^{(4)} = 0$, $\eta = 5 \text{ cm}^{-1}$).

As shown, the low region of the spectrum is completely unaffected by the terminator. In fact, each new iterations adds a new pole on the vibron, whose intensity is distributed in several poles. For this reason, converging a complex non Lorentzian shape with the continued fraction without terminator requires a lot of iterations. The terminator fixes this behaviour providing a smooth lineshape for the whole vibron, without affecting the rest of the spectrum. A similar effect can be obtained by increasing the smearing η to a value larger than the distance between two poles. However, in this way, η will affect the full spectrum, even the low frequency region.

I. COMPUTATIONAL DETAILS FOR THE HYDROGEN SIMULATION

The simulations are performed on a 2x2x1 supercell to sample the Brillouin zone for phonons (96 atoms). The *ab initio* energy landscape is simulated through DFT, with the BLYP[62] functional. For all the DFT calculations, we employed the Quantum ESPRESSO[63, 64] package, with a plane wave basis set and a norm conserving pseudo-potential from the Pseudo Dojo library[65]. The energy cutoff for the basis of the wave-functions was 60 Ry (240 Ry for the electronic density). The Brillouin zone for electrons is sampled on a 4x4x4 mesh in the phonon displaced supercell (2x2x1). Additional details can be found in ref.[26], where we published the Raman and IR signal for several pressures and focused the discussion on the high-pressure hydrogen physics.

J. HARMONIC TWO-PHONON PROPAGATOR

In this section we derive the Harmonic two-phonon propagator from the response system of Eq. (81).

The harmonic limit is obtained as $\mathbf{D}^{(3)} = 0$ and $\mathbf{D}^{(4)} = 0$. In this limit, the one-phonon and two-phonon Green functions are decoupled. The two-phonon propagation is described by the variables $\text{Re}\mathbf{A}$ and \mathbf{Y} , so we isolate these contributions in the green function (Eq. (88)).

The two phonon green function is obtained inverting the matrix:

$$G^{(2ph)}(\omega) = \begin{pmatrix} -\bar{\mathbf{X}} - \omega^2 & -\bar{\mathbf{Y}} \\ -\bar{\mathbf{X}}' & -\bar{\mathbf{Y}}' - \omega^2 \end{pmatrix}^{-1} \quad (280)$$

In the polarization basis, the tensor $\bar{\mathbf{X}}$, $\bar{\mathbf{Y}}$, $\bar{\mathbf{X}}'$ and $\bar{\mathbf{Y}}'$ are diagonal. Therefore, once we identify a couple of modes $\mu\nu$, we only need to invert a 2x2 matrix in Eq. (280).

Since we are interested in the fluctuations-fluctuations correlation function, we only need the response in the Υ block (the fluctuations are the convariance matrix Υ^{-1}). This term is:

$$G_{\mu\nu}^{(\Upsilon)}(\omega) = \frac{-\bar{Y}'_{\mu\nu\mu\nu} - \omega^2}{\bar{X}'_{\mu\nu\mu\nu}\bar{Y}_{\mu\nu\mu\nu} + (\bar{X}_{\mu\nu\mu\nu} + \omega^2)(\bar{Y}'_{\mu\nu\mu\nu} + \omega^2)} \quad (281)$$

Substituting the expression defined in F (taking care of the symmetry exchanging $\mu \leftrightarrow \nu$) we get:

$$G_{ab}^{(\Upsilon)}(\omega) = \frac{2}{\hbar(4n_a n_b + 2n_a + 2n_b + 1)} \cdot \left[\frac{-2\omega^2 \omega_a n_b - \omega^2 \omega_a - 2\omega^2 \omega_b n_a - \omega^2 \omega_b}{[(\omega_a - \omega_b)^2 - \omega^2][(\omega_a + \omega_b)^2 - \omega^2]} + \frac{2\omega_a^3 n_b + \omega_a^3 - 2\omega_a^2 \omega_b n_a - \omega_a^2 \omega_b}{[(\omega_a - \omega_b)^2 - \omega^2][(\omega_a + \omega_b)^2 - \omega^2]} + \frac{-2\omega_a \omega_b^2 n_b - \omega_a \omega_b^2 + 2\omega_b^3 n_a + \omega_b^3}{[(\omega_a - \omega_b)^2 - \omega^2][(\omega_a + \omega_b)^2 - \omega^2]} \right] \quad (282)$$

This green function has the poles in the correct posi-

tion, when:

$$\omega^2 = (\omega_a \pm \omega_b)^2$$

Since we want the fluctuation-fluctuation correlation function, we need to change variable for the Green function from Υ to Υ^{-1} . This is achieved knowing how the perturbation in $(\Upsilon^{-1})^{(1)}$ depend on those on $\Upsilon^{(1)}$:

$$(\Upsilon^{-1})_{ab}^{(1)} = - \sum_{cd} \Upsilon_{ac}^{-1} \Upsilon_{bd}^{-1} \Upsilon_{cd}^{(1)} \quad (283)$$

From this expression we can compute the fluctuation-fluctuation response function:

$$\chi_{abcd}(\omega) = G_{abcd}^{(\Upsilon^{-1})}(\omega) = - \sum_{ef} \Upsilon_{ae}^{-1} \Upsilon_{bf}^{-1} G_{efcd}^{(\Upsilon)}(\omega) \quad (284)$$

If we substitute the expressions in the polarization basis, we obtain:

$$\chi_{\mu\nu}(\omega) = - \frac{\hbar(\omega_\mu - \omega_\nu)(n_\mu - n_\nu)}{2(\omega - \omega_\mu + \omega_\nu)(\omega + \omega_\mu - \omega_\nu)\omega_\mu\omega_\nu} + \frac{\hbar(\omega_\mu + \omega_\nu)(n_\mu + n_\nu + 1)}{2(\omega^2 - (\omega_\mu + \omega_\nu)^2)\omega_\mu\omega_\nu} \quad (285)$$

That is the standard two-phonon propagator.

-
- [1] Y. Li, J. Hao, H. Liu, Y. Li, and Y. Ma, The metalization and superconductivity of dense hydrogen sulfide, *The Journal of Chemical Physics* **140**, 174712 (2014).
 - [2] F. Peng, Y. Sun, C. J. Pickard, R. J. Needs, Q. Wu, and Y. Ma, Hydrogen clathrate structures in rare earth hydrides at high pressures: Possible route to room-temperature superconductivity, *Physical Review Letters* **119**, 10.1103/physrevlett.119.107001 (2017).
 - [3] A. P. Drozdov, M. I. Erements, I. A. Troyan, V. Ksenofontov, and S. I. Shylin, Conventional superconductivity at 203 kelvin at high pressures in the sulfur hydride system, *Nature* **525**, 73 (2015).
 - [4] M. Somayazulu, M. Ahart, A. K. Mishra, Z. M. Geballe, M. Baldini, Y. Meng, V. V. Struzhkin, and R. J. Hemley, Evidence for superconductivity above 260 k in lanthanum superhydride at megabar pressures, *Physical Review Letters* **122**, 10.1103/physrevlett.122.027001 (2019).
 - [5] A. Drozdov, P. Kong, V. Minkov, S. Besedin, M. Kuzovnikov, S. Mozaffari, L. Balicas, F. Balakirev, D. Graf, V. Prakapenka, *et al.*, Superconductivity at 250 k in lanthanum hydride under high pressures, *Nature* **569**, 528 (2019).
 - [6] Y. Wang, J. Lv, L. Zhu, and Y. Ma, Crystal structure prediction via particle-swarm optimization, *Physical Review B* **82**, 10.1103/physrevb.82.094116 (2010).
 - [7] A. R. Oganov and C. W. Glass, Crystal structure prediction using ab initio evolutionary techniques: Principles and applications, *The Journal of Chemical Physics* **124**, 244704 (2006).
 - [8] C. J. Pickard and R. J. Needs, Ab initio random structure searching, *Journal of Physics: Condensed Matter* **23**, 053201 (2011).
 - [9] E. Runge and E. K. U. Gross, Density-functional theory for time-dependent systems, *Physical Review Letters* **52**, 997 (1984).
 - [10] M. A. Marques, C. A. Ullrich, F. Nogueira, K. Burke, A. Rubio, and E. K. U. Gross, *Time-Dependent Density Functional Theory* (Springer Science & Business Media, 2006).
 - [11] R. Car and M. Parrinello, Unified approach for molecular dynamics and density-functional theory, *Physical review letters* **55**, 2471 (1985).
 - [12] A. Cupo, D. Tristant, K. Rego, and V. Meunier, Theoretical analysis of spectral lineshapes from molecular dynamics, *npj Computational Materials* **5**, 10.1038/s41524-019-0220-1 (2019).
 - [13] G. Baym and N. D. Mermin, Determination of thermodynamic green's functions, *Journal of Mathematical Physics* **2**, 232 (1961).
 - [14] G. Krilov and B. J. Berne, Real time quantum correlation functions. II. maximum entropy numerical analytic continuation of path integral monte carlo and centroid molecular dynamics data, *The Journal of Chemical Physics* **111**, 9147 (1999).
 - [15] J. A. Poulsen, G. Nyman, and P. J. Rossky, Practical evaluation of condensed phase quantum correlation functions: A feynman-kleinert variational linearized path integral method, *The Journal of Chemical Physics* **119**,

- 12179 (2003).
- [16] R. Hernandez and G. A. Voth, Quantum time correlation functions and classical coherence, *Chemical Physics* **233**, 243 (1998).
 - [17] X. Sun, H. Wang, and W. H. Miller, Semiclassical theory of electronically nonadiabatic dynamics: Results of a linearized approximation to the initial value representation, *The Journal of Chemical Physics* **109**, 7064 (1998).
 - [18] S. Bonella, M. Monteferrante, C. Pierleoni, and G. Ciccotti, Path integral based calculations of symmetrized time correlation functions. II, *The Journal of Chemical Physics* **133**, 164105 (2010).
 - [19] E. Snider, N. Dasenbrock-Gammon, R. McBride, M. Debessai, H. Vindana, K. Vencatasamy, K. V. Lawler, A. Salamat, and R. P. Dias, Room-temperature superconductivity in a carbonaceous sulfur hydride, *Nature* **586**, 373 (2020).
 - [20] I. Errea, M. Calandra, and F. Mauri, Anharmonic free energies and phonon dispersions from the stochastic self-consistent harmonic approximation: Application to platinum and palladium hydrides, *Physical Review B* **89**, 10.1103/physrevb.89.064302 (2014).
 - [21] I. Errea, M. Calandra, C. J. Pickard, J. R. Nelson, R. J. Needs, Y. Li, H. Liu, Y. Zhang, Y. Ma, and F. Mauri, Quantum hydrogen-bond symmetrization in the superconducting hydrogen sulfide system, *Nature* **532**, 81 (2016).
 - [22] R. Bianco, I. Errea, M. Calandra, and F. Mauri, High-pressure phase diagram of hydrogen and deuterium sulfides from first principles: Structural and vibrational properties including quantum and anharmonic effects, *Physical Review B* **97**, 10.1103/physrevb.97.214101 (2018).
 - [23] I. Errea, F. Belli, L. Monacelli, A. Sanna, T. Koretsune, T. Tadano, R. Bianco, M. Calandra, R. Arita, F. Mauri, and J. A. Flores-Livas, Quantum crystal structure in the 250-kelvin superconducting lanthanum hydride, *Nature* **578**, 66 (2020).
 - [24] M. Borinaga, P. Riego, A. Leonardo, M. Calandra, F. Mauri, A. Bergara, and I. Errea, Anharmonic enhancement of superconductivity in metallic molecular C_{60} - 4 hydrogen at high pressure: a first-principles study, *Journal of Physics: Condensed Matter* **28**, 494001 (2016).
 - [25] M. Borinaga, I. Errea, M. Calandra, F. Mauri, and A. Bergara, Anharmonic effects in atomic hydrogen: Superconductivity and lattice dynamical stability, *Phys. Rev. B* **93**, 174308 (2016).
 - [26] L. Monacelli, I. Errea, M. Calandra, and F. Mauri, Black metal hydrogen above 360 GPa driven by proton quantum fluctuations, *Nature Physics* 10.1038/s41567-020-1009-3 (2020).
 - [27] R. Bianco, I. Errea, L. Monacelli, M. Calandra, and F. Mauri, Quantum enhancement of charge density wave in NbS_2 in the two-dimensional limit, *Nano Letters* **19**, 3098 (2019).
 - [28] R. Bianco, L. Monacelli, M. Calandra, F. Mauri, and I. Errea, Weak dimensionality dependence and dominant role of ionic fluctuations in the charge-density-wave transition of NbSe_2 , *Physical Review Letters* **125**, 10.1103/physrevlett.125.106101 (2020).
 - [29] J. S. Zhou, L. Monacelli, R. Bianco, I. Errea, F. Mauri, and M. Calandra, Anharmonicity and doping melt the charge density wave in single-layer TiSe_2 , *Nano Letters* **20**, 4809 (2020).
 - [30] U. Aseginolaza, R. Bianco, L. Monacelli, L. Paulatto, M. Calandra, F. Mauri, A. Bergara, and I. Errea, Phonon collapse and second-order phase transition in thermoelectric SnSe , *Physical Review Letters* **122**, 10.1103/physrevlett.122.075901 (2019).
 - [31] U. Aseginolaza, R. Bianco, L. Monacelli, L. Paulatto, M. Calandra, F. Mauri, A. Bergara, and I. Errea, Strong anharmonicity and high thermoelectric efficiency in high temperature SnS from first-principles, *arXiv preprint arXiv:1906.02047* (2019).
 - [32] G. A. S. Ribeiro, L. Paulatto, R. Bianco, I. Errea, F. Mauri, and M. Calandra, Strong anharmonicity in the phonon spectra of PbTe and SnTe from first principles, *Physical Review B* **97**, 10.1103/physrevb.97.014306 (2018).
 - [33] R. Bianco, I. Errea, L. Paulatto, M. Calandra, and F. Mauri, Second-order structural phase transitions, free energy curvature, and temperature-dependent anharmonic phonons in the self-consistent harmonic approximation: Theory and stochastic implementation, *Physical Review B* **96**, 10.1103/physrevb.96.014111 (2017).
 - [34] M. Lazzeri and F. Mauri, First-principles calculation of vibrational raman spectra in large systems: Signature of small rings in CrystallineSiO_2 , *Physical Review Letters* **90**, 10.1103/physrevlett.90.036401 (2003).
 - [35] M. Simoncelli, N. Marzari, and F. Mauri, Unified theory of thermal transport in crystals and glasses, *Nature Physics* **15**, 809 (2019).
 - [36] L. Monacelli, G. Batignani, G. Fumero, C. Ferrante, S. Mukamel, and T. Scopigno, Manipulating impulsive stimulated raman spectroscopy with a chirped probe pulse, *The Journal of Physical Chemistry Letters* **8**, 966 (2017).
 - [37] L. Monacelli, I. Errea, M. Calandra, and F. Mauri, Pressure and stress tensor of complex anharmonic crystals within the stochastic self-consistent harmonic approximation, *Phys. Rev. B* **98**, 024106 (2018).
 - [38] T. cheng Li and P. qing Tong, Hohenberg-kohn theorem for time-dependent ensembles, *Physical Review A* **31**, 1950 (1985).
 - [39] D. Huber and E. J. Heller, Generalized gaussian wave packet dynamics, *The Journal of Chemical Physics* **87**, 5302 (1987).
 - [40] D. Huber, E. J. Heller, and R. G. Littlejohn, Generalized gaussian wave packet dynamics, schrödinger equation, and stationary phase approximation, *The Journal of Chemical Physics* **89**, 2003 (1988).
 - [41] H. Pal, M. Vyas, and S. Tomsovic, Generalized gaussian wave packet dynamics: Integrable and chaotic systems, *Physical Review E* **93**, 10.1103/physreve.93.012213 (2016).
 - [42] J. Haegeman, J. I. Cirac, T. J. Osborne, I. Pižorn, H. Verschelde, and F. Verstraete, Time-dependent variational principle for quantum lattices, *Physical Review Letters* **107**, 10.1103/physrevlett.107.070601 (2011).
 - [43] T. Guaita, L. Hackl, T. Shi, C. Hubig, E. Demler, and J. I. Cirac, Gaussian time-dependent variational principle for the bose-hubbard model, *Physical Review B* **100**, 10.1103/physrevb.100.094529 (2019).
 - [44] L. Hackl, T. Guaita, T. Shi, J. Haegeman, E. Demler, and J. I. Cirac, Geometry of variational methods: dynamics of closed quantum systems, *SciPost Phys.* **9**, 48 (2020).
 - [45] H.-D. Meyer and G. A. Worth, Quantum molecular dynamics: propagating wavepackets and density

- operators using the multiconfiguration time-dependent hartree method, *Theoretical Chemistry Accounts* **109**, 251 (2003).
- [46] H.-P. Breuer and F. Petruccione, *The Theory of Open Quantum Systems* (Oxford University Press, 2007).
 - [47] W. Kohn and J. M. Luttinger, Quantum theory of electrical transport phenomena, *Physical Review* **108**, 590 (1957).
 - [48] A. Pribram-Jones, P. E. Grabowski, and K. Burke, Thermal density functional theory: Time-dependent linear response and approximate functionals from the fluctuation-dissipation theorem, *Physical Review Letters* **116**, 10.1103/physrevlett.116.233001 (2016).
 - [49] I. Errea, B. Rousseau, and A. Bergara, Isotope effect in the superconducting high-pressure simple cubic phase of calcium from first principles, *Journal of Applied Physics* **111**, 112604 (2012).
 - [50] O. Hellman, I. A. Abrikosov, and S. I. Simak, Lattice dynamics of anharmonic solids from first principles, *Phys. Rev. B* **84**, 180301 (2011).
 - [51] T. Tadano, Y. Gohda, and S. Tsuneyuki, Anharmonic force constants extracted from first-principles molecular dynamics: applications to heat transfer simulations, *Journal of Physics: Condensed Matter* **26**, 225402 (2014).
 - [52] J.-M. Lihm and C.-H. Park, Gaussian time-dependent variational principle for the finite-temperature anharmonic lattice dynamics, *arXiv preprint arXiv:2010.15725* (2020).
 - [53] A. Putrino and M. Parrinello, Anharmonic raman spectra in high-pressure ice from Ab Initio Simulations, *Physical Review Letters* **88**, 10.1103/physrevlett.88.176401 (2002).
 - [54] P. L. Silvestrelli, M. Bernasconi, and M. Parrinello, Ab initio infrared spectrum of liquid water, *Chemical Physics Letters* **277**, 478 (1997).
 - [55] W. Windl, P. Pavone, K. Karch, O. Schütt, D. Strauch, P. Giannozzi, and S. Baroni, Second-order raman spectra of diamond from ab initio phonon calculations, *Physical Review B* **48**, 3164 (1993).
 - [56] W. H. Press, *Numerical Recipes: The Art of Scientific Computing, Third Edition*, 3rd ed. (Cambridge University Press, 2017).
 - [57] D. Rocca, R. Gebauer, Y. Saad, and S. Baroni, Turbo charging time-dependent density-functional theory with lanczos chains, *The Journal of Chemical Physics* **128**, 154105 (2008).
 - [58] I. Errea, M. Calandra, C. J. Pickard, J. Nelson, R. J. Needs, Y. Li, H. Liu, Y. Zhang, Y. Ma, and F. Mauri, High-pressure hydrogen sulfide from first principles: A strongly anharmonic phonon-mediated superconductor, *Physical Review Letters* **114**, 10.1103/physrevlett.114.157004 (2015).
 - [59] I. Errea, Approaching the strongly anharmonic limit with ab initio calculations of materials' vibrational properties – a colloquium, *The European Physical Journal B* **89** (2016).
 - [60] I. B. Magdău and G. J. Ackland, Identification of high-pressure phases III and IV in hydrogen: Simulating raman spectra using molecular dynamics, *Physical Review B* **87**, 10.1103/physrevb.87.174110 (2013).
 - [61] C. Zhang, C. Zhang, M. Chen, W. Kang, Z. Gu, J. Zhao, C. Liu, C. Sun, and P. Zhang, Finite-temperature infrared and raman spectra of high-pressure hydrogen from first-principles molecular dynamics, *Physical Review B* **98**, 10.1103/physrevb.98.144301 (2018).
 - [62] B. Miehl, A. Savin, H. Stoll, and H. Preuss, Results obtained with the correlation energy density functionals of Becke and Lee, Yang and Parr, *Chemical Physics Letters* **157**, 200 (1989).
 - [63] P. Giannozzi, S. Baroni, N. Bonini, M. Calandra, R. Car, C. Cavazzoni, D. Ceresoli, G. L. Chiarotti, M. Cococcioni, I. Dabo, A. D. Corso, S. de Gironcoli, S. Fabris, G. Fratesi, R. Gebauer, U. Gerstmann, C. Gougoussis, A. Kokalj, M. Lazzeri, L. Martin-Samos, N. Marzari, F. Mauri, R. Mazzarello, S. Paolini, A. Pasquarello, L. Paulatto, C. Sbraccia, S. Scandolo, G. Sclauzero, A. P. Seitsonen, A. Smogunov, P. Umari, and R. M. Wentzcovitch, QUANTUM ESPRESSO: a modular and open-source software project for quantum simulations of materials, *Journal of Physics: Condensed Matter* **21**, 395502 (2009).
 - [64] P. Giannozzi, O. Andreussi, T. Brumme, O. Bunau, M. B. Nardelli, M. Calandra, R. Car, C. Cavazzoni, D. Ceresoli, M. Cococcioni, N. Colonna, I. Carnimeo, A. D. Corso, S. de Gironcoli, P. Delugas, R. A. DiStasio, A. Ferretti, A. Floris, G. Fratesi, G. Fugallo, R. Gebauer, U. Gerstmann, F. Giustino, T. Gorni, J. Jia, M. Kawamura, H.-Y. Ko, A. Kokalj, E. Küçükbenli, M. Lazzeri, M. Marsili, N. Marzari, F. Mauri, N. L. Nguyen, H.-V. Nguyen, A. O. de-la Roza, L. Paulatto, S. Poncé, D. Rocca, R. Sabatini, B. Santra, M. Schlipf, A. P. Seitsonen, A. Smogunov, I. Timrov, T. Thonhauser, P. Umari, N. Vast, X. Wu, and S. Baroni, Advanced capabilities for materials modelling with quantum ESPRESSO, *Journal of Physics: Condensed Matter* **29**, 465901 (2017).
 - [65] D. R. Hamann, Optimized norm-conserving Vanderbilt pseudopotentials, *Phys. Rev. B* **88**, 085117 (2013).